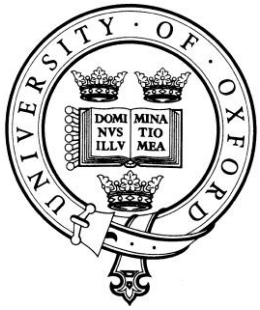
Putting marine microbes on the map: determining the global distribution of marine picophytoplankton using a combination of satellite and field data



by

Priscila Kienteca Lange

Thesis submitted to University of Oxford for the degree of Doctor of Philosophy

Department of Earth Sciences

St. John's College

Trinity Term 2017

Supervisors:

Dr Heather A. Bouman, Dr Mikhail Zubkov and Dr Shubha Sathyendranath

Declaration

I confirm that this thesis is an original work of my authorship. Operational collaborations include: the computational run of the primary production (carbon fixation) algorithm by Thomas Jackson (Plymouth Marine Laboratory) on Chapter 5; and ARGO data processing by Giorgio Dall'Olmo (Plymouth Marine Laboratory) on Chapter 4. Other collaborations have been fully acknowledged in the thesis.

Priscila Kienteca Lange

Marine microbes on the map: determining the global distribution of marine picophytoplankton using a combination of satellite and field data

Priscila Kienteca Lange, St. John's College

Thesis submitted to the University of Oxford for the degree of Doctor of Philosophy in Earth Sciences

Abstract

Picophytoplanktonic cells (0.2-2 μm) are the dominant phytoplankters in the largest marine biomes on Earth: the subtropical gyres. The overaching aim of this thesis is to develop algorithms that use remote-sensing observables to map the distribution of the smallest and most abundant member of picophytoplankton, *Prochlorococcus*, and assess its contribution to the marine carbon cycle. To understand how the photoacclimatory status and growth of *Prochlorococcus* and its sister genera *Synechococcus* are influenced by light and nutrients, experiments were conducted in the South Atlantic Gyre (SAG). Results from the manipulation experiments show that, in the central region of the SAG, nutrient addition can induce marked changes in the optical properties of *Prochlorococcus* cells when subjected to saturating light levels, leading to a decrease in cell abundance, whereas at the gyre periphery no substantive changes in cell growth or optical characteristics were observed. Since light plays a central role in shaping the distribution of cyanobacteria, an empirical algorithm based on relationships between *Prochlorococcus* abundance and remotely-sensed observables was developed. The outputs were then used in a modified primary production model to predict the vertical distribution of carbon fixation by *Prochlorococcus*. The models estimate that ~ 3.4 x 10^{27} *Prochlorococcus* cells in the global ocean fix 4.7 Gt C $year^{-1}$. Most of the cell biomass and primary productivity is concentrated in the subtropical gyres and areas near the Equatorial Convergence, and 61% of the carbon fixation occurs in the upper water column (0-45 metres), where only 43% of the cells reside. However, in the gyres, carbon fixation is highest (62%) in deeper layers (45-200m), and both cell abundance and carbon fixation show marked seasonal patterns. The models developed in this study provide an unprecedented view of the vertical distribution of *Prochlorococcus* cells and their corresponding rates of carbon fixation in the global ocean.

Marine microbes on the map: determining the global distribution of marine picophytoplankton using a combination of satellite and field data

Priscila Kienteca Lange, St. John's College

Thesis submitted to the University of Oxford for the degree of Doctor of Philosophy in Earth Sciences

Extended abstract

Subtropical ocean gyres cover ~50% of the area of the world's oceans, and has been considered to be oceanic deserts due to the chronically low nutrients and chlorophyll concentrations found in these waters. In these ecosystems, primary production is dominated by picoplanktonic cells (0.2 – 2 μm), which are comprised of the two marine cyanobacteria *Prochlorococcus* and *Synechococcus*, and photosynthetic picoeukaryotes represented by a variety of different taxonomic groups. The main goal of this thesis is to develop a series of algorithms that use Earth observations (satellites and ARGO float data) of environmental variables to predict the global distribution of picophytoplanktonic cells (i.e. *Prochlorococcus*), and their contribution to carbon fixation in the marine environment.

To achieve this aim, it was necessary to first understand how the different picophytoplankton groups respond to environmental variables such as light and nutrients. The combined influence of light and nutrients (nitrogen and iron) on the photoacclimatory status of marine cyanobacteria (*Prochlorococcus* to *Synechococcus*) was examined in experiments set in the centre and periphery of the South Atlantic Gyre. *Prochlorococcus* showed a positive growth response over time in both experiments, with cell abundances increasing by > 50% after the first cell cycle. However, in the gyre centre, nutrient addition induced marked changes in the optical properties of *Prochlorococcus* cells (decrease in red fluorescence and light scatter) when subjected to saturating light levels (> 700 μE m^{-2} s^{-1}), leading to a 38% decrease in cell abundance. In the gyre periphery, nutrient addition did not alter the optical properties and growth of *Prochlorococcus* and *Synechococcus* populations, and the increase in cell abundance was directly correlated with light intensity. These results suggest that light is the primary resource limiting the growth of *Prochlorococcus* and *Synechococcus* in subtropical gyres. Although an increase in nutrient supply often results in an increase in phytoplankton biomass, complex interactions between high light and

nutrients (possibly iron) may be harmful to cells that are highly adapted to extreme light and oligotrophic conditions such as surface populations of *Prochlorococcus*.

To develop a global algorithm to predict the large-scale vertical distribution of the functional groups of picophytoplankton, a large dataset of picophytoplankton cell abundance and environmental variables collected on 13 Atlantic Meridional Transect (AMT) cruises was assembled. The cyanobacterium *Prochlorococcus* was chosen as a model picophytoplankton group for the development of remote-sensing algorithms, since it is the dominant phytoplankter in subtropical gyres and the most numerically abundant photosynthetic organism on Earth. To ensure the comparability between datasets of flow-cytometric counts, the abundance of *Prochlorococcus* was measured using two broadly implemented flow-cytometric methods. Results using the two methods differ in less than 20%, with the highest differences found near the sea surface where the intracellular pigment content of *Prochlorococcus* cells is lowest due to the photoacclimatory response to high light.

Using the Atlantic Meridional Transect (AMT) dataset, the relationships between the abundance of the target picophytoplankton group, *Prochlorococcus*, and environmental variables that can be retrieved from satellites (e.g. temperature, light) were described using multilinear regressions. The series of equations derived from this multivariate analysis were used to develop empirical algorithms that use remote-sensing observables to describe the global vertical distribution of *Prochlorococcus*. The *Prochlorococcus* abundance model estimates the distribution of cells from the sea surface to the base of the photic zone using information on light penetration in the water column and the abundance of cells at surface, which is determined by the relationship between cell abundance and environmental variables observed from satellites. The model (R^2 = 0.58) is able to predict a deep maximum in cell abundance, and estimates that *Prochlorococcus* cells contribute approximately 171 Mt of carbon biomass (3.4×10^{27} cells) to the global ocean, with most of the biomass concentrated within the subtropical gyres and areas near the Equatorial Convergence Zone. Although no clear temporal change in cell standing stocks was observed between the years 2003 and 2014, marked seasonal variability in cell abundance followed seasonal fluctuations in light and temperature in the Atlantic gyres, where cell abundances were lowest during winter (~1.4×10^{13} cells m^{-2}), when surface cell concentrations were highest (~9.8×10^{4} cells ml^{-1}), whereas the opposite scenario was observed in the spring-summer (~2×10^{13} cells m^{-2}).

Finally, cell abundance products generated by the algorithms developed in Chapter 4 were combined with *in-situ* measurements of cell-specific carbon fixation rates to estimate carbon fixation by *Prochlorococcus* using a primary production algorithm adapted from Sathyendranath and Platt (1989). The algorithm replaces chlorophyll biomass with cell abundance biomass, and uses cell-specific photosynthetic rates measured in the Atlantic Ocean by Hartmann et al. (2014) as the maximum photosynthetic rates (P_m^{cell}) for *Prochlorococcus* at saturating irradiance. To assign the photosynthetic parameter α^{cell}, published values were taken from photosynthesis-irradiance experiments using cultures of different *Prochlorococcus* strains. The adapted cell-based primary production model uses information of light penetration in the water column to account for light-dependent changes in the photosynthetic response of *Prochlorococcus* cells. The model estimates an annual carbon fixation of 4.7 Gt C $year^{-1}$ for *Prochlorococcus*, which is roughly 10% of the global marine primary production. When integrated globally, rates of carbon fixation by *Prochlorococcus* show little seasonal variability when compared to other phytoplankton species, representing a constant background rate of carbon fixation over time in oceanic regions. In subtropical gyres, however, *Prochlorococcus* carbon fixation follows seasonal variations in light (which in turn influence both carbon fixation rates and cell abundance), and the thermal structure of the water column (another important determinant of *Prochlorococcus* abundance), being highest during spring and summer and decreasing in winter. Most of the global carbon fixation by *Prochlorococcus* (61%) occurs in the upper water column (0-45 metres), where light is highest but only 43% of the cell biomass resides. This is the combined result of the higher *Prochlorococcus* cell-specific carbon fixation rates (Hartmann et al. 2014) and high surface cell abundances measured in the Equatorial Convergence region. In gyre waters, most of the carbon fixation occurs between 45 and 200 metres, except during autumn and early winter in the North Atlantic and Pacific gyres.

In spite of their minute size, *Prochlorococcus* contributes significantly to the total phytoplankton biomass and carbon fixation in the oceans, and it is likely that previous cell abundance models have underestimated these cell stocks by not capturing variations in cell abundance at depth. The results generated by the cell abundance and primary production models provide a three-dimensional view (horizontally, vertically and temporally) of biomass and carbon fixation by *Prochlorococcus*, the most numerically abundant phytoplankton on the planet.

Acknowledgements

I am thankful to my supervisors Heather Bouman and Shubha Sathyendranath for the academic support and scientific advice during this DPhil course, especially Heather for her enthusiasm and kindness during the last 4 years. I would also like to thank my co-supervisor Mikhail Zubkov, who I consider a mentor for life, and who also hosted me in his field projects (AMT) and in his laboratory in Southampton, allowing the accomplishment of all the experimental work conducted in this DPhil thesis. In addition, I would like to thank Robert Brewin, Giorgio Dall'Olmo, and Gavin Tilstone for the support, friendship, the precious collaboration in AMT-related projects, and for advising me on any and everything related to programming and remote-sensing data processing. Thanks also to Thomas Jackson, Glen Tarran, Manuela Hartmann, and Catherine Burd for the collaboration on the research involved in this thesis, and to Trevor Platt for encouraging and supporting me in my application to this DPhil program. Special thanks to Ros Rickaby and Duncan Purdie, who agreed to be my thesis examiners in the middle of the summer, and to Babette Hoogakker, who provided essential and precious advice and supervision during the last year of my DPhil.

Thanks also to: my Brazilian friends in Oxford, especially Ivo, Sergio, Erica, Natalia, Henrique, Ariane, Alex, Lucas, Carol, Marcella, Gregorio, and Luiza, for all the shared good and bad moments during our DPhil courses; and to the Oxford handball team for the amazing experiences, accomplishments, and mostly for the fun, especially to Ai, Aitor, Thais, Barbara, Bostjan and Marija, Jan, and Marcela; to my Southampton friends Anna, Glaucia, Priscila and Rafael, and the NOC people Nina, Manuela, Sara, Cat, Kyle, Lucie, Rosie, Sam, and Andy for making the time in Southampton truly great!; to the crew of the R/v JCR on the cruises AMT 23-25, who were very helpful and kind, and to the BODCs Rob and Arwen for the help providing data to this thesis. Special thanks to my husband Rodolfo for the precious partnership, psychological and scientific support, and mostly for all the love; to the little bouncing one in my belly who kept me calm and relaxed on the last months of my DPhil; to my sister Carol piaba and my friends Rolf, Karina, Tati, Isabela, Pri, and Guga, for the conversations and shared thoughts, and for always being there; and to all the staff of Fernando's Café, for their kindness and for providing the everyday rice, beans, picanha and pudim that kept the smile on our faces.

Finally, this thesis is dedicated to the Brazilian National Council for Scientific and Technological Development (CNPq), to whom I am very thankful for sponsoring my DPhil course in Oxford, providing the scholarship and covering the involved fees. Thank you for still believing in my work at this difficult moment for our country.

Contents

Abstract i

Extended abstract ii

Acknowledgements v

Contents vi

List of Figures ix

List of Tables xviii

Chapter 1. Introduction 1

1.1 Study area 4

1.2 Picophytoplankton groups 7

1.2.1 *Prochlorococcus: the model organism of this study* 9

1.2.2 *The role of Prochlorococcus in marine biogeochemical cycles* 12

1.3 Picoplankton enumeration using flow cytometry 14

1.4 Remote-sensing models: a tool for global phytoplankton estimates 16

1.5 *In-situ* observations: the Atlantic Meridional Transect 19

1.6 Objectives 20

Chapter 2. The influence of light and nutrients on the growth of picocyanobacteria: insights on iron-induced growth inhibition of *Prochlorococcus* cells 22

2.1 Introduction 22

2.2 Material and Methods 25

2.3 Results 29

2.3.1 *Gyre periphery* 29

2.3.2 *Gyre centre* 32

2.3.3 *The growth of other picoplankton groups* 37

2.4 Discussion 38

2.4.1 *Nutrient effect on Prochlorococcus photoacclimation* 40

2.5 Conclusions 43

Chapter 3. Bleached *Prochlorococcus*: the missing phytoplankton? Assessing the efficiency of flow cytometry and filtration methods to estimate picophytoplankton biomass 46

3.1 Introduction 46

3.2 Comparison between flow cytometric methods to quantify *Prochlorococcus*: 'stained' versus 'unstained' cells 47

3.2.1 *Methods* 48

3.2.2 *Results and discussion* 51

3.3 Efficiency of GF/F filters to retain *Prochlorococcus* cells 52

3.3.1 *Methods* 52

3.3.2 *Results and discussion* 53

3.4 Conclusions 55

Chapter 4. Scratching the surface: a model to predict the vertical distribution of *Prochlorococcus* using remote sensing 57

4.1 Introduction 57

4.2 Methods 59

4.2.1 *Model parameterization* 61

4.2.2 *Prochlorococcus abundance predicted using ocean observables* 65

4.2.3 *Additional equations used in the model* 70

4.2.4 *Delineation of the area of subtropical gyres* 72

4.2.5 *In-situ measurements of environmental variables* 73

4.2.5.1 *Flow cytometric picoplankton cell counts* 74

4.2.5.2 *Calculation of in-situ variables* 74

4.3 Results 75

4.3.1 *Model validation* 75

4.3.2 *Choice of a two-component model* 79

4.3.3 *Model output* 81

4.4 Discussion 89

4.5 Conclusions 95

Chapter 5. Carbon fixation by *Prochlorococcus* in the global ocean 97

5.1 Introduction 97

5.2 Methods 100

5.2.1 *Modelling approach* 100

5.2.2 *Photosynthetic parameters for Prochlorococcus* 103

5.3 Results 107

5.4 Discussion 113

5.5 Conclusions 117

Chapter 6. Final remarks and future perspectives 119

6.1 General conclusions 119

6.2 Future perspectives 125

References 127

List of Figures

Figure 1.1. Relative contribution of the a) micro-, b) nano- and c) pico-phytoplankton to total phytoplankton biomass in the Atlantic Ocean. Figure from Brewin et al. (2010). 3

Figure 1.2. Subtropical gyres of the Atlantic Ocean. This figure was generated based on a sea surface chlorophyll (*SSChlo*) image, where subtropical gyres are determined as areas where $SSChlo < 0.075$ mg m^{-3}. 5

Figure 1.3. Vertical profiles of a) temperature, b) nitrate, and c) chlorophyll concentration across the Atlantic Ocean. Map shows the transect where measurements were taken. Data from the oceanographic expedition Atlantic Meridional Transect 22 (AMT22).. 6

Figure 1.4. Vertical profiles of *Prochlorococcus*, *Synechococcus*, and picoeukaryotes across the Atlantic Ocean. Map shows the transect where measurements were taken. Data from AMT 22 (2012). 8

Figure 1.5. Image of a cell of *Synechococcus* sp.. Credit: http://www.whoi.edu/science/B/people/ewebb/Syne.html 8

Figure 1.6. Image of a *Prochlorococcus* sp. cell (Bryant 2003)..... 9

Figure 1.7. a) Schematic view of the light path and mechanisms to detect optical signals emitted by a particle when being analysed in a flow cytometer (adapted from Shapiro (2003)); b) The flow cell of a flow cytometer. 15

Figure 1.8. Picophytoplankton groups individualized in sea water samples using the right-angle light scatter (RALS) and red fluorescence. Round tight clusters are formed by 0.5µm and 1.0µm fluorescent beads and their respective bead duplets. Figure was created using Flowing Software® (version 2.5). 16

Figure 1.9. Transects of the 13 AMT cruises used to create the empirical model to predict the abundance of *Prochlorococcus* cells. 20

Figure 2.1. Location of the two experimental sites in the South Atlantic Ocean: 26

Figure 2.2. Vertical profiles of a,c) the cell abundance of *Prochlorococcus* and *Synechococcus*, and b,d) temperature, salinity and chlorophyll from fluorometer at the stations where water was collected for the experiments at the a-b) gyre centre and c-d) gyre border..... 26

Figure 2.3. a-b) *Prochlorococcus* and c-d) *Synechococcus* cell abundance over time in the gyre border, in the a,c) control and b,d) nutrient enrichment experiments. The dark background indicates periods when incubations were kept in the dark (night). The colour-code indicates the light level to which incubations were exposed during the light hours. 30

Figure 2.4. a-b) *Prochlorococcus* and c-d) *Synechococcus* cell-specific right angle light scatter (RALS) normalized to beads' RALS over time in the gyre border, in the a,c) control and b,d) nutrient enrichment experiments. The dark background indicates periods when incubations were kept in the dark (night). The colour-code indicates the light level to which incubations were exposed during the light hours. 31

Figure 2.5. a-b) *Prochlorococcus* and c-d) *Synechococcus* cell-specific red fluorescence normalized to beads' red fluorescence over time in the gyre border, in the a,c) control and b,d) nutrient enrichment experiments. The dark background indicates periods when incubations were kept in the dark (night). The colour-code indicates the light level to which incubations were exposed during the light hours..... 31

Figure 2.6. Gyre border: a-c) *Prochlorococcus* and d-f) *Synechococcus* a,d) cell abundance, b,e) red fluorescence, and c,f) right-angle light scatter (RALS). Sample in control and nutrient treatments are plotted against each other according to the light level. The diagonal line represents a ratio whereby the data from the control and nutrient addition samples are equal. The colour gradient represents light levels (darkblue = dark; orange = highest light level (1420 to 1780 μE m^{-2} s^{-1})). 32

Figure 2.7. a-b) *Prochlorococcus* and c-d) *Synechococcus* cell abundance over time in the gyre centre, in the a,c) control and b,d) nutrient enrichment experiments. The dark background indicates periods when incubations were kept in the dark (night). The colour-code indicates the light level to which incubations were exposed during the light hours. 34

Figure 2.8. a-b) *Prochlorococcus* and c-d) *Synechococcus* cell-specific right angle light scatter (RALS) normalized to beads' RALS over time in the gyre centre, in the a,c) control and b,d) nutrient enrichment experiments. The dark background indicates periods when incubations were kept in the dark (night). The colour-code indicates the light level to which incubations were exposed during the light hours. 34

Figure 2.9. a-b) *Prochlorococcus* and c-d) *Synechococcus* cell-specific red fluorescence normalized to beads' red fluorescence over time in the gyre centre, in the a,c) control and b,d) nutrient enrichment experiments. The dark background indicates periods when incubations were kept in the dark (night). The colour-code indicates the light level to which incubations were exposed during the light hours..... 35

Figure 2.10. Gyre centre: a-c) *Prochlorococcus* and d-f) *Synechococcus* a,d) cell abundance, b,e) red fluorescence, and c,f) right-angle light scatter (RALS) in the experiments conducted at the gyre centre. Sample in control and nutrient treatments are plotted against each other according to the light level. The diagonal line represents a ratio whereby the data from the control and nutrient addition samples are equal. The color gradient represents light levels (darkblue = dark; orange = highest light level (1420 to 1780 $\mu E\ m^{-2}\ s^{-1}$)). 35

Figure 2.11. *Prochlorococcus* a) absolute increase in right-angle light scatter (RALS) during the day on day 2 (RALS increase day 2 = $RALS_{dusk}$ day 2 - $RALS_{dawn}$ day 2) *versus* absolute increase in cell abundance during the following night (abund increase night 2 = $abundance_{dawn}$ day 3 - $abundance_{dusk}$ day2); b) light level of incubation versus relative cell abundance increase during the day on day 2 (% abundance increase = ($abundance_{dusk}$ day 2 – $abundance_{dawn}$ day 2) × 100 / $abundance_{dawn}$ day 2); c) relative cell abundance increase during the day *versus* relative RALS increase during the day on day 2 (% RALS increase = ($RALS_{dusk}$ day 2 – $RALS_{dawn}$ day 2) × 100 / $RALS_{dawn}$ day 2). Circles represent experiment 4 (gyre centre) and triangles represent experiment 5 (gyre border). 36

Figure 2.12. Contribution (%) of the main picoplankton groups relative to total picoplankton abundance (cells ml^{-1}) in the a-b) gyre centre and c-d) gyre border, in a,c) control and b,d) nutrient-enriched treatments..... 37

Figure 2.13. Vertical profiles of *Prochlorococcus* cell abundance, cell-specific RALS and red fluorescence, and the downwelling PAR ($PAR_{(z)}$) measured at noon at a location in the North Atlantic Gyre (16.436^{o} N, 28.405^{o} W). Data collected on AMT24. 43

Figure 3.1. Cruise tracks of AMTs 23 and 24. 48

Figure 3.2. Picoplankton groups individualized in a) unstained samples using the right-angle light scatter (RALS) and red fluorescence, and b) stained samples using RALS and green fluorescence. Round tight clusters represent 0.5µm and 1.0µm fluorescent beads. Figures were created using the Flowing Software® (version 2.5). 50

Figure 3.3. a) Stained vs. unstained *Prochlorococcus* at the top 200 metres of the water column and in b) sub-surface samples (< 20 metres). Grey scale indicates the depth, with lighter points representing shallower depths. 51

Figure 3.4. Relationship between the relative difference between Pro_{st} and Pro_{unst} (*Rdif*) and: a) depth (all samples); b) downwelling irradiance (samples collected during the day); and c) *Prochlorococcus* red fluorescence. The depth is expressed in metres, the downwelling irradiance in W m^{-2} and log(+1) transformed, and the red fluorescence of *Prochlorococcus* cells is calculated relative to the red fluorescence of 0.5µm beads. The grey line shows the linear regression between the two plotted variables..... 52

Figure 3.5. Efficiency of GF/F filters to retain *Prochlorococcus* cells (retention efficiency) across the Atlantic Ocean, on AMT 24. 54

Figure 3.6. Relationships between the efficiency of GF/F filters to retain *Prochlorococcus* cells (retention efficiency) and a) the mean cell right-angle light scatter (RALS) in the sample before filtration, and b) the abundance of *Prochlorococcus* cells in the sample before filtration. 55

Figure 4.1. Relationship between *Prochlorococcus* cell abundance at the sea surface (Pro_{surf}) and: a) sea surface temperature (*SST*), b) remote sensing reflectance at 448 nm ($R_{rs}(488)$) and c) surface chlorophyll concentration on AMTs 12 to 24. The dashed line indicates the chlorophyll threshold used to delineate the subtropical gyres..... 62

Figure 4.2. Transects of the 13 AMT cruises used to create the empirical model to predict the abundance of *Prochlorococcus* cells. 63

Figure 4.3. Flowchart of computations used to calculate the cell abundance of *Prochlorococcus*. Variable acronyms are described in Table 4.4. 65

Figure 4.4. Vertical profiles of observed and estimated *Prochlorococcus* cell abundances a,d,g) over depth and b,e,h) over the fractional PAR *fPAR*, and c,f,i) profiles of temperature and chlorophyll from CTD casts at a site in a-c) the North Atlantic Gyre periphery (NAGP: 28°N, 35°W), d-f) inside the North Atlantic Gyre (NAG: 22°N, 50°W), and g-i) the South Atlantic Gyre (SAG: 20°S,20°W). *In situ* observations are represented by red dots, predicted profiles of *ProI* by the orange dashed line, predicted profiles of *ProII* by the blue dashed line, and predicted profiles of total *Prochlorococcus* abundance by the solid black line. Data from AMT 24 (2014)..... 69

Figure 4.5. a) Comparison between observed attenuation coefficient for photosynthetically active radiation (K_dPAR') from CTD PAR profiles *versus* predicted K_dPAR using equation [4.11] of the present work (red) and using equation [9′] from Morel et al. 2007 (blue); b) Observed and predicted K_dPAR across the Atlantic Ocean (AMTs 20 to 24)..... 70

Figure 4.6. a) Comparison between observed versus predicted depth of the deep chlorophyll maximum (Z_{DCM}) using equation [4.12] of this work; b) Observed and predicted Z_{DCM} across the Atlantic Ocean (AMTs 12 to 24). For each CTD cast, observed Z_{DCM} was determined as the depth of the maximum chlorophyll concentration measured using the CTD fluorometer..... 71

Figure 4.7. Latitudinal section of the Atlantic Ocean, showing profiles of a) the concentration of nitrate and b) the concentration of chlorophyll. Figure c) shows the relationship between the depth of the nutricline (Z_{nut}) and the depth of the deep chlorophyll maximum (Z_{DCM}), where the red line shows the 1:1 relationship, and the blue line shows the linear regression between Z_{nut} and Z_{DCM}. Data for figs. (a) and (b) from AMT 18 (1998), and data for fig. (c) from AMTs 12 to 24, provided by the British Oceanographic Data Centre (BODC). 72

Figure 4.8. Relationship between the depth of the deep chlorophyll maximum (Z_{DCM}) and the sea-surface chlorophyll (*SSChlo*). Black dots show locations where $Z_{DCM} \geq 80$ metres. Data from AMTs 12 to 24, provided by the British Oceanographic Data Centre (BODC)..... 73

Figure 4.9. Vertical profiles of *Prochlorococcus* cell abundance over depth ($Pro_{total(z)}$) a) observed *in situ* on AMTs 12 to 24 ($Pro_{total(z)}$'); b) predicted using the partial model with observed inputs of Pro_{surf} and Z_{DCM} (equations [4.1] to [4.15] excluding equations [4.3-4.5] and [4.12]); and c) predicted using the full model with remote sensing inputs (equations [4.1-4.15]). 77

Figure 4.10. Difference (residual) between predicted and observed *Prochlorococcus* cell abundance over depth ($Pro_{total(z)}$) a) using the partial model partial model where *in-situ* observations of Z_{DCM}, K_dPAR, and Pro_{surf} are used as inputs to calculate $Pro_{total(z)}^{1}$ (excluding equations [4.3-4.5] and [4.12]); and b) using the full model with remote-sensing inputs (equations [4.1] to [4.15]). 77

Figure 4.11. a) Comparison between observed and predicted *Prochlorococcus* cell abundance integrated in the water column (Pro_{int}^{1}) using the partial model where *in-situ* observations of Z_{DCM}, K_dPAR, and Pro_{surf} are used as inputs ($Pro_{total(z)}^{1}$ from equations [4.1] to [4.15] excluding equations [4.3-4.5] and [4.12]); b) Observed and predicted Pro_{int}^{1} across the Atlantic Ocean (AMTs 12 to 24). 78

Figure 4.12. a) Comparison between observed and predicted *Prochlorococcus* cell abundance integrated in the water column (Pro_{int}^{3}) using the complete model (equations [4.1] to [4.15] of the present work); b) Observed and predicted Pro_{int}^{3} across the Atlantic Ocean (AMTs 12 to 24); c) Comparison between observed and predicted *Prochlorococcus* cell abundance at the sea surface (Pro_{surf}) using equations [4.3] to [4.5] of the present work; d) Observed and predicted Pro_{surf} across the Atlantic Ocean (AMTs 12 to 24). 78

Figure 4.13. a) Comparison between observed and predicted *Prochlorococcus* cell abundance integrated in the water column (Pro_{int}) using the one-component model (equations [4.1-4.5] and [4.8-4.15], replacing equation [4.2] with equation [4.18]); b) Observed and predicted Pro_{int} across the Atlantic Ocean using the one-component model (AMT 12 to 24); c) Comparison between observed and predicted Pro_{int} using the two-component model (equations [4.1-4.15]); d) Observed and predicted Pro_{int} across the Atlantic Ocean (AMT 12 to 24) using the two-component model. 81

Figure 4.14. Annual mean of a) the predicted *Prochlorococcus* cell abundance integrated in the top 200 m of the water column (Pro_{int}^{3}) using the complete model (equations [4.1-4.15]); b) predicted maximum *Prochlorococcus* cell abundance at depth (Pro_{max}^{3}) using equation [4.7]; and c) predicted *Prochlorococcus* cell abundance at the sea surface (Pro_{surf}^{3}) from equations [4.1-4.5]. 83

Figure 4.15. Time series of a) global horizontally- and vertically-integrated *Prochlorococcus* cell stocks and c) horizontally-integrated cell abundance near the ocean surface, with corresponding anomalies and trends (b,d). Values were computed using monthly-composite input variables from the year 2002 to 2014 (NASA Ocean Color 2014). Anomalies were calculated by subtracting the monthly climatology (dashed red lines in figures (a) and (c)) from the calculated values for each month (black lines in figs. (a) and (c)). Red lines in figures (b) and (d) show the moving trend. 84

Figure 4.16. Estimated monthly distribution of the *Prochlorococcus* cells integrated in the top 200 m of the water column (Pro_{int}) (cells m^{-2}), with correspondent vertical profiles of estimated *Prochlorococcus* cell abundances (cells l^{-1}) at sites (white dots) in the North Atlantic Gyre (NAG) and South Atlantic Gyre (SAG): *ProI* is indicated by the orange dashed line, *ProII* by the blue dashed line, and the total *Prochlorococcus* abundance by the solid black line. Cell abundances were calculated based on the monthly climatology of environmental variables (NASA 2014). 86

Figure 4.17. Monthly averages of a) the areal extent of the North Atlantic Gyre (NAG) and b) South Atlantic Gyre (SAG); c) the euphotic depth Z_{eu} at the NAG and d) the SAG; e) sea surface temperature *SST* at the NAG and f) the SAG; g) the estimated *Prochlorococcus* cell abundance at the sea surface (Pro_{surf}) at the NAG and h) the SAG; i) *Prochlorococcus* cell abundance at the deep maximum (Pro_{max}) at the NAG and j) the SAG; and k) *Prochlorococcus* cell abundance integrated in the water column (Pro_{int}) at the NAG and l) the SAG. *SST* measurements were taken from monthly satellite composites from Jan./2003 to Dec./2014 (NASA Ocean Color). *Prochlorococcus* cell abundances were computed using monthly-averaged input variables for the years 2003 to 2014, at specific locations inside the Atlantic gyres: NAG: 26°N, 50°W; SAG: 20°S, 20°W. 87

Figure 4.18. Time series of a,g) the estimated *Prochlorococcus* cell abundance integrated in the water column (Pro_{int}), c,i) estimated *Prochlorococcus* cell abundance at the deep maximum (Pro_{max}), and e,k) estimated *Prochlorococcus* cell abundance at surface (Pro_{surf}). All values calculated at (a-f) one location (26°N, 50°W) in the North Atlantic Gyre (NAG), and (g-l) one location (20°S, 20°W) in the South Atlantic Gyre (SAG). Figures on the right side show the time-series anomalies (black bars) and trends (red lines). Anomalies were calculated by subtracting the monthly climatology (dashed red lines in figures on the left side) from the calculated values for each month (black lines in figures on the left side). 88

Figure 5.1. Flowchart of a) the primary production remote sensing algorithm that uses chlorophyll concentration as unit of biomass (Sathyendranath and Platt 1989), and b) the adapted primary production algorithm using cell abundance as biomass unit. ... 100

Figure 5.2. Example of a photosynthesis-irradiance (*PE*) curve for picophytoplankton in the North Atlantic gyre (13.9° N, 33.6° W), with photosynthetic parameters P_m^b (maximum carbon fixation rate per unit of biomass), α^b (initial slope), and E_k (saturating irradiance). Data from Gavin Tilstone (Plymouth Marine Laboratory), collected on AMT22. 102

Figure 5.3. a) Shape of average phytoplankton community PE curves for various Atlantic provinces (MAPPS database). Growth irradiance used in the AMT20 incubations (Hartmann et al. 2014) indicated by dashed line; b) Cell-specific carbon uptake rates (fg C $cell^{-1}$ h^{-1}) by *Prochlorococcus* (Hartmann et al. 2014) in the different oceanic biogeochemical provinces (Longhurst 1998). 105

Figure 5.4. a) Global distribution of the annual carbon fixation by *Prochlorococcus* in the euphotic layer; b) in the upper water column (surface to 45 metres depth), and; c) from 45 to 200 metres. 109

Figure 5.5. Seasonal variability in the carbon fixation rates by *Prochlorococcus* integrated in the water column (mg C m^{-2} d^{-1}) down to the depth of 200 metres, in the a) North Atlantic Gyre (22°N, 50°W), b) South Atlantic Gyre (20°S, 20°W), c) North Pacific Gyre (22°N, 166°W), d) South Pacific Gyre (20°S, 150°W), e) Northern Indian Ocean (2°S, 80°E), and f) Indian Gyre (20°S, 80°E). Light grey indicates values integrated in the upper ocean (0 to 45 metres depth), and dark grey represents carbon fixation integrated in the lower water column (45 to 200 metres deep). 111

Figure 5.6. Estimated monthly distribution of the *Prochlorococcus* carbon uptake integrated in the top 200 m of the water column (mg C m^{-2} d^{-1}). White dots indicate the location of the sites in the North Atlantic Gyre (NAG) and South Atlantic Gyre where data from Fig. 5.5 was taken from. Carbon fixation was calculated based on the monthly climatology of environmental variables (NASA 2014). 112

List of Tables

Table 2.1. Final concentrations of added inorganic nutrients in seawater samples. 27

Table 2.2. Light levels (μE m^{-2} s^{-1}) where bottles were incubated. 28

Table 4.1. AMT Cruises used in this study and corresponding dates. 63

Table 4.2. AMT cruises used to generate models to calculate the light attenuation coefficient K_dPAR, depth of the deep chlorophyll maximum Z_{DCM}, *Prochlorococcus* cell abundance at surface Pro_{surf}, and at the deep maximum Pro_{max}. 63

Table 4.3. Parameters and coefficients used in equations [4.1-4.8] and their standard deviations (σ)..... 64

Table 4.4. List of acronyms used in this chapter (input variables used in the predictive model of *Prochlorococcus* cell abundance). 66

Table 4.5. Response variables with their respective root mean square error (Ψ), bias (δ), centre-root (unbiased) mean square error (Δ), and correlation coefficient (R^2) when compared with *in situ* data from 13 AMT cruises (this work), and the PANGAEA dataset (Buitenhuis et al. 2012). Variable definitions are listed in Table 4.4. 79

Table 4.6. Predicted *Prochlorococcus* standing stock in the oceans, integrated spatially and vertically at each area. Values were computed using equations [4.1-4.15], with monthly climatology products used as input variables (Ocean Color, NASA 2014), then averaged over the year. Pro_{int}^3, Pro_{surf}^3 and Pro_{max}^3 were calculated at specific geographic locations within each Atlantic gyre (coordinates in the table)..... 82

Table 5.1. Compilation of photosynthesis-irradiance curve parameters for *Prochlorococcus*, taken from Bruyant et al. (2005), Hartmann et al. (2014) , Hopkinson et al. (2014) , Li (1994) , Moore and Chisholm (1999) , Partensky et al. (1993) , Shimada et al. (1996). Total phytoplankton E_k data provided by the MAPPS dataset (Bouman et al. 2017). 106

Table 5.2. Annual carbon fixation by *Prochlorococcus* integrated spatially and vertically at each area. Values were computed with monthly climatology products used as input variables (Ocean Color, NASA 2014), then integrated monthly and over the year. The annual mean of the daily carbon fixation was calculated at specific geographic locations within the Atlantic gyres (coordinates in the table). 108

Chapter 1.

Introduction

Phytoplankton is defined as the group of unicellular aquatic free-living photoautotrophic organisms which are unable to move actively against water currents (Boney 1976). These organisms are the main primary producers in the world oceans and, despite accounting for only 1% of the plant biomass on our planet, marine phytoplankton are responsible for approximately 50% of the photosynthesis on Earth (Field et al. 1998). Marine phytoplankton play an important role in the global carbon cycle, assimilating inorganic carbon in the form of carbon dioxide (CO_2) and transforming it into organic matter through photosynthesis. This carbon is supplied to the surface oceans through diffusion from the atmosphere and through respiration by micro- and macro-organisms (Feely et al. 2001), and supports marine food webs as herbivores feed on primary producers. Ultimately, a fraction of this fixed carbon sinks to the deep ocean in a process known as the *biological pump*, where atmospheric carbon is diffused to the surface ocean, then removed from these surface layers through biological activity and stored in the deep ocean (Ducklow et al. 2001; Barker et al. 2003; Richardson and Jackson 2007; Siegel et al. 2014).

Owing to their small size, phytoplankton exhibit high growth rates (cell division) and respond rapidly to changes in physical and chemical properties of water masses (Smayda 1958). Factors like light, temperature, and nutrient availability dictate which taxonomic group or size class inhabits a particular water mass, and fluctuations of these factors are responsible for the temporal, seasonal, and spatial variability in the phytoplankton community structure (Margalef 1968; Winder and Sommer 2012; Striebel et al. 2016).

Phytoplankton cells are conventionally divided into three size classes: micro- (20-200 μm), nano- (2-20 μm) and picophytoplankton (< 2 μm) (Sieburth et al. 1978). Cell size is an important determinant of the physiological response of a cell to environmental forcing. It is widely believed that the nutrient uptake rate by a cell is proportional to the surface-area-to-volume (*s/v*) ratio of this cell, thus smaller cells tend to be favoured in nutrient-depleted waters by their large *s/v* ratio (Legendre and Le Févre 1989). In such oligotrophic areas, nutrient uptake depends on the viscosity of the water (dictated by the water temperature and salinity) and turbulence, which influence nutrient diffusion rates towards the cell's surface (Berg and Purcell 1977; Kiørboe 1993). Therefore, picoplanktonic organisms (cyanobacteria and flagellates) are dominant in central areas of the ocean basins (i.e. subtropical gyres) (**Fig. 1.1a**) where nutrient concentrations are drastically low in the euphotic zone of the water column (Raimbault et al. 2008; Torres-Valdés et al. 2009; Landolfi et al. 2016), hampering the growth of larger phytoplankton cells (Marañón 2014). Conversely, in nutrient-replete environments, large cells are favoured by their faster metabolism and higher growth rates, as the competition for nutrients is sporadic (Marañón 2014). Thus, micro-sized cells (diatoms, dinoflagellates, and some chain-forming cyanobacteria) are most abundant in nutrient-replete areas such as coastal and shelf seas, and nutrient-rich open ocean areas such as the polar oceans (**Fig. 1.1c**) (Brewin et al. 2011). In these areas, microphytoplankton contributes a significant fraction of the total carbon fixation through photosynthesis and total phytoplankton biomass, fuelling marine food webs (Berglund et al. 2007; Marquis et al. 2007; Chen and Liu 2010), in addition to contributing to the carbon burial in the deep ocean when sinking (Ducklow et al. 2001; Moran et al. 2012; Tilstone et al. 2017). The nanoplanktonic constituents of phytoplankton (flagellates, small diatoms and dinoflagellates) form a constant background of phytoplankton biomass, being significantly abundant in all water masses (Li 2007) (**Fig. 1.1b**).

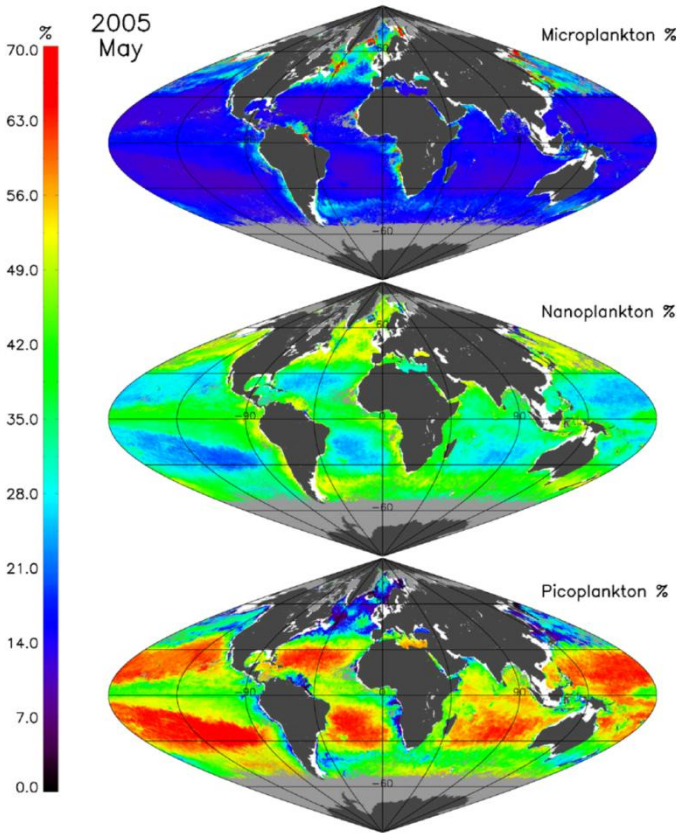


Figure 1.1. Relative contribution of the **a)** micro-, **b)** nano- and **c)** pico-phytoplankton to total phytoplankton biomass in the Atlantic Ocean. Figure from Brewin et al. (2010b).

Due to their global significance to carbon fixation and phytoplankton biomass, this study is focused on the smallest fraction of the phytoplankton community and most abundant phytoplankton on the planet, the picophytoplankton, thus most attention is driven to the warm waters of the ocean gyres and equatorial convergence region of the Atlantic Ocean. With a final goal of understanding the spatial distribution and temporal dynamics of picophytoplankton on a global scale, the cyanobacterium *Prochlorococcus* was chosen as a model organism, and its response to environmental forcing was used to develop algorithms that allow the use of remotely-sensed observables to assess the global distribution and temporal variability of this important phytoplankter, and quantify its global biomass and annual carbon fixation budget.

To elucidate ecology and physiology of these small primary producers, their ecological roles and their importance to biogeochemical cycles, this introductory chapter describes their habitat and its environmental conditions, the taxonomic groups that represent the picophytoplankton size class, and physiological and ecological strategies used by these taxonomic groups to thrive in extreme light and nutrient conditions. As the remote-sensing algorithms developed in this thesis were focused on *Prochlorococcus*, this chapter also explores the biogeochemical and ecological importance as well as the physiological characteristics of this cyanobacterium in more detail.

1.1 Study area

The marine Trade Biome is defined as the region of the oceans governed by trade winds. These regions are characterized by a positive heat flux from the atmosphere to the surface ocean that implies very low input of kinetic energy in the water column, increasing stability, with a permanent thermocline that shows little seasonal oscillation compared to other oceanic biomes (Longhurst 1998). The Trade Biome ranges from tropical waters near the Equatorial Convergence Zone (ECZ) to subtropical regions that include the subtropical gyres (**Fig. 1.2**), located roughly between the latitudes of 10^{o} and 30^{o}, both North and South.

Subtropical gyres (**Fig. 1.2**) are the largest oceanic ecosystems on our planet (Longhurst 1998; Karl 1999; Hirata et al. 2008), accounting for ~50% of the world ocean's surface area. In the central subtropical gyres, extreme high-light conditions hamper phytoplankton growth at the sea surface and lead to very low intracellular pigment concentrations (Westberry et al. 2008; Behrenfeld et al. 2015). Because of the low chlorophyll observed at the sea surface, subtropical gyres were considered to be oceanic deserts until the early 1980s.

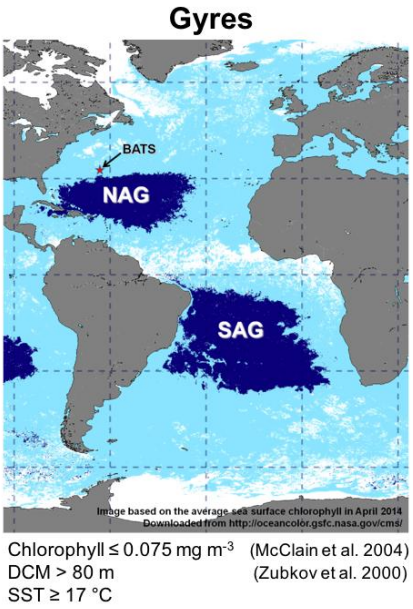


Figure 1.2. Subtropical gyres of the Atlantic Ocean. This figure was generated based on a sea surface chlorophyll (*SSChlo*) image, where subtropical gyres are determined as areas where $SSChlo < 0.075$ mg m^{-3}.

The water column of the gyres is strongly structured vertically due to the large volume of warm water trapped in the surface 150 metres (**Fig. 1.3a**). The surface warm water leads to strong stratification, which decreases the transport of nutrients from deep waters to the euphotic zone, making surface waters nutrient-depleted (oligotrophic) (**Fig. 1.3b**). As a consequence, a deep chlorophyll maximum (DCM) is formed in the region where nutrients are available and light is still sufficient to support photosynthesis and, consequently, phytoplankton and growth (Cullen 1982; Aiken et al. 2016). The DCM is formed because phytoplankton attain net growth which leads to an accumulation of phytoplankton biomass, and because these cells that live under extreme low light conditions increase their intracellular pigment concentration to be able to absorb sufficient light for photosynthesis (Cullen 1982; Behrenfeld et al. 2015). The DCM occurs at a depth that varies between 60 and 130 meters (**Fig. 1.3c**), and can account for up to 43% of the integrated primary production at locations inside the subtropical gyres (Karl et al. 2001; Pérez et al. 2006). In the Atlantic gyres, picophytoplankton represent up to 76% of total chlorophyll-*a* concentration in the DCM and > 60% in surface waters (Pérez et al. 2006).

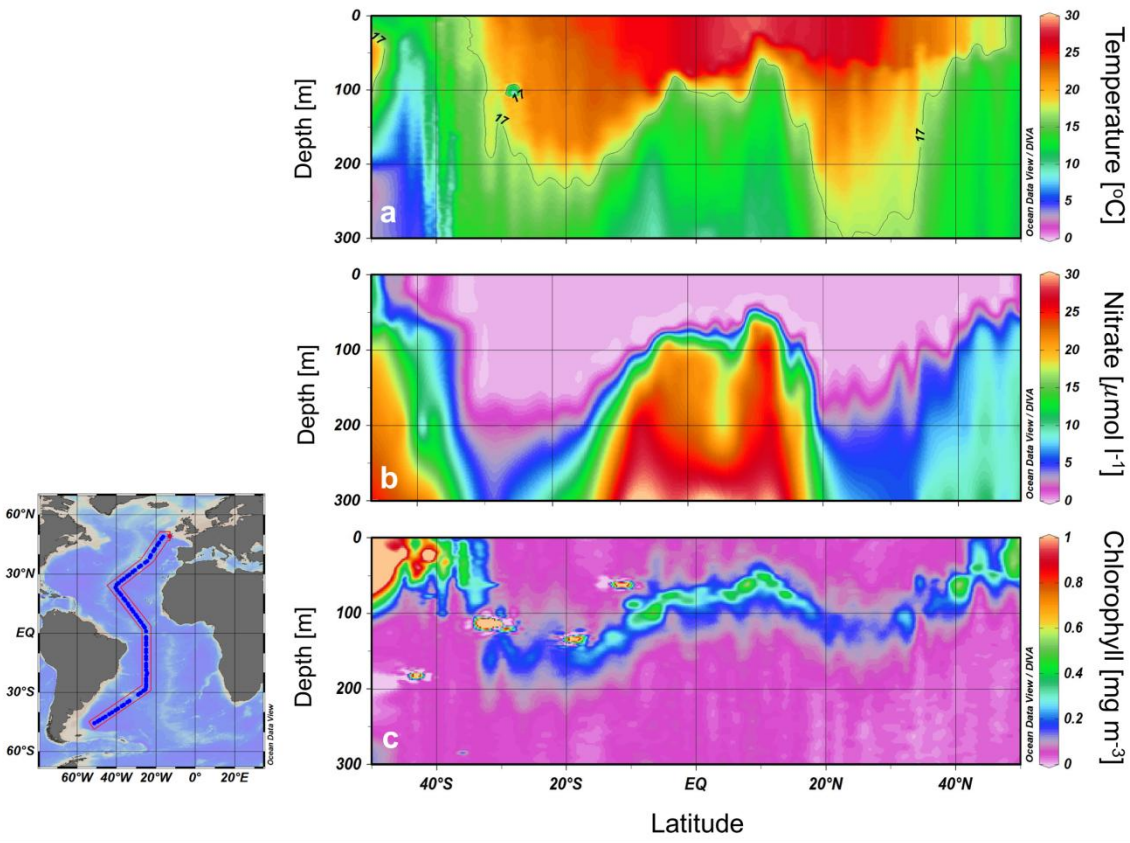


Figure 1.3. Vertical profiles of **a)** temperature, **b)** nitrate, and **c)** chlorophyll concentration across the Atlantic Ocean. Map shows the transect where measurements were taken. Data from the oceanographic expedition Atlantic Meridional Transect 22 (AMT22, September-November 2012).

In the late 1980s, the use of shipboard flow cytometry adapted to study small phytoplankton cells allowed Chisholm, Olson, Waterbury and colleagues to describe and quantify two ubiquitous species of marine phytoplankton that were so small that they could not be observed using traditional microscopy, but more abundant than any other photosynthetic organism in the oceans: the cyanobacteria *Prochlorococcus* (Chisholm et al. 1988) and *Synechococcus* (Waterbury et al. 1986). Flow cytometry also allowed scientists to better explore an important multi-taxonomic group of eukaryotic picophytoplankton (Kirkham et al. 2011, 2013). The flow-cytometric assessment of picoplankton community increased the accuracy of biomass estimates and the analysis of the contribution of different taxonomic groups to phytoplankton primary production, especially in oligotrophic areas

where these cells are dominant among primary producers. By then, the scientific community started to realize that the ecological and biogeochemical importance of the subtropical gyres was greater than previously thought.

1.2 Picophytoplankton groups

Picophytoplankton is composed of three functional groups: the cyanobacteria *Prochlorococcus* and *Synechococcus*, and several eukaryotic taxa such as haptophytes, prymnesiophytes and prasinophytes denominated collectively as photoautotrophic picoeukaryotes (PPE) (Tarran et al. 2006; Grob et al. 2011; Kirkham et al. 2011).

Prochlorococcus and *Synechococcus* constitute a significant fraction of the total biomass in the oligotrophic ocean, in particular in subtropical gyres (Partensky and Garczarek 2010; Zhang et al. 2008) (**Fig. 1.4a,b**), whereas photosynthetic picoeukaryotes are a diverse and cosmopolitan group that have been shown to replace their cyanobacterial counterparts in polar seas, in addition to represent an important amount of biomass at the DCM in subtropical waters (Tarran et al. 2006; Li 2007; Kirkham et al. 2011) (**Fig. 1.4c**): At the deepest DCMs of subtropical gyres, *Prochlorococcus* is dominant, beneath which a mixed assemblage of picoeukaryotes is found (Kirkham et al. 2011; Tarran et al. 2006; Veldhuis and Kraay 2004; Zubkov et al. 1998; Zubkov et al. 2000a). Surface waters are inhabited mostly by the cyanobacterium *Prochlorococcus* in the central region of the subtropical gyres, whereas the contribution of *Synechococcus* and picoeukaryotes sharply increases at the gyres' periphery as the availability of nutrients progressively increases (Bouman et al. 2011; Mouriño-Carballido et al. 2016; Zubkov et al. 2000a).

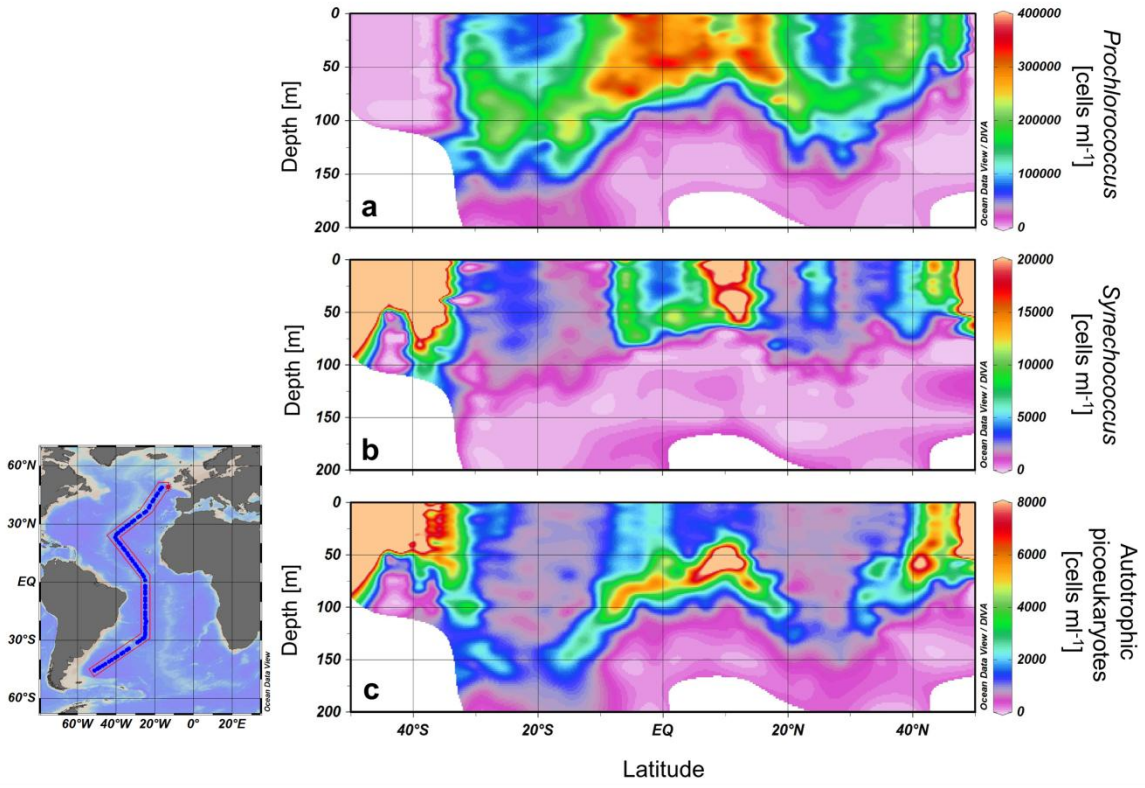


Figure 1.4. Vertical profiles of *Prochlorococcus*, *Synechococcus*, and picoeukaryotes across the Atlantic Ocean. Map shows the transect where measurements were taken. Data from AMT 22 (2012).

The discovery of picocyanobacteria is relatively recent (Waterbury et al. 1979, 1986; Chisholm et al. 1988) and, due to their importance to the global primary production and ocean biogeochemical processes, studies on their physiology, ecology and genomics are progressively increasing (Scanlan and West 2002; Partensky and Garczarek 2010).

Synechococcus (**Fig. 1.5**) inhabits tropical and temperate waters, being most representative in the periphery of subtropical gyres, where the water column becomes slightly less stratified than in the inner gyres (Zubkov et al. 2000b; Heywood et al. 2006). *Synechococcus* cells contain high concentrations of phycoerythrin, a light-harvesting

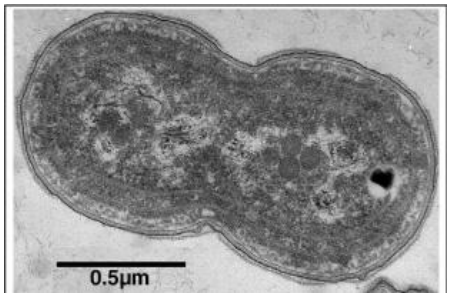


Figure 1.5. Image of a cell of *Synechococcus* sp.. Credit: http://www.whoi.edu/science/B/people/ewebb/Syne.html

phycobiliprotein that assists in the energy acquisition for photosynthesis (Wyman et al. 1985; Shukla et al. 2012) and makes these cells easily detectable using flow cytometry due to its unique orange fluorescence (Olson et al. 1990). This pigment is characteristic for its efficiency to absorb blue and green light, which allows *Synechococcus* to take advantage of the energy in a light spectral band that is weakly absorbed by other phytoplankton (Sathyendranath and Platt 2007; Stomp et al. 2007; Hickman et al. 2009).

1.2.1 *Prochlorococcus: the model organism of this study*

Prochlorococcus (**Fig. 1.6**) are the smallest known photoautotrophic prokaryotic phytoplankton on the planet, having a DNA average size of 0.6 to 0.8 Am (Veldhuis et al. 2005), which approaches the minimum size necessary to maintain a living cell (considering the number of genes coding the minimal amount of essential proteins) (Raven 1994). *Prochlorococcus* exists in a variety of ecotypes (i.e. populations of the same species which have parts of the genome that are unique to that population), which share approximately 1,000 core genes and present a diverse combination of 'flexible' genes that allow them to better acclimate to different light levels and uptake distinct forms of nutrients (Biller et al. 2014a). When all *Prochlorococcus* ecotypes are combined, the number of described genes to date approaches 13,000 (Biller et al. 2014a), but model projections estimate a pan-genome of more than 84,000 genes (Urbach et al. 1992; Kettler et al. 2007), which is four times the size of the human genome.

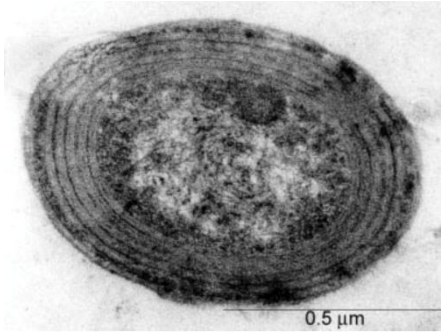


Figure 1.6. Image of a *Prochlorococcus* sp. cell (Bryant 2003).

The average abundance of *Prochlorococcus* cells in subtropical and tropical waters (Heywood et al. 2006; Rabouille et al. 2007; Malmstrom et al. 2010; Bouman et al. 2011) is in the same order of magnitude of most phytoplankton blooms where a single species of alga typically reaches cell abundances of 10^4 to 10^5 cells ml^{-1} (Smayda 1997). However, due to the small size of *Prochlorococcus* cells and its consequent low intracellular carbon content of 50 fg C $cell^{-1}$ (Bertilsson et al. 2003), *Prochlorococcus* actually contributes a much lower biomass than blooms of other phytoplankton with cell abundances in the same order of magnitude. On the other hand, *Prochlorococcus* is ubiquitous in an extensive area of the globe that ranges from the latitude of 40°N to 40°S (Partensky et al. 1999), being the dominant phytoplankton in oligotrophic waters, which makes them the most numerically abundant photosynthetic organism on Earth (Karl 1999; Longhurst 1998). Thus, despite its reduced cell size and intracellular carbon content, biomass estimates escalate when global budgets are considered: previous estimates of their global biomass are in the order of 10^{27} cells representing 180 Mt C (Williams and Follows 2011; Flombaum et al. 2013), which is more than any other phytoplankton species in the world's oceans.

Prochlorococcus occurs in warm waters (> 13 °C) with strong thermal stratification (Zubkov et al. 2000b; Schauer et al. 2003; Rabouille et al. 2007; Zinser et al. 2007; Malmstrom et al. 2010; Šantić et al. 2011; Bouman et al. 2011) and limited availability of nutrients. To grow in such oligotrophic conditions, different *Prochlorococcus* strains can utilize not only nitrate (Berube et al. 2015), but also other forms of nitrogen such as urea, ammonia (Moore et al. 2002), amino-acids and other organic forms (Zubkov et al. 2003; Gómez-Pereira et al. 2013), besides their ability to uptake organic phosphorus as an alternative phosphorus source (Rippka et al. 2000; Casey et al. 2016). The assimilation of organic compounds utilizes the energy of light in a process called *photoheterotrophy* (Zubkov 2009), which also occurs in some heterotrophic bacteria that inhabit subtropical

waters such as *SAR11* (Gómez-Pereira et al. 2013). Thus, *Prochlorococcus* utilizes light energy not only to uptake carbon dioxide through photosynthesis, but also to metabolize organic nutrients.

Taking light dependency into account, *Prochlorococcus* can cope with extreme light conditions, and inhabits a wide depth range: from the sea surface to the bottom of the photic zone, which may extend down to 200 metres (Johnson 2006; Karl 1999; Zubkov et al. 2000a). Despite the presence of potentially damaging UV and visible radiation, *Prochlorococcus* cells are frequently most abundant at the sea surface. In regions where surface chlorophyll concentrations are extremely low such as the central area of subtropical gyres, cell abundance can slightly increase with depth and peak a few metres above the DCM (Zubkov et al. 1998b; Heywood et al. 2006; Rabouille et al. 2007; Mella-Flores et al. 2012; Buitenhuis et al. 2012).

The ability of *Prochlorococcus* cells to grow in extreme high and low light conditions is in part supported by their particular array of intracellular pigments, which includes unique photosynthetic pigments, the divinyl derivatives of chlorophylls *a* and *b* (Chisholm et al. 1992; Goericke and Repeta 1993), and the photoprotective pigment zeaxanthin. *Prochlorococcus* also possesses a different light harvesting chlorophyll antenna, with a distinct form of phycoerythrin, whereas other phycobilins are absent, making the phycobilisomes incomplete (Steglich et al. 2003). Despite lacking phycobilisomes, *Prochlorococcus* cells are able to synthesize different types of phycoerythrin, which is an efficient adaptation to extreme light conditions: high-light adapted ecotypes synthesize phycoerythrin with only the alpha-subunit, whereas low-light strains possess phycoerythrin with both an alpha- and a beta-subunit (Wiethaus et al. 2010). The lower complexity of the photosystem II allowing a rapid degradation and replacement of the phycobilisomes is a strong adaptation to the extreme light conditions present in subtropical gyres, where the

mixed-layer depth is deep and light intensity is very high in surface waters (Hartmann et al. 2014).

For that reason, *Prochlorococcus* ecotypes are collectively grouped in two main types: high light-adapted (HL) and low light-adapted ecotypes (LL) (West and Scanlan 1999; Johnson et al. 2006). As examples of light adaptation, cells of HL *Prochlorococcus* ecotypes are smaller and become very transparent when subjected to extremely high light, with such small pigment content being below the detectable limit of most fluorometers. Conversely, cells of LL *Prochlorococcus* ecotypes are larger and contain a high pigment per cell concentration and natural fluorescence (Moore and Chisholm 1999; Bruyant et al. 2005). Additionally, it has been observed that, within an ecotype, cells can quickly change their intracellular photosynthetic pigment concentrations, fluorescence properties and photosynthetic rates in order to adapt to different light levels, and these changes are sometimes larger than the differences observed between HL and LL ecotypes (Moore and Chisholm 1999).

1.2.2 *The role of Prochlorococcus in marine biogeochemical cycles*

Prochlorococcus was first believed to play a minor role in the biogeochemical cycling of elements due to their small cell size, which implies low contribution to carbon export (carbon sink), combined with low rates of nutrient and carbon assimilation estimated based on cell division rates (Williams and Follows 2011). However, recent findings show that the biogeochemical significance of this small cyanobacterium has been underestimated. Measurements of cell-specific carbon fixation (Hartmann et al. 2014) and uptake of nutrients such as nitrate, phosphate and organic molecules with nitrogen and phosphorus (Berube et al. 2015; Mary et al. 2008a, 2008b; ; Zubkov et al. 2004; Zubkov and Tarran

2005) show significant rates of assimilation of these elements. In turn, it has been reported that microbial mixotrophs and heterotrophic eukaryotes graze on *Prochlorococcus* cells (Hartmann et al. 2013), transmitting the assimilated energy and nutrients to diverse levels of the food web. Additionally, agglomerates in collagenous material containing a relevant amount of *Prochlorococcus* biomass have been shown to contribute significantly to carbon export from the euphotic zone to deeper layers of the water column (Richardson and Jackson 2007; Johnson and Lin 2009; Lomas and Moran 2011).

Another important feature of *Prochlorococcus* cells is the production of lipid vesicles that contain genetic material (DNA and RNA) and proteins. These vesicles are abundant in the marine environment and protect *Prochlorococcus* cells from phage infections (Biller et al. 2014b). They are also reported to stimulate the growth of heterotrophic bacteria, showing this can have an important protective role for microbial communities against viruses or be an important pathway of nutrients between different microbial niches (Biller et al. 2014b). In addition, *Prochlorococcus* excretes a variety of proteins (lanthipeptides) called *prochlorosins*, of which the ecological function is still unknown, and sugars such as glycolate, which are assimilated by some heterotrophic bacteria (Cubillos-ruiz et al. 2017). These bacteria, in turn, are able to scavenge and metabolize toxic reactive oxygen species, an ability that *Prochlorococcus* lacks (Morris et al. 2011). Because of this cooperative relationship between *Prochlorococcus* and some heterotrophic bacteria (Morris et al. 2008), each having its biochemical role in the environment, cultures of *Prochlorococcus* are rarely axenic since the growth of *Prochlorococcus* cells is facilitated by the presence of some specific heterotrophic bacteria that occur in the natural environment, such as *SAR11* (Biller et al. 2014a).

1.3 Picoplankton enumeration using flow cytometry

The first picophytoplanktonic species, a photosynthetic picoeukaryote, was described in the 1950s (Butcher 1952) using an optical fluorescence microscope, which can detect the fluorescence emitted by algal photosynthetic pigments when illuminated by an ultra-violet lamp (Renz 2013). Epifluorescence microscopy was extensively used to quantify pico- and nano-phytoplankton cells until the 1990s.

Flow cytometers were initially developed for the clinical analysis of blood cells, and became popular in the late 1970s, allowing not only improvements in clinical analyses but also new insights on the composition of marine microbial communities (Waterbury et al. 1979). Ten years later, an improved flow cytometric technique (Olson et al. 1993) allowed the discovery of the smallest picophytoplankton species (Chisholm et al. 1988; Waterbury et al. 1986), which were confirmed by electron microscopy. Since then, flow cytometric counts of picophytoplankton abundance became increasingly popular and are now routinely included as core measurements in international oceanographic programmes. This is due in part to the recognition of the importance of picophytoplankton in global biogeochemical cycles and to the speed, accuracy and ease of the sample processing (Vaulot et al. 2008).

A flow cytometer is composed of a *flow cell* that hydrodynamically focuses particles (cells) to flow in single file through a volume illuminated by a laser beam or a beam of another strong light source (**Fig. 1.7b**). When illuminated, the particle scatters light which is directed to different sensors: the light scattered forward is detected by a sensor of forward light scatter; the light scattered laterally at 90^{o} is detected by a right-angle light scatter (RALS) sensor, and colour-filtered before reaching sensors that detect the light emitted in specific wavelengths. The instrument used in this study was equipped with sensors for red (light fluoresced by chlorophyll and divinyl-chlorophyll molecules), green,

and orange light (fluorescence of the pigment phycoerythrin in *Synechococcus* cells) (**Fig. 1.7a**) (Shapiro 2003).

Considering cells of each phytoplankton species emit a unique combination of fluorescence and RALS signals when illuminated by UV light, it is possible to identify different phytoplankton groups. The computer coupled to the flow cytometer processes the data and returns plots on demand that can combine any of the measured optical signals. Typically, picophytoplankton groups are identified using the combination of RALS and red fluorescence, which distinguishes autotrophic from heterotrophic cells, and discriminates different phytoplankton groups due to their differences in RALS and red fluorescence (**Fig. 1.8**). Other combinations can be used such as orange fluorescence and red fluorescence, which discriminates *Synechococcus* cells from the rest of the phytoplankton community. More information on flow cytometric techniques can be found in **Chapter 1**.

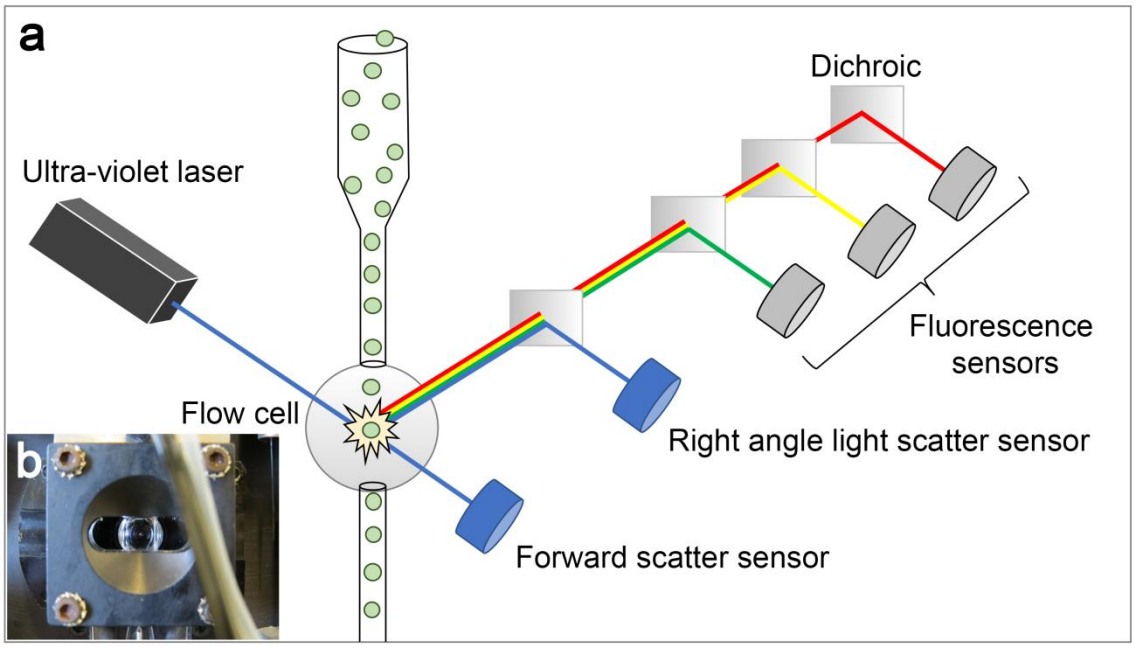


Figure 1.7. a) Schematic view of the light path and mechanisms to detect optical signals emitted by a particle when being analysed in a flow cytometer (adapted from Shapiro (2003)); **b)** The flow cell of a flow cytometer.

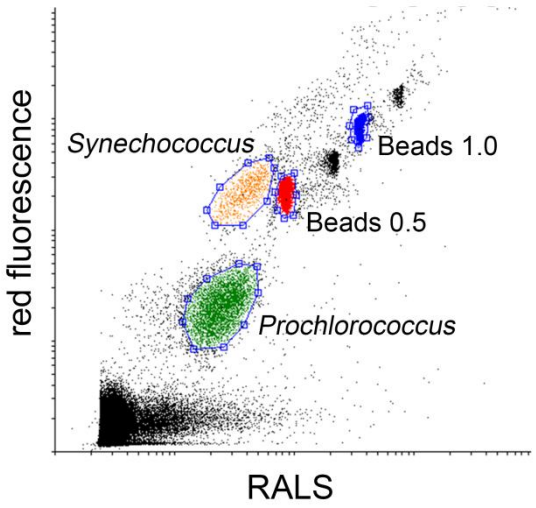


Figure 1.8. Picophytoplankton groups individualized in sea water samples using the right-angle light scatter (RALS) and red fluorescence. Round tight clusters are formed by 0.5µm and 1.0µm fluorescent beads and their respective bead duplets. Figure was created using Flowing Software® (version 2.5).

Flow cytometry significantly improved the analysis of picoplankton communities, and reduced drastically the time of processing, allowing sample analysis shortly after collected. This brought important advances in studies of the ecology and physiology of these microorganisms.

1.4 Remote-sensing models: a tool for global phytoplankton estimates

Although the quantification of picoplanktonic cells by flow cytometry has increased our understanding of the contribution of this phytoplankton size-fraction to the total phytoplankton biomass in the global ocean, especially in the subtropical gyres, data coverage in these vast and remote oligotrophic areas remains poor. Optical sensors mounted on earth-orbiting satellites provide a synoptic view of the global distribution of environmental variables such as sea surface temperature, reflectance of light at various wavebands (remote sensing reflectance, R_{rs}), and the photosynthetically active radiation

(visible light) incident on the sea surface (Ocean Color, NASA 2014). However, the observed signals come from the sea surface and thus these sensors are blind to changes in the physical and biological properties of the ocean beneath the first tens of metres (Gordon and Morel 1983). To obtain a three-dimensional view of the ocean environment, ARGO floats and ocean gliders equipped with sensors of temperature, salinity, and pressure (which determines depth) provide important information on the vertical structure of the water column (Hosoda et al. 2008).

Remote-sensing data can be used in mathematical models, which in turn are constructed and applied to describe the dynamics of the marine ecosystem. Much interest at present is concerned with the autotrophic element of ecosystem models, specifically with the question of how much detail is desirable in the description of phytoplankton properties. Various international groups of modellers have partitioned the autotrophic component of ecosystem models based on the explicit biogeochemical role of certain phytoplankton taxa and the distinct physiological, environmental and nutrient requirements that they appear to possess. This has led to the division of the autotrophic pool into so-called Phytoplankton Functional Types (PFTs) (Le Quéré et al. 2005). Models are also extensively used to estimate the biomass of different phytoplankton groups PFTs (Nair et al. 2008) and size-fractions (Brewin et al. 2010b; Brewin et al. 2014; Roy et al. 2017) using remote-sensing observables.

In addition to semi-analytical techniques that use the light absorption and backscatter by suspended particles in the water column to distinguish phytoplankton functional types and size classes (Sathyendranath et al. 2004; Nair et al. 2008; Roy et al. 2017), recent empirical studies have used relationships between environmental variables detected from satellite (i.e. sea surface temperature, chlorophyll, reflectance) and flow cytometric cell abundance counts, diagnostic pigments, and phytoplankton absorption to determine the

global distribution and temporal variability of picophytoplankton (Uitz et al. 2008, 2010; Brewin et al. 2011) and the functional groups *Prochlorococcus* and *Synechococcus* (Li 2002; Flombaum et al. 2013). In these studies, light is an important factor governing the vertical structure from the level of species to ecotypes (Hickman et al. 2009; Kletou and Hall-Spencer 2010). For example, the chlorophyll biomass of different phytoplankton size classes was determined using satellite models based on relationships between remote-sensing observables and pigments measured *in situ* using different techniques, such as size-fractionated filtration for the determination of size-partitioned chlorophyll (Brewin et al. 2013, 2014), or diagnostic pigments for different phytoplankton taxa, which are dominant in each phytoplankton size-class, measured using High Performance Liquid Chromatohraphy (Uitz et al. 2010). Size-fractionated filtration can be aggressive to the most delicate cells (e.g. cyanobacteria) causing the rupture of cell membranes, which could lead to underestimates of the biomass of the pico-fraction of phytoplankton. On the other hand, the use of diagnostic pigments to estimate the chlorophyll biomass of different size classes can be inappropriate in some environments because the taxa that dominates a determined size class can vary. As an example, picoeukaryotes can be the dominant picophytoplankton in some areas, but this method considers that only taxa containing divinyl-chlorophylls (i.e. picocyanobacteria) belong to the pico-fraction, thus the measured biomass in such an area would be attributed to the nano-fraction of phytoplankton. Advantages, disadvantages, and the uncertainty of these types of models are associated with the environment being investigated, with each model being more appropriate to certain environmental conditions (Brewin et al. 2013).

Nevertheless, the use of species-specific cell counts (e.g. using microscopy or flow cytometry) to develop empirical models has the advantage of an increased precision of the *in-situ* quantification of the target species, decreasing the uncertainty of the model.

Regarding picophytoplankton groups, an empirical model has been developed to estimate the abundance of cyanobacterial cells using satellites (Flombaum et al. 2013). However, this model is based on some assumptions that neglect changes in cell abundance at depth, distorting the vertical and horizontal cell distributions, as assessed in **Chapter 4**. Developing a robust way of extrapolating field-based measurements of picophytoplankton abundance and biomass in an operational way using remote sensing will aid in our assessment of the spatial and temporal dynamics of these key members of marine ecosystems and allow us to estimate their contribution to the global carbon cycle.

1.5 *In-situ* observations: The Atlantic Meridional Transect

The Atlantic Meridional Transect (AMT) is an international oceanographic program founded and funded by NERC, with the objective of surveying and studying remote regions of the Atlantic Ocean such as the subtropical waters (Aiken et al. 2016). Created in 1995, the AMT is mostly focused on plankton studies, but research conducted on board of AMT cruises also include oceanic and atmospheric chemistry, and physical processes in the surface ocean. The AMT has generated more than 300 publications, most of which have high impact to the knowledge of the functioning and biogeochemical cycles of the different marine biomes in the Atlantic, including subtropical oligotrophic zones and productive upwelling regions (more information on www.amt-uk.org).

The AMT dataset covers a broad spatial range of the Atlantic Ocean (**Fig. 1.9**), providing a 22-year time-series of information of physicochemical properties of the surface ocean such as temperature, salinity, pigments and nutrients, and of a variety of planktonic organisms that occupy various niches of the marine food web, from bacteria to macrozooplankton. This dataset was the primary source of information for the present study, allowing an interdisciplinary assessment of the ecology and biogeochemical role of the target organisms, picophytoplankton, in the Atlantic Ocean.

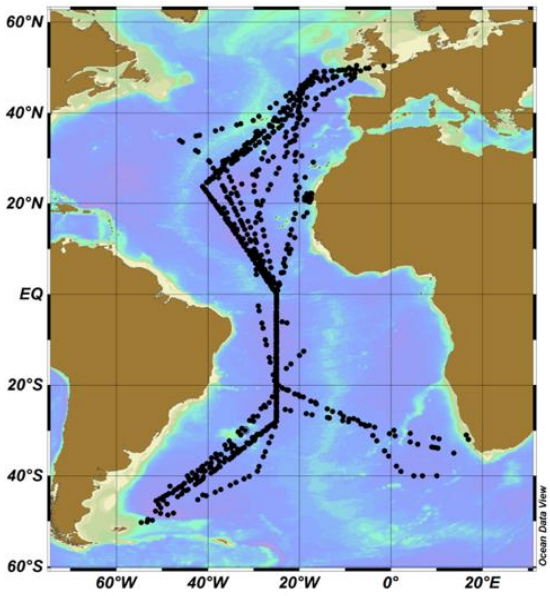


Figure 1.9. Transects of the 13 AMT cruises used to create the empirical model to predict the abundance of *Prochlorococcus* cells.

1.6 Objectives

Oceanic gyres cover a vast area of the global ocean, and the small picoplanktonic organisms that dominate these areas are collectively believed to be significant contributors to marine primary production (Brewin et al. 2010a, 2017; Roy et al. 2017), the carbon pump (Johnson and Lin 2009) and energy input to the marine food web (Williams and Follows 2011; Hartmann et al. 2013). Yet, most of the generalizations on the relative importance of these marine microbes in terms of biomass and primary production are based on discrete measurements, and the understanding of their contribution to the carbon cycle on basin to global scales is still poorly constrained.

This study aims to assess the ecological and physiological response of the smallest and most abundant phytoplankton, the picophytoplankton, to environmental forcing, and use this information to create an empirical model using Earth observables (satellite and ARGO data) to predict the contribution of our model organism, the cyanobacterium *Prochlorococcus*, to the global phytoplankton biomass and carbon fixation. Using this approach, the distribution and biomass of *Prochlorococcus* can be assessed on a global scale, allowing the investigation of temporal and spatial changes in the distribution in response to climate variations. The specific objectives of the thesis are as follows:

1) To understand how major environmental factors (light and nutrients) influence the growth and physiological response of pico-cyanobacteria;

2) To assess potential bias in cell counts of surface populations of *Prochlorococcus* using cruise data from conventional flow cytometric analysis, with the aim of constructing a robust database of picophytoplankton abundance;

3) To derive a robust and quantitative algorithm to predict the vertical profile of the abundance and biomass of our model picophytoplankton taxon, the cyanobacterium *Prochlorococcus*, using remote-sensing observations; to test the algorithm using independent datasets; and to estimate the global distribution of *Prochlorococcus* cells using ocean-colour time-series from the MODIS satellite sensors.

4) To estimate the contribution of *Prochlorococcus* to global phytoplankton carbon fixation using remote-sensing observables, carbon fixation rates measured *in situ*, and the cell abundance distribution maps generated by the previous model.

This work not only provides the oceanographic community with a powerful new satellite product but also allows the examination of the phenology of an important component of the marine picophytoplankton during a period of climate change.

Chapter 2.

The influence of light and nutrients on the growth of picocyanobacteria: insights on iron-induced growth inhibition of *Prochlorococcus* cells

2.1 Introduction

Light and nutrients govern phytoplankton growth in the oceans (Kirk 2011). In subtropical gyres, extreme conditions of high light and low nutrients caused by the high stratification of the water column lead to the prevalence of the pico- fraction amongst primary producers (Zubkov et al. 2000b; Partensky and Garczarek 2010). The marine microbial community is dominated by prokaryotes, with the heterotrophic fraction represented mainly by the alphaproteobacterium *SAR11* (Morris et al. 2002). Photosynthetic constituents are composed by the cyanobacteria *Prochlorococcus* and *Synechococcus* (Zubkov et al. 2000b; Heywood et al. 2006; Zhang et al. 2008; Partensky and Garczarek 2010), with an increase in the contribution of picoeukaryotes at the deep chlorophyll maximum (Zubkov et al. 1998b, 2000b; Tarran et al. 2006; Kirkham et al. 2011).

The dominance of *Prochlorococcus* in such extensive areas makes them the most numerically abundant photosynthetic organism on Earth (Longhurst 1998; Karl 1999), thanks to their ability to adapt to extreme conditions of light and low nutrients provided by the genetic plasticity and genome simplicity of the different *Prochlorococcus* ecotypes (Biller et al. 2014a). *Synechococcus* inhabits tropical and temperate waters, being most representative in the periphery of subtropical gyres, where the water column becomes slightly less stratified than in the inner gyres (Zubkov et al. 1998b; Heywood et al. 2006).

Both natural populations and cultured strains of *Prochlorococcus* and *Synechococcus* present a fairly synchronized diel cell cycle, with cell growth occurring during the light period, followed by cell division at night (Vaulot et al. 1995; Zubkov et al. 2000a; Lefort and Gasol 2014). This diel cell cycle is related to changes in cell metabolism and corresponding marked diel variations in the optical properties of these cells. Flow cytometers measure the cell specific forward- and right-angle light scatter (FALS and RALS, respectively), which are often associated with cell size in ecological studies of pico- and small nano-plankton groups (DuRand and Olson 1998; Mann and Chisholm 2000; Jacquet et al. 2001; Claustre et al. 2002; Bruyant et al. 2005; Lin et al. 2013). However, it has been shown that changes in the cell's refractive index, which in turn is a function of the cell's chemical composition, may be equally important to explaining the diel variability in FALS and RALS (Stramski and Morel 1990; Stramski and Reynolds 1993; Stramski et al. 1995; DuRand et al. 2002).

Cell-specific red fluorescence, which is also measured by flow cytometers, is a broadly used proxy for chlorophyll *a* and divinyl-chlorophyll *a* contents (Roy et al. 2013) because chlorophyll molecules emit part of the absorbed light in the form of a "red photon", and most of the red fluorescence in natural waters is provided by chlorophyll molecules (Huot and Babin 2010). In turn, the concentrations of chlorophyll *a* and its derivative divinyl chlorophyll *a* are used as an indicator of phytoplankton biomass, as all phytoplankton cells possess one of these important photosynthetic pigments. Chlorophyll fluorescence is also influenced by other factors such as non-photochemical quenching (NPQ): when light levels are high, phytoplankton cells deviate the excess absorbed energy to cellular components other than chlorophyll (e.g. photoprotective pigments that dissipate absorbed light energy as heat). This leads to lower red fluorescence per unit chlorophyll molecule, and consequently less energy is left to support photosynthesis (Raven 2011; Roesler and

Barnard 2013). Since NPQ occurs at high light, and phytoplankton cells tend to synthesize more pigments to improve their light harvesting capacity at low light (Raven 2011), red fluorescence per cell is expected to increase as light decreases.

As phytoplankton synthesize more photosynthetic pigments, it requires more iron. Iron is a key limiting element for photosynthesis (Moore et al. 2013), being present in light harvesting and electron transport units such as the photosystems I and II (PSI and PSII, respectively), cytochrome-b_6f, and ferredoxin molecules (Briat et al. 2015). *Prochlorococcus* possesses genes related to iron scavenging and storage (Morrissey and Bowler 2012), being able to store 2 to 4 times more iron than required for its daily metabolic activities (Shire and Kustka 2015), although the adaptations of HL *Prochlorococcus* to iron depletion vary among ecotypes (Rusch et al. 2010). Primary production also relies on the ability of photosynthetic cells to control the intracellular Fe homeostasis (Marchetti et al. 2009) which, in turn, regulates the photosynthetic and general metabolic circadian cycles in many photosynthetic organisms (Tissot et al. 2014; Briat et al. 2015). When photosynthetic electron fluxes are high (i.e. in high-light conditions), cyanobacteria use a number of alternative electron transport pathways (Lea-Smith et al. 2016), and primary production is limited by the activity of other enzymes, mainly the ones involved in the Calvin cycle such as the carbon-fixing catalyst ribulose-1,5-bisphosphate carboxylase/oxygenaseas (RuBisCO) (Berepiki et al. 2016).

As light and nutrients are important for the cell growth cycle, the lack or excess of light and/or nutrient supply over the day will result in changes in cell growth and abundance over time. For example, iron fertilization increased growth and cell division rates of *Prochlorococcus* in the Equatorial Pacific (Mann and Chisholm 2000), but the combined effect of excess iron availability under different light conditions has not yet been assessed. Microbial metabolic rates are also highly influenced by light. In the Atlantic and

Pacific Oceans, light availability has been demonstrated to stimulate amino-acid uptake rates by photoautotrophic (i.e. *Prochlorococcus*, *Synechococcus*) and photoheterotrophic organisms (i.e. SAR11, low nucleic-acid (LNA) bacteria) when compared to dark incubations (Church et al. 2004; Mary et al. 2008b; Gómez-Pereira et al. 2013).

The combined effect of light and nutrient availability on cyanobacterial populations is reflected in the observed seasonal variability of *Prochlorococcus* and *Synechococcus* in the Atlantic subtropical gyres, with higher abundances occurring in spring/summer, and lower during autumn (Zubkov et al. 2000b; DuRand et al. 2001). This seasonality has an apparent link with changes in the gyre surface area, which varies with the seasonality of the light regime and variations in horizontal and vertical nutrient fluxes (Polovina et al. 2008).

In order to understand the combined effect of nutrient and light conditions on populations of picocyanobacteria that inhabit surface waters of the Atlantic subtropical gyres, this study evaluates changes in cell abundance and optical attributes of *Prochlorococcus* and *Synechococcus* cells as a response to different light levels and nutrient availability in the South Atlantic subtropical gyre (SAG).

2.2 Material and Methods

Water samples were taken from a representative depth of the mixed layer (depth = 30 metres) at 14:00, using a *Go Flo* bottle (OceanTest Equipment, Inc.). The *Go Flo* and associated parts were acid cleaned in 10% hydrochloric acid prior to use. Deployment of the *Go Flo* was performed on the fore deck of the RRS James Clark Ross, in conjunction with the solar noon CTD cast. Experiments were conducted at the SAG centre (22.158^{o} S, 25.087^{o} W, on 23/10/2015), where *Prochlorococcus* is numerically dominant, and the SAG periphery (33.332^{o} S, 31.074^{o} W, on 27/10/2015), where the contribution of *Synechococcus*

is also significant in surface waters (**Fig. 2.1**). Vertical profiles of *Prochlorococcus* and *Synechococcus* cell abundances, photosynthetically active radiation (PAR), temperature, salinity, and nutrients at the two contrasting stations are shown in **Fig. 2.2**.

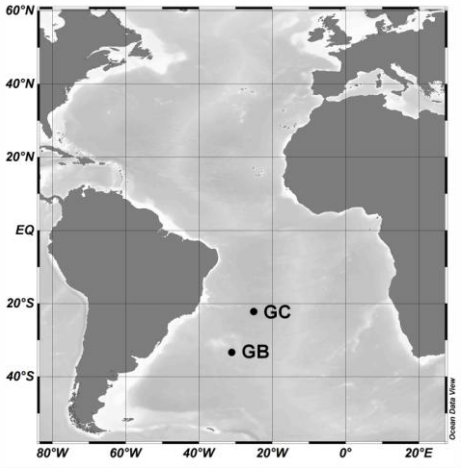


Figure 2.1. Location of the two experimental sites in the South Atlantic Ocean:
GC - Gyre centre (*Prochlorococcus*-dominated);
GB - Gyre border (*Prochlorococcus*/*Synechococcus* co-dominated)

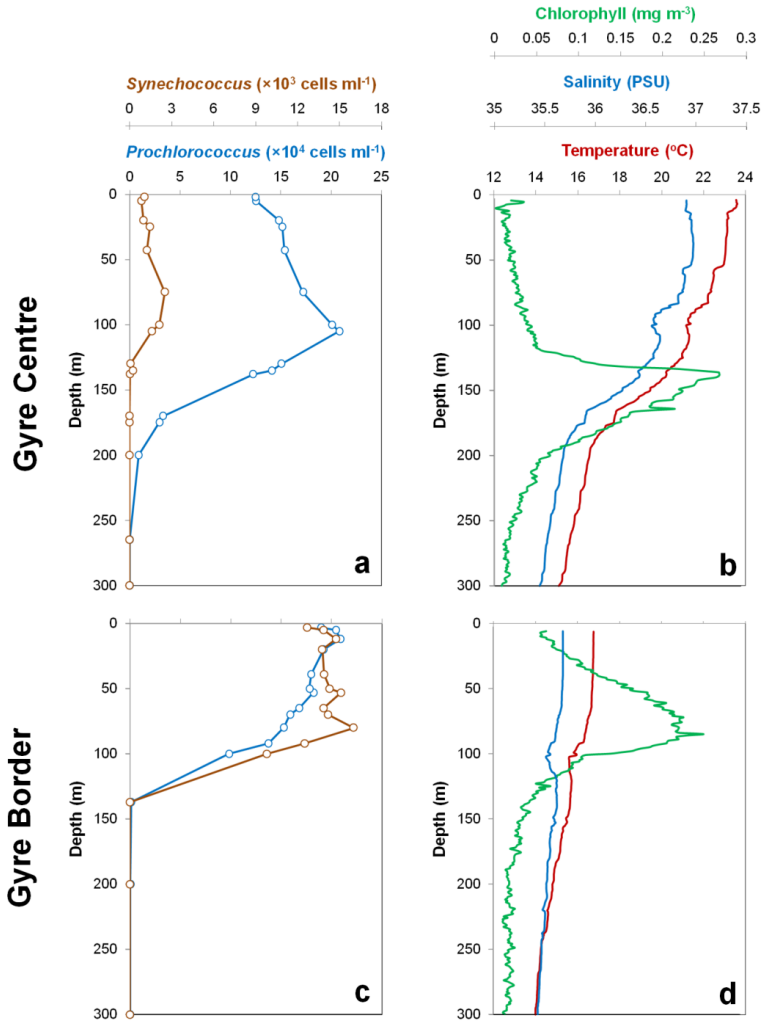


Figure 2.2. Vertical profiles of **a,c)** the cell abundance of *Prochlorococcus* and *Synechococcus*, and **b,d)** temperature, salinity and chlorophyll from fluorometer at the stations where water was collected for the experiments at the **a-b)** gyre centre and **c-d)** gyre border.

Seawater was incubated in 60 ml polycarbonate bottles, pre-washed with HCl (10%) and rinsed with the same seawater. Photosynthetrons illuminated by 50 W, 12 V tungsten halogen lamps were used to incubate the seawater at different light levels. The temperature in the photosynthetrons was kept stable by a constant flow of sea surface water provided by the ship's underway system. The temperature in the incubators was measured every three hours to ensure it is similar to the *in situ* temperature at the time of sample collection, and decreased less than 2^{o} C in the end of the experiments when compared to the beginning.

Two sets of incubations were performed for each experiment, with nutrients added to one of the sets, as detailed in **Table 2.1**. In each experiment, seawater was incubated under nine light levels, as described in **Table 2.2**. In order to observe the circadian variations of abundance and optical properties of the different taxonomic groups, picoplankton populations were quantified by flow cytometry in subsamples taken from each light treatment every 3 hours, over a 24 hour period, as well as after 36 and 48 hours. At each time point, two subsamples (0.8 ml and 1.6 ml) were taken from each bottle for flow cytometric analysis of picoplankton populations.

Table 2.1. Final concentrations of added inorganic nutrients in seawater samples.

			Final concentration of added nutrient (µM)	
Experiment ID	**Location (latitude N)**	**Experiment set**	**Ammonium chloride (NH_4Cl)**	**Iron(III) chloride ($FeCl_3$)**
#1	-22.158^{o}	Control	0	0
		Nutrients	1	0.002
#2	-33.332^{o}	Control	0	0
		Nutrients	1	0

Table 2.2. Light levels (µE m^{-2} s^{-1}) where bottles were incubated.

bottle	**Light levels (µE m^{-2} s^{-1})**			
	Experiment #1		**Experiment #2**	
	Control	**Nutrients**	**Control**	**Nutrients**
1	1780	1620	1495	1450
2	830	800	750	750
3	510	500	493	490
4	380	380	365	360
5	250	250	240	235
6	110	105	112	100
7	65	60	65	59
8	45	45	46	40
9	Dark	Dark	Dark	Dark

Prochlorococcus and *Synechococcus* cells were quantified using a FACSCalibur (Becton Dickinson) flow cytometer. Cell abundance, red fluorescence, and the right-angle light scatter (RALS) of *Prochlorococcus* and *Synechococcus* cells were evaluated following the 'unstained' method, whereas heterotrophic bacteria were quantified using the 'stained' method. Details on these flow cytometric methods are described in the next chapter of this thesis (**Chapter 3**). The extracted flow cytometry data was pre-processed using Microsoft Excel, and then analysed using R. Differences between treatments were tested using a paired Student t-test. Statistical calculations were done using the R packages *stats* (R Core Team 2017), *ggplot2* (Wickham 2009), and *devtools* (Wickham and Chang 2016).

2.3 Results

The response of cyanobacteria, particularly *Prochlorococcus*, to nutrient addition showed a marked difference between the two sample locations. In the gyre centre, nutrient addition negatively affected *Prochlorococcus* population growth, and this decrease in cell abundance was correlated with light availability, with a largest decrease in cell abundance at high light, associated with a decrease in RALS. In the gyre border, where only ammonium was added to the incubations, *Prochlorococcus* and *Synechococcus* did not respond to nutrient addition, which suggests that ambient ammonium concentrations are not limiting for cells in the SAG periphery, and/or that the ammonium concentration does not significantly affect the growth and metabolism of cyanobacteria. *Prochlorococcus* was the most abundant picophytoplankton group and the second most abundant microbe at the initial time point of both experiments, representing 20 and 15% of the total microbial abundance in the gyre centre and border, respectively. *Synechococcus* represented less than 1% of the population in the gyre centre, and 3% in its periphery.

2.3.1 *Gyre periphery*

At the gyre periphery (border), nutrient addition did not influence the growth of *Prochlorococcus* or *Synechococcus* (**Fig. 2.3**), and cell abundances only increased at light levels above 200 μE m^{-2} s^{-1}, especially after the second cell division. This increase in cyanobacterial cell abundance occurred mainly during the night, when cells divide. RALS and red fluorescence increased during the day, with the magnitude of this increase associated to the light level (**Fig. 2.4**; **Fig. 2.5**), and decreased at night when cells divide.

RALS and red fluorescence were slightly higher in the nutrient-enriched samples, but it did not result in an increase in cell abundance (**Fig. 2.6a,d**). The increase in *Prochlorococcus* RALS and cell abundance were greatest at ~250 µE m^{-2} s^{-1} regardless of the nutrient treatment (**Fig. 2.4**), whereas *Synechococcus* reached higher cell abundances and RALS at high light (> 700 µE m^{-2} s^{-1}). Red fluorescence varied similarly in both cyanobacteria, reaching highest values at 100 µE m^{-2} s^{-1} and decreasing gradually with increasing light (**Fig. 2.5**).

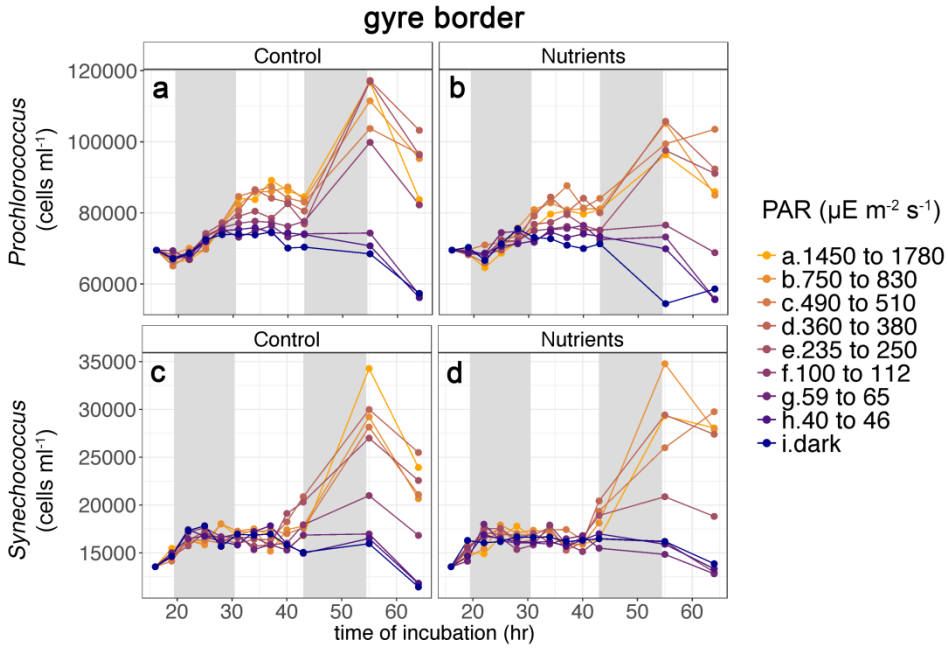


Figure 2.3. a-b) *Prochlorococcus* and **c-d)** *Synechococcus* cell abundance over time in the gyre border, in the **a,c)** control and **b,d)** nutrient enrichment experiments. The dark background indicates periods when incubations were kept in the dark (night). The colour-code indicates the light level to which incubations were exposed during the light hours.

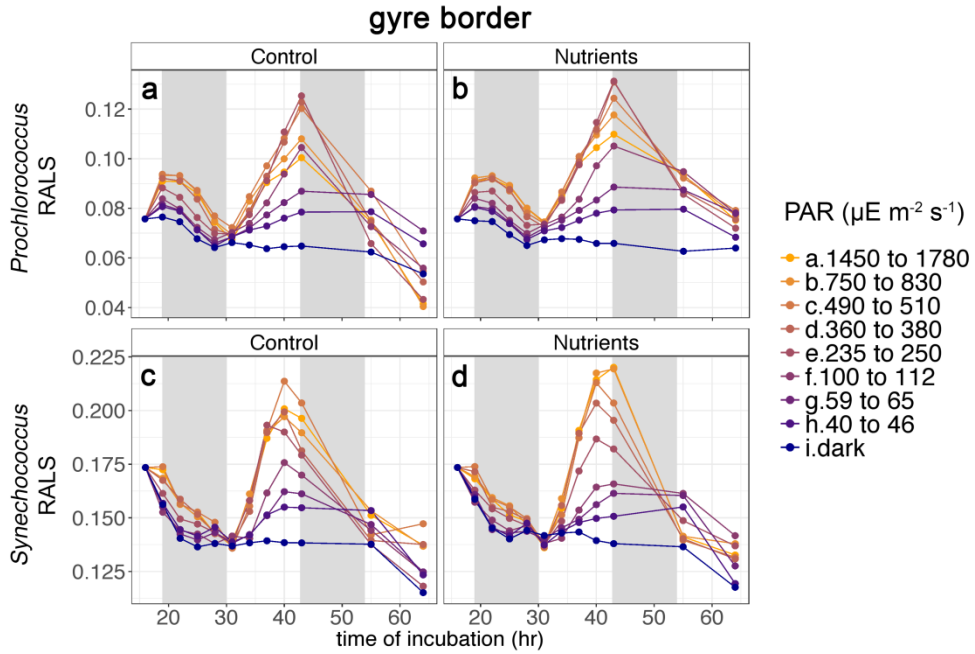


Figure 2.4. a-b) *Prochlorococcus* and **c-d)** *Synechococcus* cell-specific right angle light scatter (RALS) normalized to beads' RALS over time in the gyre border, in the **a,c)** control and **b,d)** nutrient enrichment experiments. The dark background indicates periods when incubations were kept in the dark (night). The colour-code indicates the light level to which incubations were exposed during the light hours.

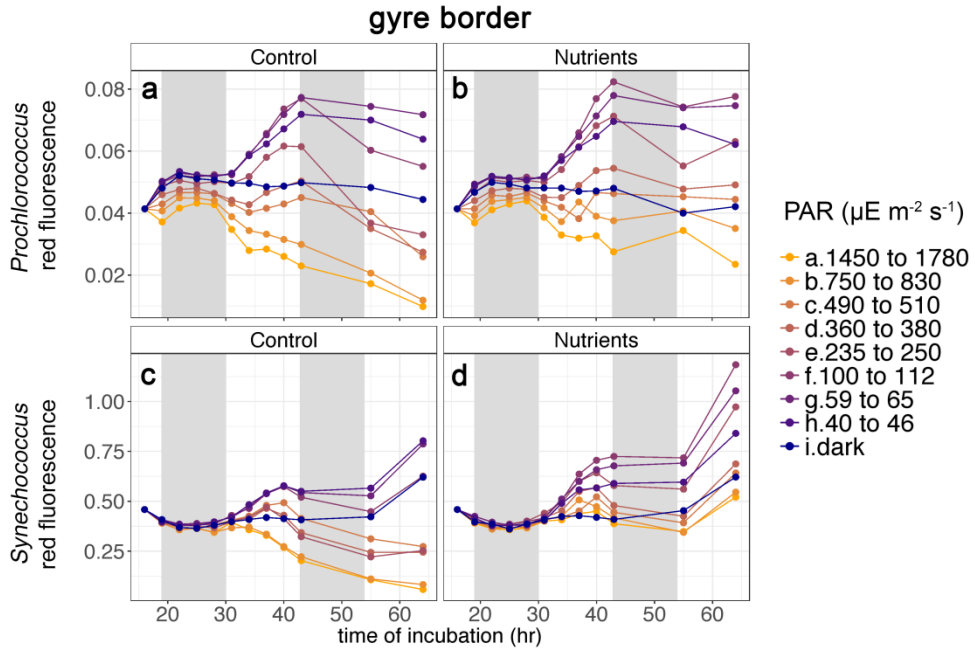


Figure 2.5. a-b) *Prochlorococcus* and **c-d)** *Synechococcus* cell-specific red fluorescence normalized to beads' red fluorescence over time in the gyre border, in the **a,c)** control and **b,d)** nutrient enrichment experiments. The dark background indicates periods when incubations were kept in the dark (night). The colour-code indicates the light level to which incubations were exposed during the light hours.

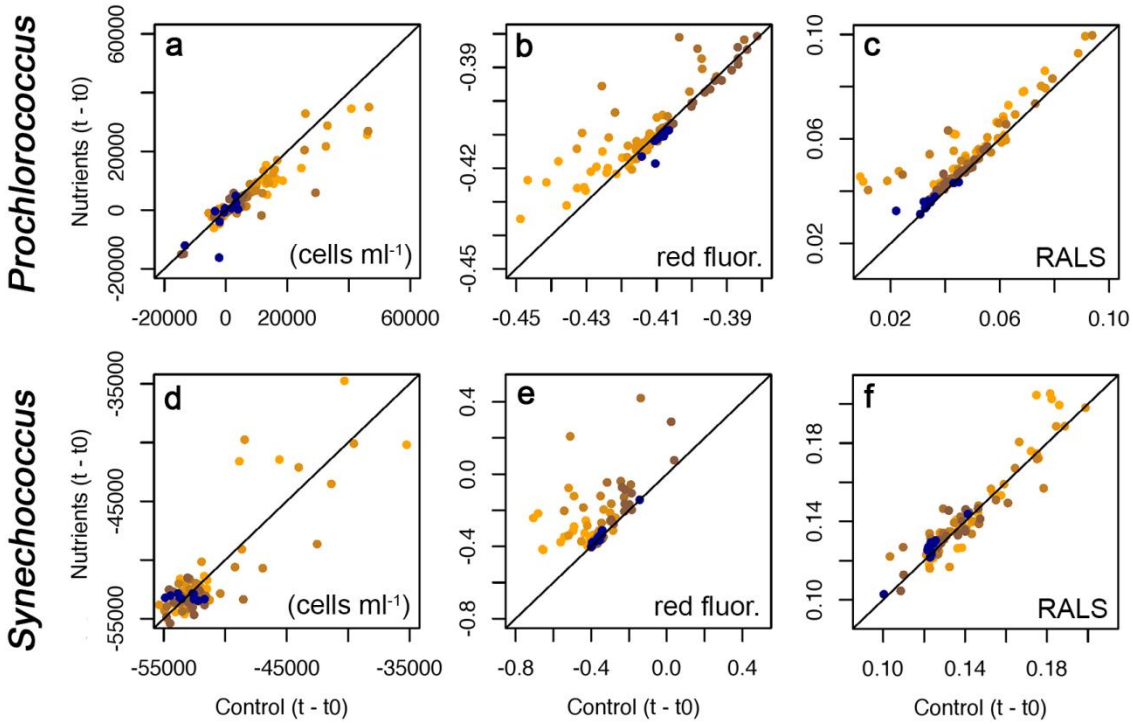


Figure 2.6. Gyre border: **a-c)** *Prochlorococcus* and **d-f)** *Synechococcus* **a,d)** cell abundance, **b,e)** red fluorescence, and **c,f)** right-angle light scatter (RALS). Sample in control and nutrient treatments are plotted against each other according to the light level. The diagonal line represents a ratio whereby the data from the control and nutrient addition samples are equal. The colour gradient represents light levels (darkblue = dark; orange = highest light level (1420 to 1780 µE m^{-2} s^{-1})).

2.3.2 *Gyre centre*

In the gyre centre, there was an increase in cell abundance over time at all light levels (**Fig. 2.7a**). However, this increase in cell abundance was slightly smaller when nutrients were added (**Fig. 2.7a,b**), and was restricted to light levels below 700 µE m^{-2} s^{-1}, with no growth at higher light levels (**Fig. 2.7b**). The observed decrease in *Prochlorococcus* population growth under high light was accompanied by changes in the light scatter properties of these cells. Cell-specific right angle light scatter (RALS) increased proportionally to the ambient light and the time of exposure to light, decreasing overnight (**Fig. 2.8a,b**) when cells divide (Claustre et al. 2002; Vaulot et al. 1995; Zinser et al.

2009). This increase in RALS was higher in the control treatment than in nutrient incubations (paired t-test p value < 0.001), especially at high light (> 700 μE m^{-2} s^{-1}) (**Fig. 2.8b**), proportionally to the significantly lower increase in cell abundance (paired t-test p value < 0.01) (**Fig. 2.10a,b**). *Prochlorococcus* red fluorescence increased over time, but to lower levels when nutrients were added (**Fig 2.9a,b**, **Fig. 2.10c**). *Synechococcus* occurred in very low cell abundances in the surface waters of the gyre centre, decreasing in abundance over time in all incubations, in both treatments (**Fig. 2.7c,d**). Variations in RALS did not show a clear pattern (**Fig. 2.8c,d**), and red fluorescence increased over time (**Fig. 2.9c,d**). It is important to note that, in the first 12 hours of incubation (first afternoon and first night), changes in cell abundance reflect cell growth over the first day, which includes the morning period before samples were taken from the environment. Cell division and consequent increase in cell abundance overnight were correlated to the increase in RALS during the day (**Fig. 2.11a**). This suggests that environmental conditions during the day closely regulate the growth of cyanobacteria, provided that grazing rates during the night do not vary significantly. The decrease in *Prochlorococcus* cell abundance that occurred during the day (incubation day 2) when nutrients were added was more significant at high light (**Fig. 2.11b**), and proportional to the relative decrease in RALS (**Fig. 2.11c**).

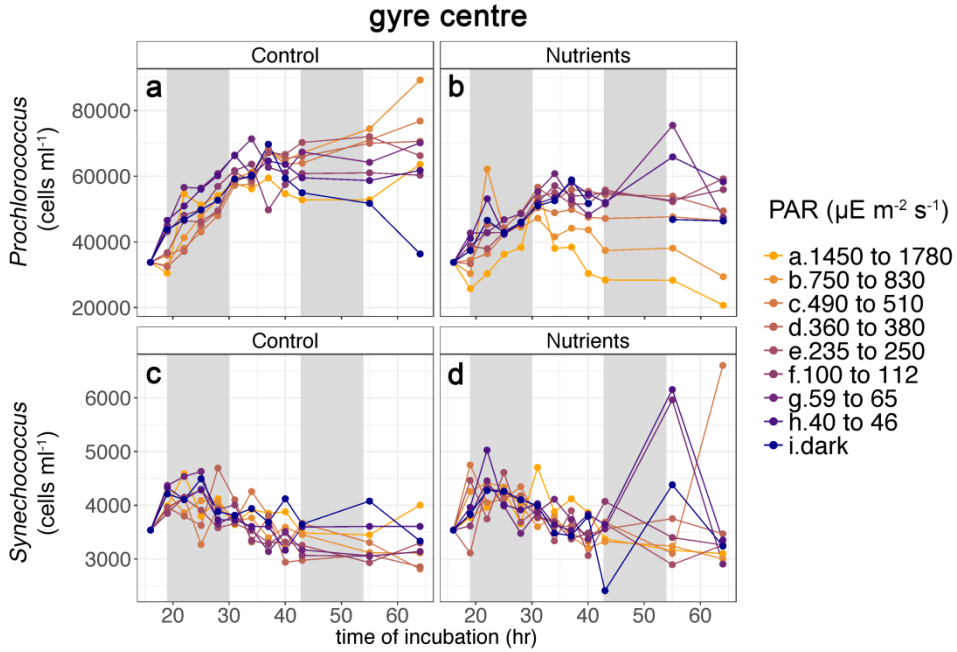


Figure 2.7. a-b) *Prochlorococcus* and **c-d)** *Synechococcus* cell abundance over time in the gyre centre, in the **a,c)** control and **b,d)** nutrient enrichment experiments. The dark background indicates periods when incubations were kept in the dark (night). The colour-code indicates the light level to which incubations were exposed during the light hours.

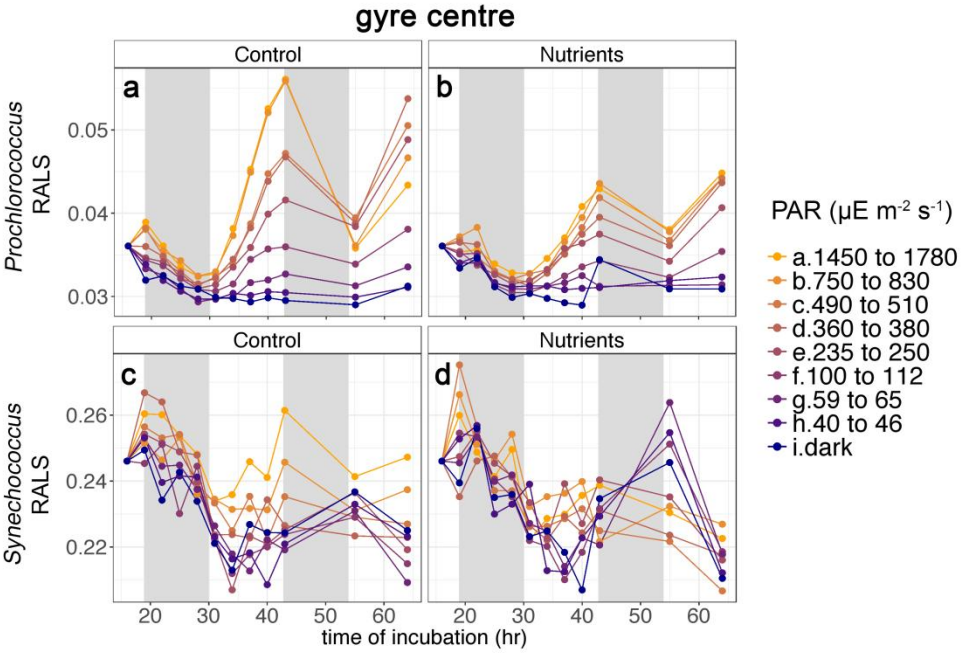


Figure 2.8. a-b) *Prochlorococcus* and **c-d)** *Synechococcus* cell-specific right angle light scatter (RALS) normalized to beads' RALS over time in the gyre centre, in the **a,c)** control and **b,d)** nutrient enrichment experiments. The dark background indicates periods when incubations were kept in the dark (night). The colour-code indicates the light level to which incubations were exposed during the light hours.

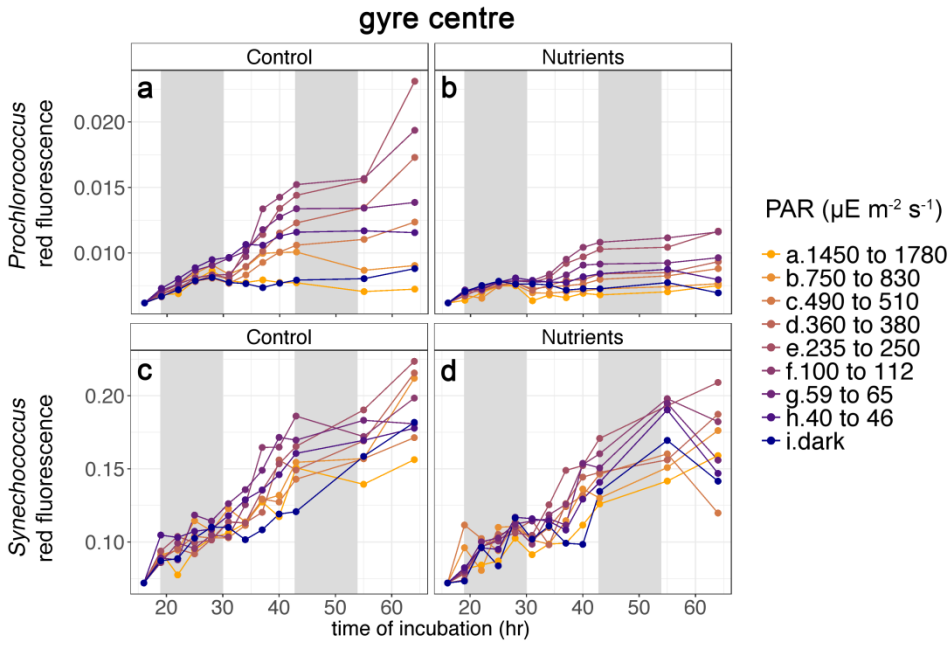


Figure 2.9. a-b) *Prochlorococcus* and **c-d)** *Synechococcus* cell-specific red fluorescence normalized to beads' red fluorescence over time in the gyre centre, in the **a,c)** control and **b,d)** nutrient enrichment experiments. The dark background indicates periods when incubations were kept in the dark (night). The colour-code indicates the light level to which incubations were exposed during the light hours.

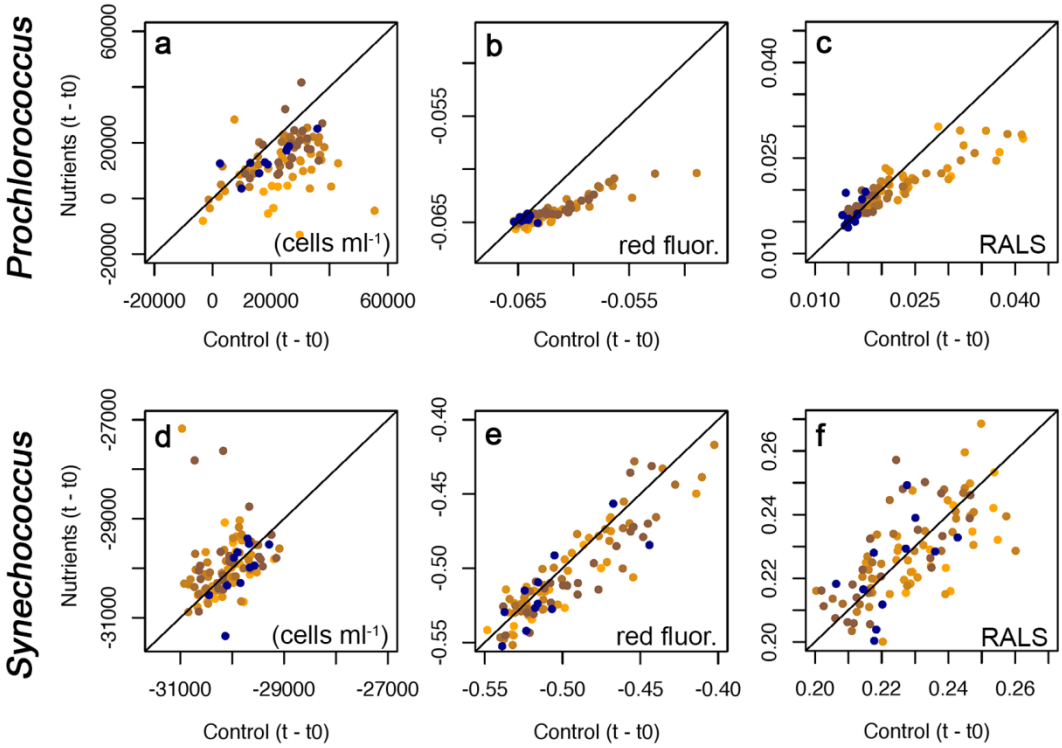


Figure 2.10. Gyre centre: **a-c)** *Prochlorococcus* and **d-f)** *Synechococcus* **a,d)** cell abundance, **b,e)** red fluorescence, and **c,f)** right-angle light scatter (RALS) in the experiments conducted at the gyre centre. Sample in control and nutrient treatments are plotted against each other according to the light level. The diagonal line represents a ratio whereby the data from the control and nutrient addition samples are equal. The color gradient represents light levels (darkblue = dark; orange = highest light level (1420 to 1780 µE m^{-2} s^{-1})).

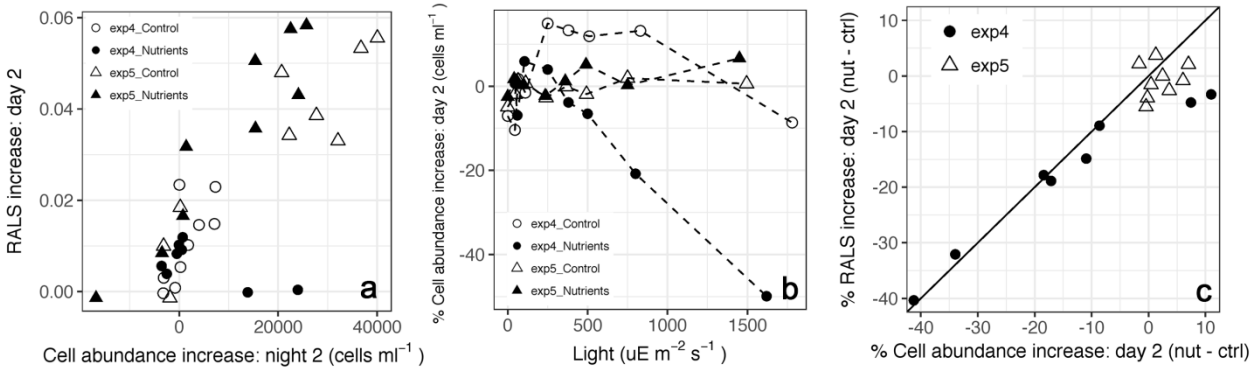


Figure 2.11. *Prochlorococcus* **a)** absolute increase in right-angle light scatter (RALS) during the day on day 2 (RALS increase day 2 = $RALS_{dusk}$ day 2 - $RALS_{dawn}$ day 2) *versus* absolute increase in cell abundance during the following night (abund increase night 2 = $abundance_{dawn}$ day 3 - $abundance_{dusk}$ day2); **b)** light level of incubation versus relative cell abundance increase during the day on day 2 (% abundance increase = ($abundance_{dusk}$ day 2 – $abundance_{dawn}$ day 2) × 100 / $abundance_{dawn}$ day 2); **c)** relative cell abundance increase during the day *versus* relative RALS increase during the day on day 2 (% RALS increase = ($RALS_{dusk}$ day 2 – $RALS_{dawn}$ day 2) × 100 / $RALS_{dawn}$ day 2). Circles represent experiment 4 (gyre centre) and triangles represent experiment 5 (gyre border).

In summary, at the gyre centre, *Prochlorococcus* showed a positive growth response in both experiments, with cell abundances increasing by > 50% after the first cycle. However, nutrients inhibited the photoacclimatory response of *Prochlorococcus* to high light: when nutrients were added at light levels above 700 μE m^{-2} s^{-1}, a decrease of up to 38% in cell abundance combined with a reduction in cell-specific red fluorescence and RALS were observed after 48 hours. In the gyre periphery, nutrient addition did not alter the optical properties and growth of *Prochlorococcus* and *Synechococcus* populations, and the increase in cell abundance was directly correlated with light, suggesting that the availability of ammonium and iron does not limit their growth in this region.

2.3.3 *The growth of other picoplankton groups*

The picoplanktonic community structure was numerically dominated by LNA bacteria (predominantly *SAR11*), followed by *Prochlorococcus* (**Fig. 2.12**). However, when nutrients were added in both experiments, the population of a large bacterium with high nucleic-acid content (LHNA bacteria) increased 10-33 times in 48h, reaching up to 30% of the total cell abundance after 36h of incubation (**Fig. 2.12**). The population of *Synechococcus* was numerically reduced when compared to other taxonomic groups, although more representative in the gyre border (**Fig. 2.12**).

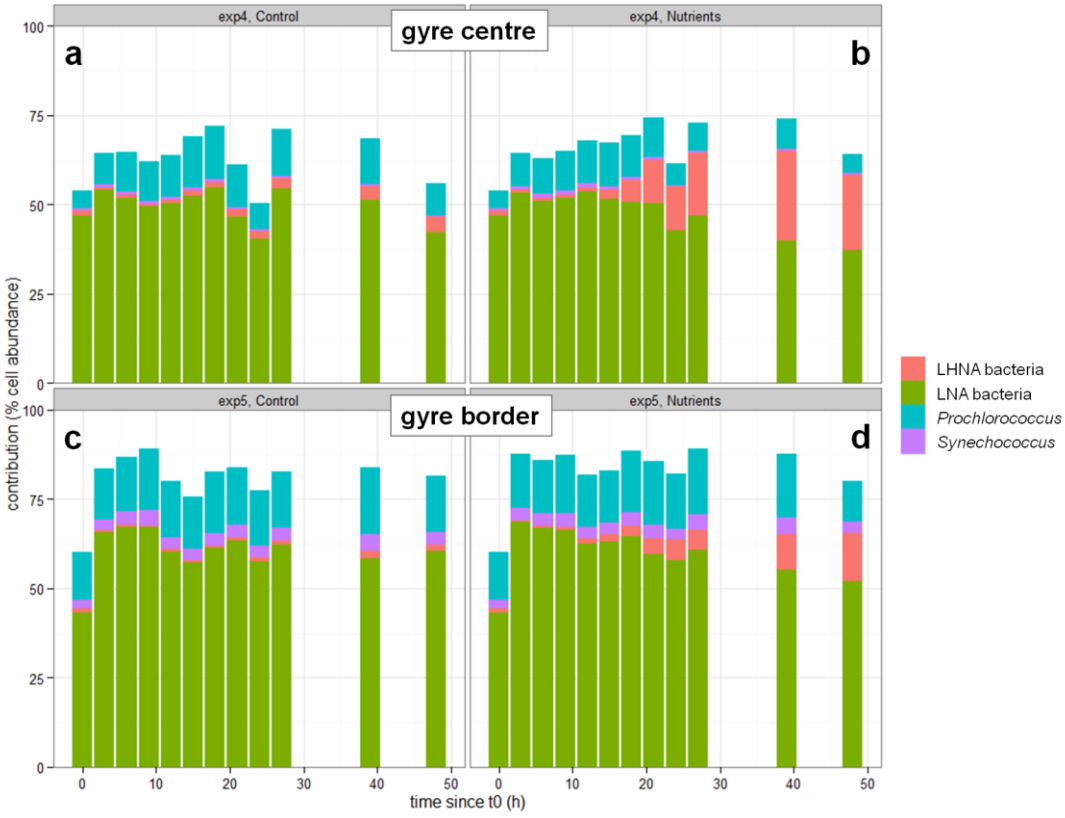


Figure 2.12. Contribution (%) of the main picoplankton groups relative to total picoplankton abundance (cells ml^{-1}) in the **a-b)** gyre centre and **c-d)** gyre border, in **a,c)** control and **b,d)** nutrient-enriched treatments.

2.4 Discussion

In this study, changes in the RALS and red fluorescence of *Prochlorococcus* cells related to the incident light level could already be noticed in the first three hours of incubation, indicating the fast acclimation capacity of this cyanobacterium to extreme light conditions. Additionally, *Prochlorococcus* and *Synechococcus* cell concentrations, right-angle light scatter (RALS) and red fluorescence showed marked diel cycles, as previously observed in many culture (Jacquet et al. 2001; Claustre et al. 2002; Bruyant et al. 2005; Zinser et al. 2009; Hynes et al. 2015) and *in situ* studies (Vaulot et al. 1995; Mann and Chisholm 2000; Jacquet et al. 2001; Lin et al. 2013; Lefort and Gasol 2014; Ribalet et al. 2015). However, when analysed over a few hours, the observed changes in cell abundance were correlated with the variability in the optical properties of these cyanobacteria.

In-situ observations show that, in the Atlantic Ocean, *Prochlorococcus* cells are more abundant in surface waters, where their red fluorescence (or divinyl-chlorophyll content) is the lowest, contrary to other phytoplankton that occur in higher concentrations where their red fluorescence is highest (Zubkov et al. 2000b; Veldhuis et al. 2005; Bouman et al. 2006). Accordingly, *Prochlorococcus* amino-acid uptake rates are highest at surface when compared to depth (Zubkov et al. 2004), despite the cell's lower pigment content, suggesting the photosynthetic performance of these high light-acclimated *Prochlorococcus* cells is not as tightly correlated to their intracellular pigment red fluorescence as it is in other phytoplankton groups (Veldhuis et al. 2005; Hartmann et al. 2014; Zubkov 2014). Conversely, when different regions are compared, higher amino-acid uptake rates are observed in areas where cells are more pigmented such as the gyre periphery, if compared to the gyre centre (Zubkov and Tarran 2005b). In our experiment

at the gyre periphery, the increase in *Prochlorococcus* and *Synechococcus* cell abundances over time was largest at high light where cellular red fluorescence was reduced, in agreement with what is observed *in situ*. The increase in intracellular photosynthetic pigment content and/or reduction of the non-photochemical quenching (NPQ) at light levels < 200 μE m^{-2} s^{-1} led to an increase in red fluorescence, and the amount of light energy acquired by these cyanobacteria was enough to sustain the cell metabolism but insufficient to lead to cell division and consequent increase in cell abundance. These results suggest that the relationship between red fluorescence and nutrient uptake efficiency may vary drastically between *Prochlorococcus* ecotypes, but within an ecotype, the growth of *Prochlorococcus* is optimized when cells are less pigmented.

While light was the main limiting factor for cyanobacterial growth at the gyre periphery, nutrients played an important role dampening the growth of *Prochlorococcus* and reducing RALS and red fluorescence at the gyre centre. This suggests that *Prochlorococcus* populations have a physiological mechanism to adapt to high light that is associated to nutrient depletion. The reduction in cellular red fluorescence upon nutrient addition could have been caused by an increase in NPQ and consequent reduction of the proportional amount of energy directed to photosynthesis, in which case an increase in cell-specific RALS would be expected because *Prochlorococcus* cells with more photoprotective pigments tend to scatter more light (Mella-Flores et al. 2012). Red fluorescence could also have been reduced because of an increase in energy flux through the photosynthetic machinery that led to lower energy dissipation as fluorescence by chlorophyll molecules. This reduction in red fluorescence upon nutrient addition caused a slight decrease in cell growth, but the influence of variations in cell-specific RALS was much more significant. Cell-specific RALS is often used as a proxy for cell size (i.e.

higher RALS indicates a larger cell) because it is directly correlated with the cell cross-section (Marañón et al. 2007; Lefort and Gasol 2014), but also associated with changes in the intracellular content of carbon and other elements and molecules that can potentially change the cell's refractory index (Stramski et al. 1995; Claustre et al. 2002). Therefore, a reduction in cell RALS can be an indicator of lower cell size, which would influence cell division, or reflect changes in the cell metabolism and elemental content, being unrelated with cell size (Robertson et al. 1998; Zubkov et al. 1999).

Variations in *Prochlorococcus* and *Synechococcus* cell-specific RALS were affected mainly by light, but also influenced by nutrients in the gyre centre. The diel cycle in cyanobacterial cell RALS was observed in both experiments, with lower magnitude in low light and dark incubations. Particularly in the gyre periphery, RALS did not change significantly during the day when light levels were lower than 200 μE m^{-2} s^{-1}, and consequently cells did not replicate at night (i.e. remained in G1 phase), leading to a decrease in cell abundance. This suggests that, especially in the gyre border, there is a minimum amount of daily light of approximately 2500 μE m^{-2} day^{-1} (200 μE m^{-2} s^{-1} for 12.5 hours) for *Prochlorococcus* and *Synechococcus* to grow enough in biomass to be able to divide, but this threshold was not clear at the gyre centre, reinforcing that nutrient depletion is possibly the main factor regulating the growth of cyanobacteria in this extreme high-light environment.

2.4.1 *Nutrient effect on Prochlorococcus photoacclimation*

Particularly in the gyre centre, *Prochlorococcus* cell-specific RALS and red fluorescence were reduced when nutrients were added, leading to a lower population gross growth at light levels below 700 μE m^{-2} s^{-1}: In the first 24 hours, the number of cells

increased 83% on average in control treatments, and only 50% when nutrients were added. At the highest light level (1620 μE m^{-2} s^{-1}), however, the abundance of *Prochlorococcus* decreased by 10% after the 24 hours, reaching a reduction of 38% after 48 hours, when similarly the number of cells decreased by 10% under 800 μE m^{-2} s^{-1}. This reduction in cell abundance was correlated with the reduction in cell RALS when nutrients were added. One explanation that may reconcile the changes in growth response and the bio-optical characteristics of *Prochlorococcus* cells with nutrient addition, in particular iron, is that the nutrient amended conditions made the cells more vulnerable to photodamage, especially at high light.

In our experiment at the gyre centre, the uptake of additional iron may have increased the photosynthetic electron transfer (Lea-Smith et al. 2016), inducing the lower fluorescence by photosynthetic pigments observed at all light levels, and the lower light scatter observed at high light (> 700 μE m^{-2} s^{-1}). This increase in energy flow towards photosynthesis could damage other components further down the photosynthesis reaction chain, such as RuBisCO (Berepiki et al. 2016). Therefore, under high light, photodamage could be enhanced by nutrient addition, especially if light exceeded levels as high as 700 μE m^{-2} s^{-1}. The increased cell death caused the reduction in cell abundance observed at high light when nutrients were added in the gyre centre.

Mann and Chisholm (2000) observed similar response to increasing Fe input in the Equatorial Pacific, where iron fertilization enhanced cell division rates of *Prochlorococcus*, but also increased cell loss by herbivory, transport, and cell death, maintaining a constant cell abundance. Therefore, iron limitation is possibly important to regulate energy transfer through the cell photosynthetic apparatus and avoid photodamage in the extreme high light conditions of the South Atlantic gyre surface waters. Once iron is available, it is possible that the photosynthetic machinery of *Prochlorococcus* is

overloaded with energy and this would hamper the ability of these cells to survive high light. In waters where iron is available in higher concentrations than at the gyre centre, such as the gyre borders or the equatorial region (Moore et al. 2013), light attenuation is higher, and phytoplankton cells are not subjected to such high light conditions in the mixed layer. Under such conditions, iron becomes beneficial to *Prochlorococcus*, which utilizes it to enhance photosynthetic rates (Berepiki et al. 2016; Lea-Smith et al. 2016). The reduction of red fluorescence from increased energy dissipation through NPQ could imply a higher photoprotective pigment content in these cells, and consequently, higher cell-specific RALS. However, this contradicts the observed reduced RALS at high light in nutrient-enriched incubations.

Other factors may also contribute to the reduction of RALS in nutrient-replete incubations at high light, such as an increase in the production of photoprotective pigments (such as zeaxanthin). As photoprotective pigments absorb light but do not fluoresce, light absorption by these pigments would lead to a decrease in scattered light by the cell, as observed in our experiment. It is also possible that *Prochlorococcus* cells produce another compound which scatters light and increases the cell's refractive index (Stramski and Reynolds 1993; Stramski et al. 1995) to protect intracellular components against photodamage. A final explanation to the different variability in cell abundance in nutrient and control treatments is oscillations in loss rates. The effects of nutrient addition to viral activity and to the growth and grazing pressure of mixotrophic herbivores such as pico- and nano-flagellates (Hartmann et al. 2013) were not examined in this study. However, we take into account that, by using flow cytometric counts, we evaluate the net growth of these populations, which already includes cell loss by any means (Zubkov 2014). We also consider that the grazing pressure, predominantly by flagellates, does not

change with the light intensity to which these incubations are exposed (Hartmann et al. 2014).

The results of this study show that the addition of nutrients increased the sensitivity of *Prochlorococcus* to high light. This would not be adverse to *Prochlorococcus* natural populations because frequently the supply of nutrients to the surface ocean is linked to a decrease in the water column stratification and an increased surface mixing which, in turn, decreases the average light cells are exposed to within in the mixed layer. In such case, a nutrient-induced increase in light harvesting would be beneficial to the cells.

In the oceans, *Prochlorococcus* cells that occur near the surface usually show lower red fluorescence, lower RALS, and are presumably smaller than those that occur at depth (Zubkov et al. 2004b). Therefore, *in-situ* RALS and red fluorescence are positively and strongly correlated, suggesting pigments influence cell-specific light scatter substantially. Here, experiments were set with a population of *Prochlorococcus* cells that had the same initial cell size and optical properties. The observed increase in light scatter at high light contradicts the relationships between cell size, red fluorescence, and light scatter observed *in situ*, where cells present lower RALS under high light (**Fig. 2.13**).

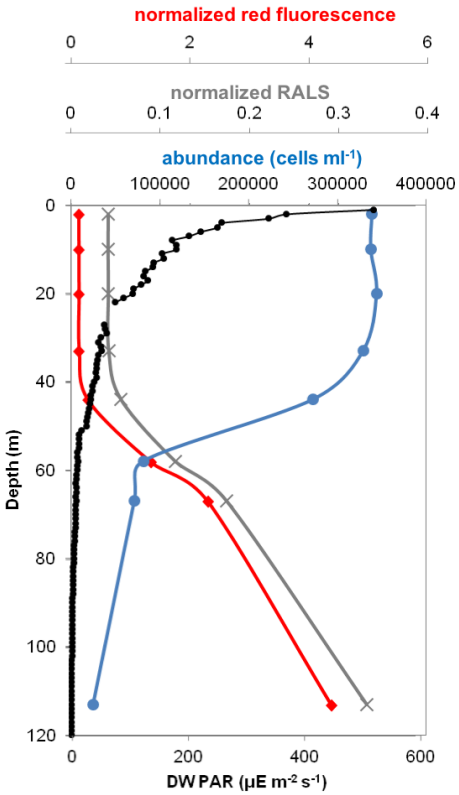


Figure 2.13. Vertical profiles of *Prochlorococcus* cell abundance, cell-specific RALS and red fluorescence, and the downwelling PAR ($PAR_{(z)}$) measured at noon at a location in the North Atlantic Gyre (16.436° N, 28.405° W). Data collected on AMT24 (08/10/2014).

2.5 Conclusions

In surface waters of the South Atlantic gyre, the primary environmental factors that regulate growth and the photoacclimatory response of cyanobacteria differ between the inner part of the gyre and its periphery. At the gyre periphery, the growth and optical attributes of *Prochlorococcus* and *Synechococcus* cells depend mostly on the light conditions, and nutrients (particularly nitrogen) are not limiting to these cells. However, in the gyre centre, *Prochlorococcus* growth and cellular optical properties rely on nutrient limitation to allow photoacclimation to the extreme high light, characteristic of these surface waters. The observed reduction in the cell-specific red fluorescence combined with reduced right-angle light scatter (RALS) upon nutrient addition, especially at light levels above 700 μE m^{-2} s^{-1}, suggests that the excess iron possibly led to an increase in energy flow through the photosynthetic machinery, reducing energy emission in the form of fluorescence by photosynthetic pigments.

Relationships between cell-specific RALS and red fluorescence observed in these experiments suggest that the cell's light scattering properties were influenced by features other than cell size, such as the intracellular pigment content and metabolic processes that involve light harvesting and energy acquisition and dissipation, leading to changes in intracellular molecular constituents. Because of the plasticity of HL *Prochlorococcus* ecotypes to regulate their intracellular divinyl-chlorophyll content according to extreme light conditions, we do not recommend red fluorescence to be used as a proxy for *Prochlorococcus* biomass in the surface mixed layer of subtropical gyres.

Our results suggest that changes in environmental conditions of the Atlantic subtropical gyres that affect the availability of nutrients and light in the euphotic layer can potentially influence stocks of cyanobacteria in surface waters. Nutrient enrichment,

especially that of micronutrients like iron, would impair the growth of the particular high light *Prochlorococcus* ecotypes that are predominant in surface waters of subtropical gyres, but would benefit *Synechococcus*, other *Prochlorococcus* ecotypes, and possibly other phytoplankton groups in other areas of the ocean where light exposure is reduced due to a change in phytoplankton community composition and biomass.

Chapter 3.

Bleached *Prochlorococcus*: the missing phytoplankton?

Assessing the efficiency of flow cytometry and filtration methods to estimate picophytoplankton biomass

3.1 Introduction

Picophytoplankton biomass is conventionally determined either by quantifying cell abundance, or measuring species-specific pigment concentrations in water samples. The abundance of these small phytoplankton cells is typically quantified in water samples using flow cytometry (Olson et al. 1993), whereas filtered samples are analysed to determine the concentration and absorptive properties of pigments using High Performance Liquid Chromatography (HPLC) and spectrophotometry (Roy et al. 2013), respectively.

Due to the relatively short time and high accuracy in the analysis of picophytoplankton communities (Vaulot et al. 2008), flow cytometric counts are now routinely included as core measurements in international oceanographic programmes such as the AMT. Recent syntheses of large datasets of picophytoplankton abundance have shown consistent patterns in their vertical distribution in the open ocean, with light being an important factor governing the vertical structure from the level of species to ecotypes (Johnson et al. 2006; Bouman et al. 2006; Hickman et al. 2009; Kletou and Hall-Spencer 2010). The adaptation of *Prochlorococcus* populations to different light environments is reflected in their cellular characteristics: high light-acclimated *Prochlorococcus* cells are smaller and transparent, with such low pigment content that their fluorescence is below the detectable limit of conventional fluorometers and flow cytometers, whereas

Prochlorococcus that inhabit low light environments are larger and contain a high pigment content per cell (Biller et al. 2014a).

In order to develop an empirical model to predict the abundance of picophytoplankton cells based on environmental predictors, the compilation of a large dataset is required, as a higher number of observations leads to an increase in accuracy of the predictive factors used in this predictive model. Yet, when assembling such a dataset, it is vital to examine whether measurements of picophytoplankton biomass provided by different sources are comparable and thus can be combined with confidence that the error between analysis techniques is minimal. In this study, differences between broadly implemented flow cytometric methods are assessed. The efficiency of the conventional filtration method used for pigment and phytoplankton light absorption analyses is also examined for samples dominated by picophyoplankton (cells < 2 μm), which is often the case in subtropical oceanic waters.

3.2 Comparison between flow cytometric methods to quantify *Prochlorococcus*: 'stained' *versus* 'unstained' cells

Flow cytometers discriminate between cell types according to their side and forward light scatter and their fluorescence properties. Optical sensors are able to measure the natural fluorescence of pigmented low light-acclimated *Prochlorococcus* cells, but the red fluorescence signal becomes undetectable when *Prochlorococcus* cells are acclimated to high light and their intracellular pigment concentrations are extremely low, which often occurs near the surface of the water column in clear oligotrophic waters. The objective of this work is to assess potential biases in cell counts of surface populations of *Prochlorococcus* by analysing the differences between flow cytometric counts of

'stained' (Zubkov et al. 2007; Gómez-Pereira et al. 2013) and 'unstained' (Olson et al. 1993) *Prochlorococcus* cells, which are the two most frequently used methods for quantifying picophytoplankton cells using flow cytometry.

3.2.1 *Methods*

Sampling and analysis were carried out during two consecutive Atlantic Meridional Transect cruises: AMT23 (2013) and AMT24 (2014) (**Fig. 3.1**). On both cruises, water samples were collected at 8 to 12 depths at each sampling station using Niskin bottles installed on a CTD rosette profiling system, and fixed with paraformaldehyde (3%) immediately after sampled.

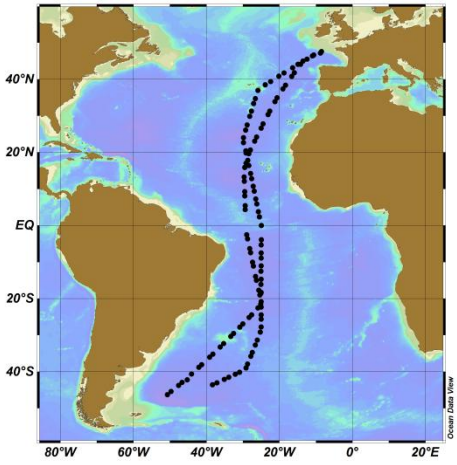


Figure 3.1. Cruise tracks of AMTs 23 and 24.

Prochlorococcus cells were quantified concomitantly using a FACSCalibur and a FACSort (Becton Dickinson) flow cytometer and using the methods briefly summarized below:

a) 'Unstained' analysis: 0.8ml samples were taken and immediately analysed using a FACSort (Becton Dickinson) flow cytometer. These samples were analysed fresh (without fixation). *Prochlorococcus* populations were evaluated based on their red fluorescence and right-angle light scatter (RALS) (**Fig. 3.2a**), using the method described in Olson et al. (1993). This analysis provided information on cell counts, cell-specific red fluorescence and RALS.

b) 'Stained' analysis: 1.6ml samples were fixed using paraformaldehyde and stained with a 1% commercial stock solution of SYBR Green 1 (Molecular Probes, Inc.) in Milli-Q water, then mixed with 300mM tripotassium citrate (24.5 mM final concentration) (Zubkov et al. 2007). The samples were analysed using a FACSCalibur (Becton Dickinson) flow cytometer. Cell size (forward and right-angle light scatter) and DNA content (green fluorescence) of the auto- and hetero-trophic picoplanktonic populations, and photosynthetic pigment content (red fluorescence) of cyanobacteria and autotrophic picoeukaryotes were determined (**Fig. 3.2b**) (Olson et al. 1993; Zubkov et al. 2000b, 2007). Yellow-green 0.5 and 1.0 μm reference beads (Fluoresbrite Microparticles, Polysciences, Warrington, PA, USA) were used as an internal standard for both fluorescence and flow rates (Zubkov and Burkill 2006). Through this analysis, it is possible to identify different species of heterotrophic bacteria and distinguish *Prochlococcoccus* cells from other picophytoplankton, regardless of their intracellular chlorophyll content (red fluorescence).

The identified picoplankton groups using the 'stained' and 'unstained' methods can be seen in **Fig. 3.2**. The WinMDI, version 2.0, free software (Joseph Trotter) was used to extract and visualize flow cytometric data.

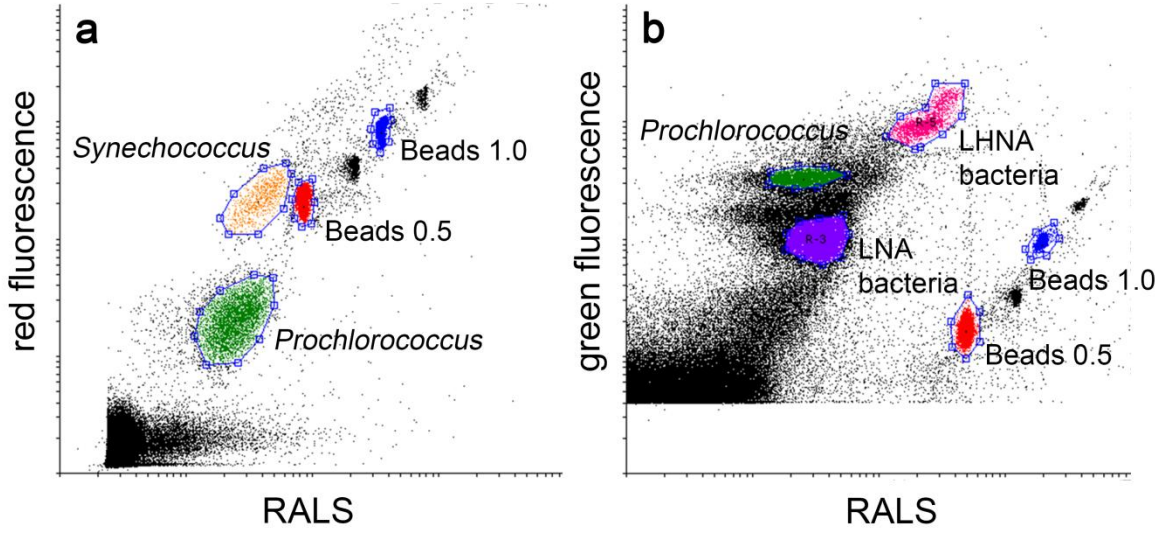


Figure 3.2. Picoplankton groups individualized in **a)** unstained samples using the right-angle light scatter (RALS) and red fluorescence, and **b)** stained samples using RALS and green fluorescence. Round tight clusters represent 0.5µm and 1.0µm fluorescent beads. Figures were created using the Flowing Software® (version 2.5).

The main difference between the two methods used to determine the abundance of different picoplankton groups is that the 'unstained' method quantifies *Prochlorococcus* cells based on their red fluorescence (originated from chlorophyll molecules found within the photosynthetic apparatus of the cell) and right-angle light scatter (RALS), whereas the 'stained' method also uses the green fluorescence of the DNA-specific dye (SYBR Green) that is added to the samples prior to the flow cytometric analysis.

The relative difference (*Rdif*) between *Prochlorococcus* cells quantified using the 'unstained' method (Pro_{unst}) and the 'stained' method (Pro_{st}) was calculated in equation [3.1]:

$$Rdif = \frac{Pro_{st} - Pro_{unst}}{Pro_{st}} \quad [3.1]$$

3.2.2 *Results and discussion*

Results from tests in the two AMT cruises show that *Prochlorococcus* cell concentrations were slightly higher when quantified using the 'stained' method (**Fig. 3.3a**), especially near the sea surface (**Fig. 3.3b**). Pro_{unst} was, on average, 17% (± 19%) lower than Pro_{st} (i.e. Pro_{unst} is 83% of Pro_{st}, thus Pro_{unst} is part of Pro_{st}), and fall within a similar range to what was reported by (Zubkov et al. 2000b) and Hartmann et al. (2014). When considering exclusively surface samples (taken at depths < 20 m), the relative difference between Pro_{st} and Pro_{unst} increased to 25% (± 14%) due to their low intracellular pigmentation.

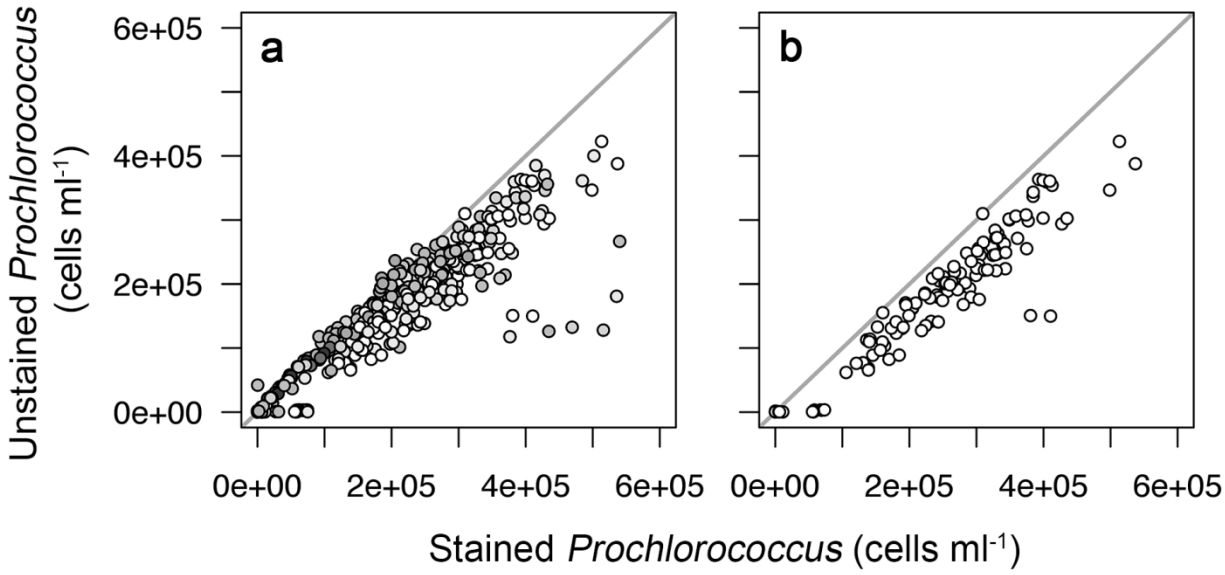


Figure 3.3. a) Stained vs. unstained *Prochlorococcus* in the top 200 metres of the water column and in **b)** sub-surface samples (< 20 metres). Grey scale indicates the depth, with lighter points representing shallower depths.

To examine the influence of the vertical distribution of irradiance in the water column and the photoacclimatory response of *Prochlorococcus* cells on the difference between the two flow cytometric methods, *Rdif* was compared with depth (m), the intensity of downwelling irradiance (W m^{-2}), and the average cell red fluorescence (a

proxy for intracellular pigment concentration). The relative difference between Pro_{st} *and* Pro_{unst} decreased with depth (**Fig. 3.4a**), due to depth-dependent variations in irradiance (**Fig. 3.4b**), highlighting that the low red fluorescence found in cells acclimated to high light near the sea surface (**Fig. 3.4c**) resulted in an underestimation in the cell abundance of *Prochlorococcus* using the 'unstained' method when compared to the 'stained' method.

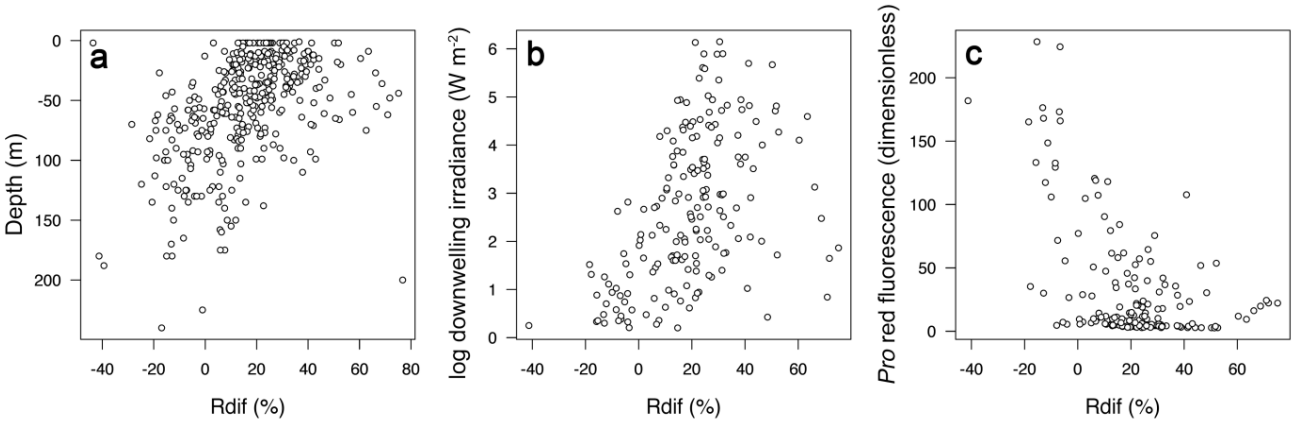


Figure 3.4. Relationship between the relative difference between Pro_{st} and Pro_{unst} (*Rdif*) and: **a)** depth (all samples); **b)** downwelling irradiance (samples collected during the day); and **c)** *Prochlorococcus* red fluorescence. The depth is expressed in metres, the downwelling irradiance in W m^{-2} and log(+1) transformed, and the red fluorescence of *Prochlorococcus* cells is calculated relative to the red fluorescence of 0.5µm beads.

3.3 Efficiency of GF/F filters to retain *Prochlorococcus* cells

3.3.1 *Methods*

Samples collected to measure phytoplankton absorption and pigments are routinely filtered through GF/F filters (0.7µm equivalent pore size, pressure = 10mm Hg), but it has been observed that a significant amount of *Prochlorococcus* cells can pass through GF/A and GF/C filters (with a similar pore size to GF/F filters) due to the reduced size of these

cells, especially in surface oligotrophic waters (Zubkov et al. 1998a). As a consequence, it is possible that phytoplankton pigments and absorption datasets could be biased if they are missing a fraction of the *Prochlorococcus* population that is not retained in GF/F filters when attempting to account for the optical and pigment signatures of the total phytoplankton community. This could potentially lead to significant errors in global picophytoplankton biomass distribution models, as this species is the most abundant phytoplankton in the oceans and, even when weakly pigmented, contribute significantly to the bulk primary production in the gyres (Hartmann et al. 2014).

To determine whether all *Prochlorococcus* cells are retained by GF/F filters, 200 ml of all samples taken from near surface depths (5 to 15 metres) on AMT 24 (2014) were filtered through GF/F filters, and the abundance of cells in the seawater samples (pre-filtration) and in the filtrate (post-filtration) were evaluated by flow cytometry using the 'stained' technique. To estimate how efficient GF/F filters are in retaining *Prochlorococcus* cells, the retention efficiency (*RE*) was calculated using equation [3.2]:

$$RE = \left(1 - \frac{Pro\ cell\ abundance\ in\ the\ filtrate}{Pro\ cell\ abundance\ in\ the\ sample}\right) \times 100 \qquad [3.2]$$

where *RE* is expressed as the percentage of cells from the original sample that is retained in the filter.

3.3.2 *Results and discussion*

The results show that GF/F filters retained more than 80% of *Prochlorococcus* cells throughout the entire AMT transect (**Fig. 3.5**), with a mean retention efficiency of 94 ± 5 %. Therefore, GF/F filters are efficient to retain even the smallest phytoplankton when samples are filtered under low pressure.

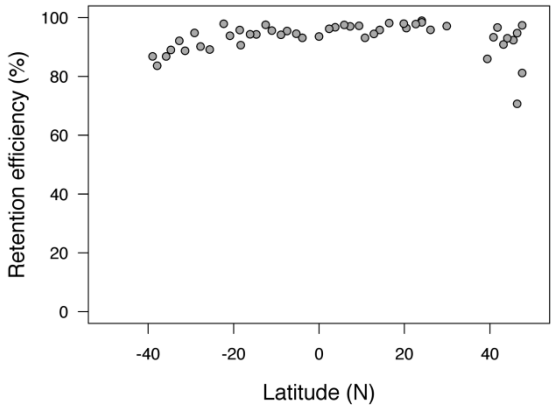


Figure 3.5. Efficiency of GF/F filters to retain *Prochlorococcus* cells (retention efficiency) across the Atlantic Ocean, on AMT 24.

A lower efficiency of GF/F filters to retain *Prochlorococcus* cells was expected in samples with low average cell right-angle light scatter (RALS), a flow-cytometric measurement often associated with cell size and volume (Stramski and Morel 1990; Stramski and Reynolds 1993; Stramski et al. 1995; DuRand et al. 2002). However, contrary to what was expected, a negative relationship between the retention efficiency and the average cell RALS in the samples was observed (**Fig. 3.6a**). The reason for this unexpected result is that more cells passed through the filter in samples where cell abundance was lower, and coincidentally cell RALS was higher in these samples. Consequently, the retention efficiency was higher in samples with higher cell concentrations (**Fig. 3.6b**), possibly due to filter clogging caused by the agglomeration of cells, leading to a decrease in the average pore size. Thus, cell abundance has a stronger effect influencing the filtration efficiency than cell size (RALS).

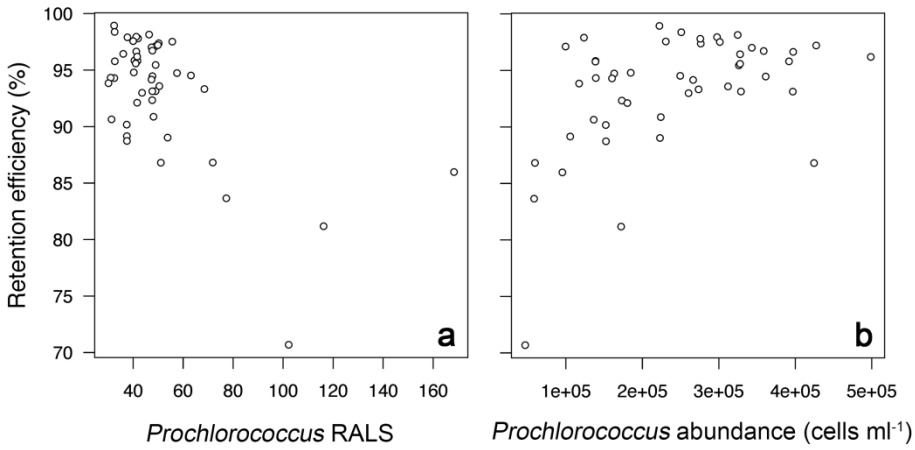


Figure 3.6. Relationships between the efficiency of GF/F filters to retain *Prochlorococcus* cells (retention efficiency) and **a)** the mean cell right-angle light scatter (RALS) in the sample before filtration, and **b)** the abundance of *Prochlorococcus* cells in the sample before filtration.

3.4 Conclusions

Given that the results from AMT24 show that the difference between flow cytometric techniques to quantify *Prochlorococcus* cells is less than 20%, it can be concluded that datasets of *Prochlorococcus* cell abundance over the AMT time series and other datasets are comparable regardless of the flow cytometric technique used to quantify *Prochlorococcus* cells. As a result of these findings, a combined AMT dataset of *Prochlorococcus* abundance was exploited, where both approaches are used to capture a wide range of oceanographic conditions over which this important cyanobacterium dominates.

Additionally, pigment and absorption measurements conventionally used as proxy for cyanobacterial biomass are not subject to significant loss of *Prochlorococcus* cells through filtration, as on average 95% of the cells are retained in GF/F filters.

This supports the use of phytoplankton pigments and their optical signatures that are explored in ocean-colour algorithms as robust proxies of water column turbidity and

marine productivity, even when studying the smallest phytoplankton size fraction. Moreover, these results provide reassurance that ocean-colour algorithms used to estimate pigment concentration and phytoplankton absorption in the most oligotrophic waters of the open ocean are not prone to a systematic bias in the determination of total phytoplankton pigment and absorption through the loss of sub-micron size cells.

Chapter 4.

Scratching the surface: a model to predict the vertical distribution of *Prochlorococcus* using remote sensing

4.1 Introduction

Until the early 1980s, the largest marine ecosystems on our planet, referred collectively as the subtropical gyres (Longhurst 1998; Karl 1999; Hirata et al. 2008), were considered to be oceanic deserts as they are characterized by low biological primary production and occur at similar latitudes to terrestrial deserts and savannahs (Olson et al. 2001). In the central subtropical gyres, extreme high-light conditions hamper phytoplankton growth at the sea surface and lead to very low intracellular pigment concentrations (Westberry et al. 2008; Behrenfeld et al. 2015). Yet, lying beneath this seemingly barren surface layer, a deep chlorophyll maximum (DCM) is commonly observed at depths between 80 to 120 metres (Cullen 1982; Aiken et al. 2016). This peak in pigment concentration is the result of light penetrating sufficiently deep in the water column to reach depths where pulses of nutrients are supplied from below the euphotic layer (Kirk 2011). Cells found at this depth can therefore attain net growth by increasing their intracellular pigment concentration to thrive at low light levels, which results in the formation of the DCM (Cullen 1982; Behrenfeld et al. 2015). This allocation of biomass at depth in the subtropical gyres makes these gyre ecossystems more similar to terrestrial savannahs than deserts: like the subtropical gyres, savannahs have most of its biomass buried below ground, protected from direct contact with the surface (Grace et al. 2006).

Although the DCM provides an enhancement in biomass, the chorophyll-derived biomass in subtropical gyres is still low when compared with coastal marine

environments and shelf seas (Cullen 1982). However, in 1988, the use of shipboard flow cytometry to study small phytoplankton cells allowed the discovery of a small and ubiquitous species of marine phytoplankton: the cyanobacterium *Prochlorococcus* (Chisholm et al. 1988). *Prochlorococcus* is the dominant phytoplankton in subtropical and tropical waters, where it occurs in cell abundances of 10^4 to 10^5 cells ml^{-1} (Zubkov et al. 2000b; Rabouille et al. 2007; Malmstrom et al. 2010; Bouman et al. 2011). Despite its diminutive size (~ 1μm) and consequently low cell biomass (~ 50 fg C $cell^{-1}$; Bertilsson et al. 2003), the contribution of *Prochlorococcus* to the global phytoplankton stock is considerable: the integrated biomass of their astronomically numerous 10^{27} cells (Williams and Follows 2011; Flombaum et al. 2013) is higher than the biomass of any other phytoplankton species in the world's oceans.

The knowledge about the distribution and ecology of *Prochlorococcus* increased drastically after flow cytometric analysis of phytoplankton became a norm (Waterbury et al. 1979; Vaulot et al. 2008). Nevertheless, there are still remote areas of the ocean, especially in subtropical gyres, where data coverage is poor. Remote-sensing observables such as temperature, remote-sensing reflectance (R_{rs}), and the photosynthetically active radiation (PAR) are important tools to aid the understanding of the global distribution of this species, although satellite sensors capture optical signals from only a few metres underneath the ocean's surface ocean (Gordon and Morel 1983). As a complement to remote-sensing satellite observations, a three-dimensional view of the ocean environment is provided by ARGO floats and ocean gliders that measure temperature, salinity, and pressure (which determines depth) at deeper layers of the water column (Hosoda et al. 2008).

It is widely known that the biogeography of *Prochlorococcus* is governed by changes in environmental gradients of temperature, light, and chlorophyll (Johnson et al. 2006; Rabouille et al. 2007; Zinser et al. 2007; Williams and Follows 2011). As

Prochlorococcus is the numerically dominant phytoplankter in large areas of the world's oceans, it is important to be able to predict how *Prochlorococcus* populations might vary temporally and spatially in response to environmental and climate changes, and to assess seasonal and long term changes inflicted by biogeochemical processes and trophic interactions in oceanic food webs. To date, estimates of global standing stocks of *Prochlorococcus* (Williams and Follows 2011) and their distribution in the world's oceans (Flombaum et al. 2013) take into account the vertical change in cell abundance with depth by assuming that the response of *Prochlorococcus* cells to environmental conditions at depth is similar to what occurs at the surface, disregarding the deep maximum in cell abundance that is commonly observed in oligotrophic systems such as the North Pacific Gyre (Karl 1999; Rabouille et al. 2007) and the North and South Atlantic Gyres (Zubkov et al. 1998b, 2000b; Veldhuis and Kraay 2004; Heywood et al. 2006). This can potentially lead to an underestimation in global standing stocks. Here, an empirical model that uses two ocean-observing systems (Aqua-MODIS and ARGO) was developed and applied to estimate the vertical and spatial distribution of *Prochlorococcus* at a basin scale. This approach captures both seasonal and inter-annual variations in the vertical distribution of *Prochlorococcus* cells, thus providing a powerful tool to examine the large-scale dynamics of global standing stocks and their contribution to the marine organic carbon cycle.

4.2 Methods

The *Prochlorococcus* abundance model estimates the distribution of cells from the surface to the base of the photic zone using information on light penetration in the water column. The vertical distribution of *Prochlorococcus* has a form similar to the typical

profile of primary production, which is determined by light availability and the photosynthetic response of phytoplankton to available light. Recognising that primary production may indeed have a role in determining the vertical distribution of this phytoplankton species in the ocean, equations analogous to that of the photosynthesis-irradiance curve (Platt et al. 1980) were used to describe the relationship between cell abundance and the percentage of surface irradiance available at each depth, henceforth referred to as the fractional PAR ($fPAR_{(z)}$).

Although *Prochlorococcus* ecotypes adapted to different light levels can coexist in a determined water body, the model is based on the assumption that there are only two sub-populations of *Prochlorococcus*: *ProI*, which dominates under high-light conditions found near the sea surface, and *ProII*, which has a preference for low-light conditions near the deep chlorophyll maximum (*DCM*). When these two populations are added, the result is a vertical profile of total *Prochlorococcus* cells, $Pro_{total(z)}$, which peaks above the depth of the *DCM* (Z_{DCM}). Vertical profiles of *ProI* and *ProII* are estimated from $fPAR_{(z)}$.

The series of equations used to estimate the vertical distribution of *Prochlorococcus* cells relies on four parameters that define the magnitude of the vertical profile of cell abundance: *Prochlorococcus* abundance at surface (Pro_{surf}) and at the deep maximum (Pro_{max}), used to calculate *ProI* and *ProII*, respectively; the attenuation coefficient for PAR (K_dPAR), used to calculate *fPAR* at each depth; and the depth of the deep chlorophyll maximum Z_{DCM}, used in the calculation of Pro_{max}. To estimate these four parameters, their empirical relationships were explored with environmental predictors that can be obtained from ocean observables or estimated using geographic locations and time of the year.

4.2.1 *Model parameterization*

Environmental variables that can potentially influence K_dPAR, Z_{DCM}, and the growth of *Prochlorococcus* cells (Pro_{surf} and Pro_{max}) were selected, such as: sea-surface temperature (*SST*), remote sensing reflectance at 443 ($R_{rs}(443)$) and 488 nm ($R_{rs}(488)$), the photosynthetically active radiation (*PAR*), the temperature at 200m estimated from the Argo array (T_{200}), the solar zenith angle at noon (θ_s), and the daylength (*DL*). The selection of these variables took into consideration some factors known to determine the distribution of this phytoplankton species. For example, *Prochlorococcus* is restricted to warm waters, thus a thermal threshold was used. Additionally, the difference between *SST* and T_{200} is here used as a proxy for ocean stratification (de Boyer Montégut et al. 2004); Remote sensing reflectance of solar radiation in the visible domain is inversely related to light absorption by phytoplankton pigments and other light-absorbing substances, such that $R_{rs}(443)$ and $R_{rs}(488)$ are closely related to the concentration of chlorophyll at the sea surface. Therefore, the correlation between $R_{rs}(443)$ and the depth of the *DCM* (Z_{DCM}) is relatively strong, as Z_{DCM} tends to be deeper when there is less chlorophyll at the sea surface (Morel and Berthon 1989).

At the sea surface, the surface reflectance at blue wavelengths typically increases as the biomass of most phytoplankton decreases (thus reducing light absorption). When the abundance of only *Prochlorococcus* cells is plotted against $R_{rs}(488)$ (sr^{-1}), we see that R_{rs} decreases with the increase in cell abundance, but after a certain threshold is reached, further decrease in R_{rs} is independent of *Prochlorococcus* cell concentrations, suggesting that the presence of phytoplankton other than *Prochlorococcus* might determine changes in R_{rs} below the threshold (**Fig. 4.1**). The underwater light field is determined by K_dPAR in the model, which directly influences Z_{DCM} and the vertical distribution of

Prochlorococcus cells. Light availability in the water column is also a function of the *DL*, which governs the daily-integrated irradiance at the sea surface, and θ_s, which dictates the pathlength of light per unit vertical distance within the water column (i.e. lower θ_s lead to a longer light path and lower light attenuation).

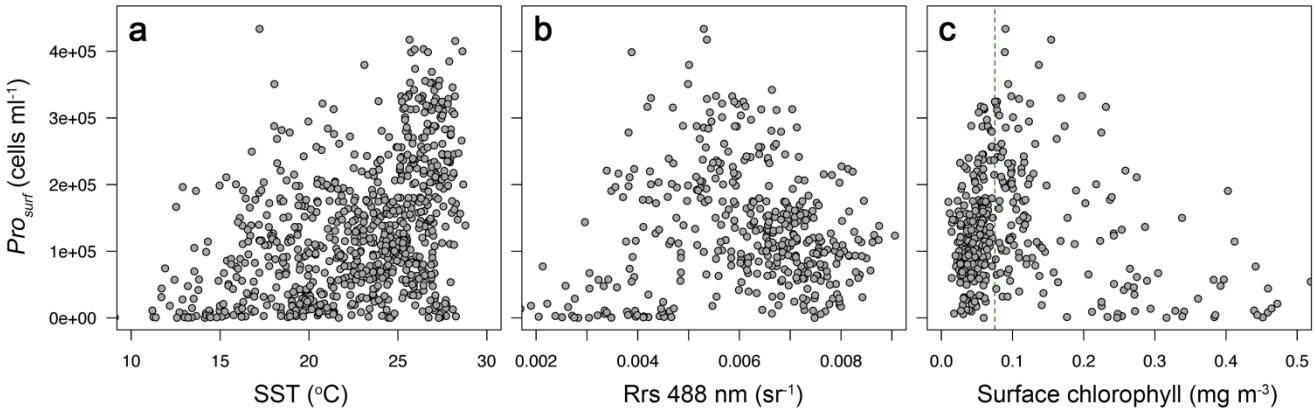


Figure 4.1. Relationship between *Prochlorococcus* cell abundance at the sea surface (Pro_{surf}) and: **a)** sea surface temperature (*SST*), **b)** remote sensing reflectance at 448 nm ($R_{rs}(488)$) and **c)** surface chlorophyll concentration on AMTs 12 to 24. The dashed line indicates the chlorophyll threshold (0.075 mg ml^{-1}) used to delineate the subtropical gyres.

Multilinear relationships between each parameter (K_dPAR, Z_{DCM}, Pro_{surf}, and Pro_{max}) and the above-mentioned environmental variables were analysed in a compilation of data from 13 Atlantic Meridional Transect (AMT) cruises (AMT 12-24) (**Fig. 4.2, Table 4.1**), which cover a broad area of the Atlantic Ocean. For each cruise, vertical profiles of temperature, chlorophyll fluorescence, and downwelling PAR (British Oceanographic Data Centre - BODC) were measured alongside flow-cytometric *Prochlorococcus* cell counts. Details of the flow-cytometric analysis, the calculation of *in-situ* variables (K_dPAR' and Z_{DCM}, where the prime denotes *in-situ* data), and programming languages and packages used for all calculations and data management are described in **section 4.2.5**. Remote-sensing reflectance data were acquired from matching 8-day composites satellite imagery (Ocean Color, NASA 2014).

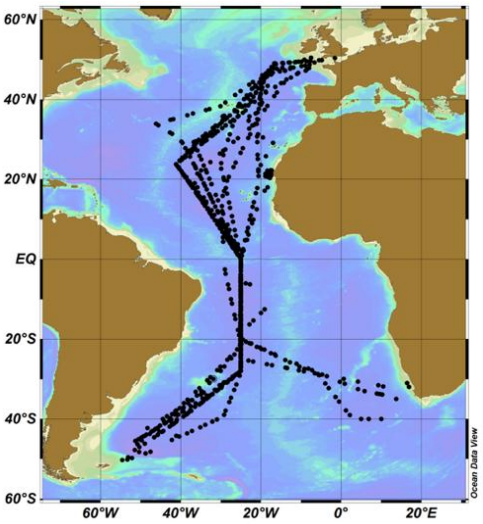


Figure 4.2. Transects of the 13 AMT cruises used to create the empirical model to predict the abundance of *Prochlorococcus* cells.

Table 4.1. AMT Cruises used in this study and corresponding dates.

cruise	dates		
AMT 12	12.05.2003	-	17.06.2003
AMT 13	17.06.2003	-	14.10.2003
AMT 14	26.04.2004	-	2.06.2004
AMT 15	19.09.2004	-	29.10.2004
AMT 16	19.05.2005	-	29.06.2005
AMT 17	15.10.2005	-	28.11.2005
AMT 18	3.10.2008	-	10.11.2008
AMT 19	13.10.2009	-	1.12.2009
AMT 20	12.10.2010	-	25.11.2010
AMT 21	29.09.2011	-	14.11.2011
AMT 22	10.10.2012	-	24.11.2012
AMT 23	7.10.2013	-	8.11.2013
AMT 24	21.09.2014	-	6.11.2014

Table 4.2. AMT cruises used to generate models to calculate the light attenuation coefficient K_dPAR, depth of the deep chlorophyll maximum Z_{DCM}, *Prochlorococcus* cell abundance at surface Pro_{surf}, and at the deep maximum Pro_{max}.

variable	AMT cruises for parameterization	AMT cruises for validation
K_dPAR	20 , 21 , 22 , 23 , 24	12 - 20
Z_{DCM}	12 , 13 , 17 , 18 , 20 , 22 , 24	14, 15, 16, 19, 21, 23
Pro_{surf}	12 , 13 , 17 , 18 , 20 , 22 , 24	14, 15, 16, 19, 21, 23
Pro_{max}	12 , 13 , 17 , 18 , 20 , 22 , 24	14, 15, 16, 19, 21, 23

Based on a subset of AMT cruises (**Table 4.2**), henceforth called *subdataset*, a group of variables was selected to predict each parameter using the backward stepwise selection method in multilinear regressions (Venables and Ripley 2002). The *subdataset* was randomly resampled allowing repetition of random data to generate the same number of observations as the original *subdataset* (Monte-Carlo test with 2000 bootstrap permutations). In each *subdataset*, the multilinear relationship between the response and the selected explanatory variables was assessed, and algorithm coefficients computed (Brewin et al. 2015). The mean of each coefficient was used in the predictive algorithms. Mean coefficients in the model equations and their standard deviations (σ) are listed in **Table 4.3**. Other variables were initially included such as mixed-layer depth, stratification index ($SST - T_{200}$) (de Boyer Montégut et al. 2004), and the downwelling irradiance (PAR) at the sea surface. These variables were excluded both using the backward stepwise selection method, and using the Akaike Information Criteria (AIC) to select the equation with the best fit to the response variable.

Table 4.3. Parameters and coefficients used in equations [4.1-4.8] and their standard deviations (σ).

Output	Input (s)	Equation	Parameter	Parameter value	Parameter σ
K_dPAR		[4.11]	intercept	0.776×10^{-1}	0.020×10^{-1}
	$R_{rs}(443)$	[4.11]	slope	-3.1673×10^{0}	0.195×10^{0}
Z_{DCM}		[4.12]	intercept	1.241×10^{1}	0.786×10^{1}
	$R_{rs}(443)$	[4.12]	$slope_1$	1.021×10^{4}	0.066×10^{4}
	θ_s	[4.12]	$slope_2$	2.227×10^{-1}	2.381×10^{-1}
Pro_{surf}	SST	[4.3-4.5]	a_3	3.254×10^{4}	0.030×10^{4}
	$R_{rs}(488)$	[4.3-4.5]	b_3	9.762×10^{7}	0.104×10^{7}
	DL	[4.3-4.5]	c_3	-2.080×10^{4}	0.043×10^{4}
	T_{200}	[4.3-4.5]	d_3	-2.117×10^{4}	0.029×10^{4}
	$SST, R_{rs}(488)$	[4.3-4.5]	e_3	-4.421×10^{6}	0.041×10^{6}
Pro_{max}		[4.7]	a_7	-1.153×10^{5}	0.194×10^{5}
	Z_{DCM}	[4.7]	b_7	1.837×10^{3}	0.014×10^{3}
	Pro_{surf}	[4.7]	c_7	2.951×10^{-1}	0.087×10^{-1}

4.2.2 *Prochlorococcus abundance predicted using ocean observables*

K_dPAR, Z_{DCM}, Pro_{surf}, and Pro_{max} were estimated based on their empirical relationships with six environmental variables: sea-surface temperature (*SST*), remote sensing reflectance at 443 ($R_{rs}(443)$) and 488 nm ($R_{rs}(488)$), and the temperature at the depth of 200m (T_{200}), the daylength (*DL*) and the solar zenith angle at noon (θ_s). Sea surface temperature (*SST*) and remote sensing reflectance at 443 ($R_{rs}(443)$) and 488 nm ($R_{rs}(488)$) acquired by the satellite Aqua-MODIS were provided by the NASA Ocean Color group (NASA 2014). Monthly climatological data of water temperature at 200 metres depth (T_{200}) (Hosoda et al. 2008) was extracted from ARGO vertical temperature profiles. Satellite and ARGO data products were re-gridded to 4-by-4 km resolution, and every grid cell was used as input data to the *Prochlorococcus* cell abundance model. The workflow of all calculations, from satellite input variables, through derived input variables, to the final product of *Prochlorococcus* cell abundance integrated in the water column, is displayed in **Fig. 4.3**, with variables and their acronyms listed in **Table 4.4**. Details on how the empirical formulas were derived and validated for the calculation of K_dPAR, Z_{DCM}, *DL*, and θ_s are described in **section 4.2.3**.

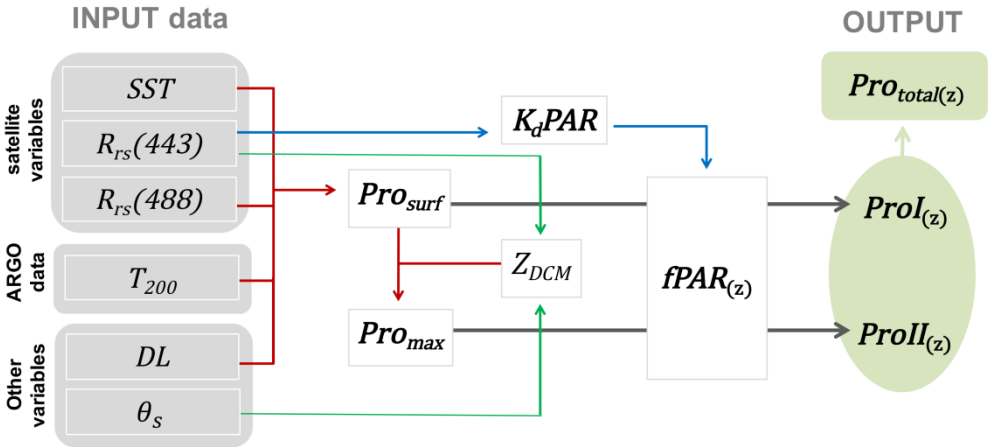


Figure 4.3. Flowchart of computations used to calculate the cell abundance of *Prochlorococcus*. Variable acronyms are described in **Table 4.4**.

Table 4.4. List of acronyms used in this chapter (input variables used in the predictive model of *Prochlorococcus* cell abundance).

Acronym	variable	units	source
SST	Sea surface temperature	^{o}C	a
Rrs_{443}	Remote sensing reflectance at 443 nm	sr^{-1}	a
Rrs_{488}	Remote sensing reflectance at 488 nm	sr^{-1}	a
T_{200}	Temperature at the depth of 200 m	^{o}C	b
DL	Day length	hours	c
θ_s	Solar zenith angle at noon	degrees	d
K_dPAR	Calculated attenuation coefficient for the photosynthetically active radiation	m^{-1}	f
K_dPAR'	Measured attenuation coefficient for the photosynthetically active radiation	m^{-1}	e
DCM	Deep chlorophyll maximum		
DPM	Deep *Prochlorococcus* maximum		
Z_{DCM}	Calculated depth of the deep chlorophyll maximum	metres	f
Z_{DCM}'	*In situ* depth of the deep chlorophyll maximum	metres	f
$fPAR_{(z)}$	Fractional PAR (proportion of surface PAR) at depth z	%	f
Pro_{surf}	Calculated *Prochlorococcus* cell abundance at the surface	cells ml^{-1}	f
Pro_{surf}'	*In situ Prochlorococcus* cell abundance at the surface	cells ml^{-1}	f
Pro_{max}	*Prochlorococcus* cell abundance at the DPM	cells ml^{-1}	f
ProI	Calculated cell abundance of *Prochlorococcus* distributed over depth near the surface	cells ml^{-1}	f
ProII	Calculated cell abundance of *Prochlorococcus* distributed over depth near the DPM	cells ml^{-1}	f
$Pro_{total(z)}$	Calculated total *Prochlorococcus* cell abundance distributed over depth	cells ml^{-1}	f
Pro_{int}	Calculated cell abundance of *Prochlorococcus* integrated in the surface 200 meters of the water column	cells m^{-2}	f

a. Aqua-MODIS, Ocean Color, NASA (2014); **b.** ARGO dataset (http://argo.jcommops.org); **c.** Behrenfeld and Falkowski (1997); **d.** Cooper (1969); **e.** Kirk (2011); **f.** This work

The two subpopulations of *Prochlorococcus*, $ProI_{(fPAR)}$ and $ProII_{(fPAR)}$, are expressed as a function of *fPAR* (**Fig. 4.4b,e,h**). The fractional PAR at depth ($fPAR_{(z)}$) was calculated using K_dPAR values in equation [4.1] from Kirk (2011):

$$fPAR_{(z)} = \exp(-K_dPAR \;\; z) \; . \qquad [4.1]$$

where *z* is depth in metres.

$ProI_{(fPAR)}$ is estimated based on the assumptions that these cells occur at depths where *fPAR* >= 1% (0.01), and that this sub-population is adapted to high light, with an

E_k = 2.5% (where E_k is the light saturation index for the accumulation of cells). $ProI_{(\mathrm{fPAR})}$ is calculated using equation [4.2]:

$$ProI_{(\mathrm{fPAR})} = Pro_{surf} \left[1 - \exp\left(- \frac{fPAR_{(z)} - 0.01}{0.025} \right) \right], \quad [4.2]$$

with $ProI_{(\mathrm{fPAR})}$ = 0 if $fPAR$ <= 0.01 (1%). Photoinhibition of cell accumulation (i.e. the photoinhibition component of a PE curve equation in Platt et al. (1980)) is not exhibited by this sub-population, thus the maximum cell concentration of $ProI_{(fPAR)}$ is equal to the concentration of *Prochlorococcus* cells at the high light intensities found at the sea surface (Pro_{surf}). Pro_{surf} is calculated using equations [4.3-4.5]

$$Pro_{surf} = n_0 \left[a_3\, SST + b_3\, R_{rs}(488) + c_3\, DL + d_3\, T_{200} + e_3 \left(SST \times R_{rs}(488) \right) \right], \quad [4.3]$$

$$n_1 = 1 - \left(\frac{17 - SST}{17 - 13} \right), \quad [4.4]$$

and

$$n_2 = 1 - \left(\frac{0.004 - Rrs_{488}}{0.004 - 0.001} \right), \quad [4.5]$$

where a_3, b_3, c_3, d_3, and e_3 are empirical coefficients listed in **Table 4.3**, $n_0 = n_1$ if $SST < 17^{o}$C, $n_0 = n_2$ if $R_{rs}(488) < 0.004$ and $SST - T_{200} < 10$, and $n_0 = 1$ otherwise. The model assumes that *Prochlorococcus* is restricted to warm waters, thus cell abundance progressively decreases as sea surface temperatures (*SST*) fall below 17^{o}C, and become absent where *SST* is less than 13^{o}C (equation [4.4]) (see **Fig. 4.1a**). The model also adopts a widely-held view that *Prochlorococcus* cells are absent in productive waters with high surface chlorophyll concentrations (thus low remote sensing reflectance (equation [4.5])), which is shown by the gradual decrease in cell abundance once $R_{rs}(488)$ is lower than 0.004 (see **Fig. 4.1b**).

To estimate the abundance of $ProII_{(\mathrm{fPAR})}$ in equation [4.6], a photoinhibition component is included:

$$ProII_{(\mathrm{fPAR})} = Pro_{max} \left[1 - \exp\left(-\frac{fPAR_{(z)}}{0.005}\right)\right] \exp\left(-\frac{fPAR_{(z)}}{0.1}\right). \quad [4.6]$$

$ProII_{(\mathrm{fPAR})}$ cells are adapted to lower light intensities (E_k = 1%), reaching a subsurface maximum cell concentration represented by Pro_{max}, which in turn is calculated using equation [4.7]

$$Pro_{max} = a_7 + b_7 Z_{DCM} + c_7 Pro_{surf}, \quad [4.7]$$

where Z_{DCM} is the depth of the deep chlorophyll maximum, and a_7, b_7, and c_7 are coefficients listed in **Table 4.3**.

After computing the depth (in metres) associated with a particular *fPAR* using equation [4.8] from Kirk (2011),

$$z = -\frac{\ln\left(fPAR_{(z)}\right)}{K_d PAR}, \quad [4.8]$$

the total *Prochlorococcus* cell abundance at any depth *z* ($Pro_{total(z)}$) is determined as the sum of $ProI_{(z)}$ and $ProII_{(z)}$ in equation [4.9]:

$$Pro_{total\,(z)} = ProI_{(z)} + ProII_{(z)}, \quad [4.9]$$

and then integrated over the top 200 metres of the water column (Pro_{int}) in equation [4.10]:

$$Pro_{int} = \int_{z=0}^{200} Pro_{total(z)}\, dz. \quad [4.10]$$

Examples of *Prochlorococcus* cell abundance profiles ($Pro_{total(z)}$) observed *in situ* and predicted by the model as the sum of *ProI* and *ProII* within the North and South Atlantic Gyres and in the gyre periphery (areas outside the gyre limits, where surface chlorophyll > 0.075 mg ml^{-1}, and also outside the ECZ, where SST < 25^{o}C) are shown in **Fig. 4.4**.

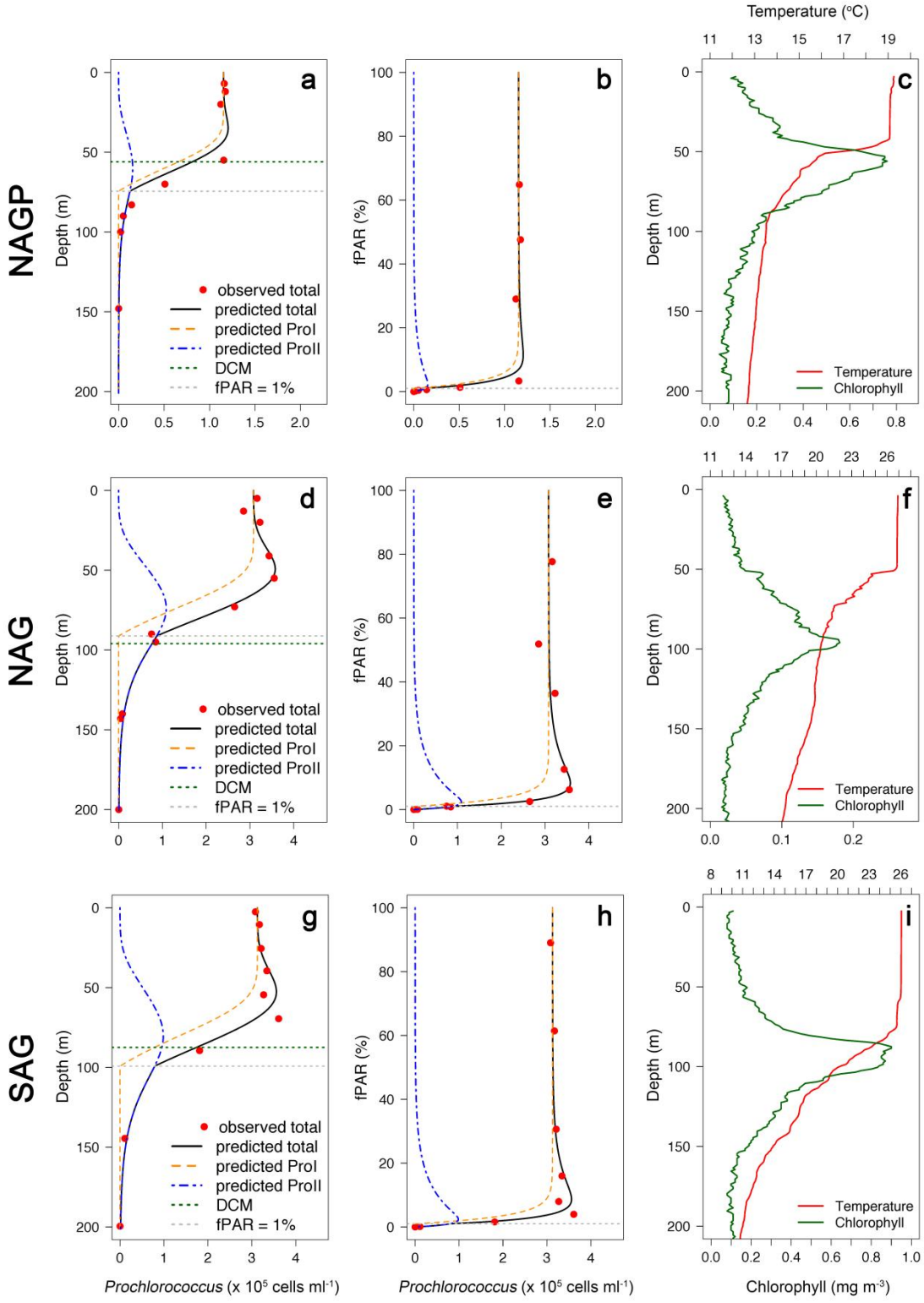


Figure 4.4. Vertical profiles of observed and estimated *Prochlorococcus* cell abundances **a,d,g)** over depth and **b,e,h)** over the fractional PAR *fPAR*, and **c,f,i)** profiles of temperature and chlorophyll from CTD casts at a site in **a-c)** the North Atlantic Gyre periphery (NAGP: 28°N, 35°W), **d-f)** inside the North Atlantic Gyre (NAG: 22°N, 50°W), and **g-i)** the South Atlantic Gyre (SAG: 20°S,20°W). *In situ* observations are represented by red dots, predicted profiles of *ProI* by the orange dashed line, predicted profiles of *ProII* by the blue dashed line, and predicted profiles of total *Prochlorococcus* abundance by the solid black line. Data from AMT 24 (2014).

4.2.3 *Additional equations used in the model*

This section describes the equations used to calculate K_dPAR, Z_{DCM}, DL, and θ_s , which are input variables in the *Prochlorococcus* abundance model.

K_dPAR was estimated from satellites using equation [4.11]:

$$K_dPAR = 0.0776 - 3.1673\, R_{rs}(443)\,, \qquad [4.11]$$

derived from the correlation between *in-situ* K_dPAR (K_dPAR') and $R_{rs}(443)$ ($R^2 = 0.75$). In clear waters, such as the subtropical gyres where *Prochlorococcus* is most abundant and K_dPAR is the lowest, equation [4.11] provided better estimates of K_dPAR than those using equation [9′] from Morel et al. (2007) (**Fig. 4.5**). As *Prochlorococcus* is dominant in clear waters, it is more important to have better K_dPAR estimates where K_dPAR is low than in productive waters where K_dPAR is high. Considering that, we chose to use equation [4.11] of the present work to predict K_dPAR.

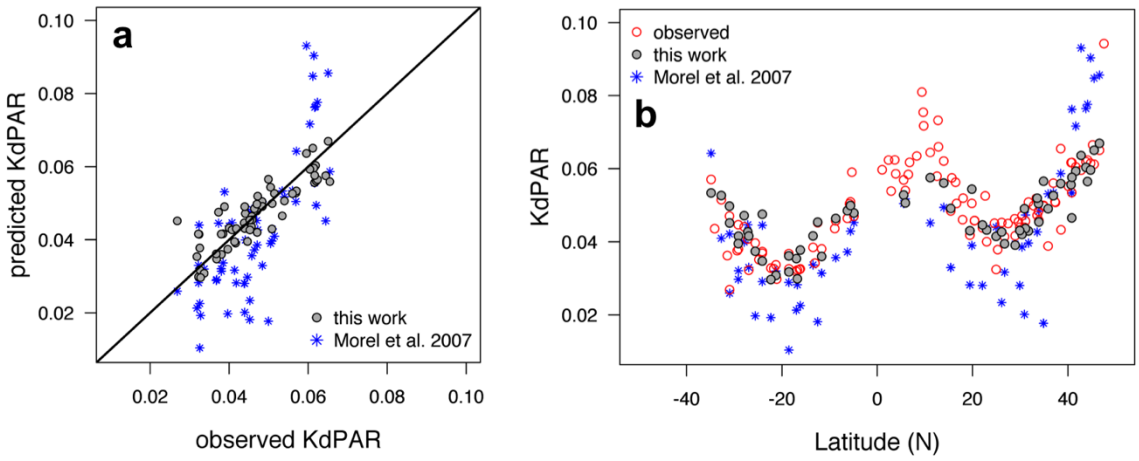


Figure 4.5. a) Comparison between observed attenuation coefficient for photosynthetically active radiation (K_dPAR') from CTD PAR profiles *versus* predicted K_dPAR using equation [4.11] of the present work (red) and using equation [9′] from Morel et al. 2007 (blue); **b)** Observed and predicted K_dPAR across the Atlantic Ocean (AMTs 20 to 24).

The depth of the deep chlorophyll maximum (Z_{DCM}) was determined in equation [4.12]:

$$Z_{DCM} = 12.41 + 10210\, R_{rs}(443) - 0.2227\, \theta_s\,, \qquad [4.12]$$

and used to estimate Pro_{max} (maximum cell abundance of the *ProII* profile). Equation [4.12] was derived from the multi-linear relationship between observed Z_{DCM} (Z_{DCM}'), Rrs_{443} and θ_s (r^2 = 0.73; **Fig. 4.6**) in the selected cruises listed in **Table 4.2**.

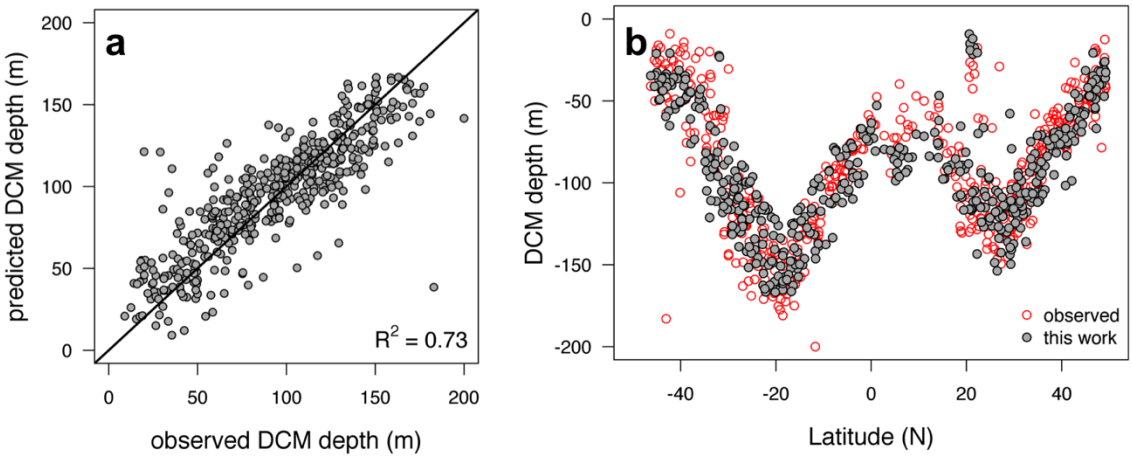


Figure 4.6. a) Comparison between observed versus predicted depth of the deep chlorophyll maximum (Z_{DCM}) using equation [4.12] of this work; **b)** Observed and predicted Z_{DCM} across the Atlantic Ocean (AMTs 12 to 24). For each CTD cast, observed Z_{DCM} was determined as the depth of the maximum chlorophyll concentration measured using the CTD fluorometer.

The daylength (*DL*) was calculated according to (Behrenfeld and Falkowski 1997), using equation [4.13]:

$$DL = \left[\left(-1\, \cos\frac{Jday}{57.295}\ \left(\sin\frac{Lat}{57.295}\right)^3\right) + 1\right] 12 \qquad [4.13]$$

where *Jday* is the Julian day, and *Lat* is the latitude (degrees N). The absolute solar zenith angle at noon was derived from the sun declination (Cooper 1969), calculated using equations [4.14] and [4.15]:

$$\delta' = \left[23.45\ \sin\left(\frac{360}{365}\ (284 + Jday)\right)\right]\left[\frac{\pi}{180}\right] \qquad [4.14]$$

$$\theta_s = Lat - \delta' \quad [4.15]$$

where δ' is the sun declination (degrees), and θ_s is the solar zenith angle at noon (degrees).

4.2.4 *Delineation of the area of subtropical gyres*

Subtropical gyres are vast oligotrophic areas, usually in the centre of ocean basins. These areas present very low chlorophyll concentrations at the sea surface due to the limitation of nutrients, as they are remote to any nutrient source and, usually, the pycnocline is deep and strong, slowing the transport of nutrients from depth to the euphotic zone.

As the depth of the nutricline commonly coincides with the depth of the deep chlorophyll maximum (Z_{DCM}) (**Fig. 4.7**), Z_{DCM} can be used as a proxy for nutrient supply from depth in these areas.

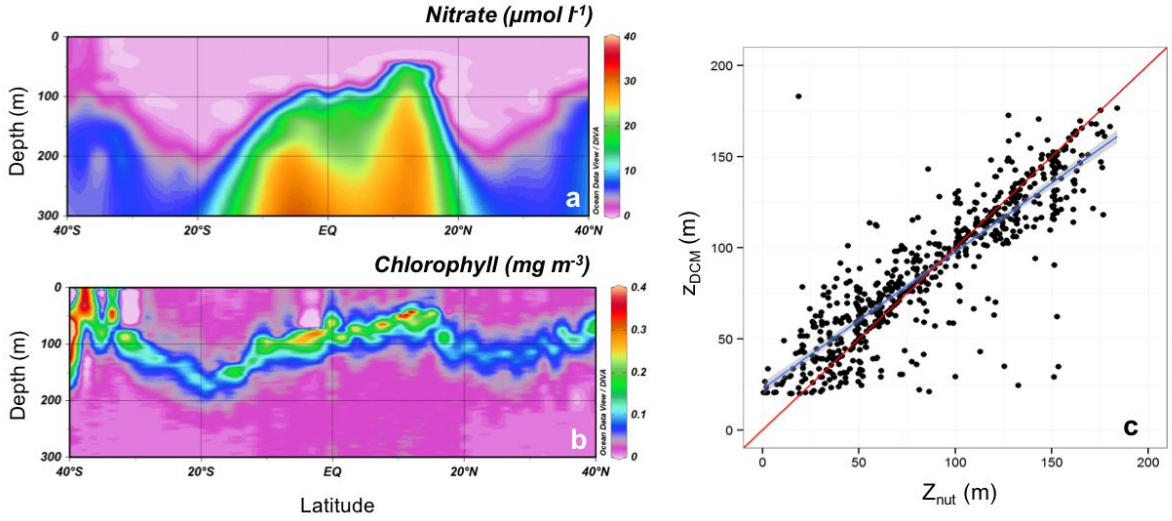


Figure 4.7. Latitudinal section of the Atlantic Ocean, showing profiles of **a)** the concentration of nitrate and **b)** the concentration of chlorophyll. Figure **c)** shows the relationship between the depth of the nutricline (Z_{nut}) and the depth of the deep chlorophyll maximum (Z_{DCM}), where the red line shows the 1:1 relationship, and the blue line shows the linear regression between Z_{nut} and Z_{DCM}. Data for figs. **(a)** and **(b)** from AMT 18 (1998), and data for fig. **(c)** from AMTs 12 to 24, provided by the British Oceanographic Data Centre (BODC).

Some criteria are commonly used to delineate the ocean gyres, such as:

a) Sea surface chlorophyll ≥ 0.07 mg m^{-3} (McClain et al. 2004);

b) The depth of the deep chlorophyll maximum (Z_{DCM}) ≥ 80 metres (Zubkov et al. 2000b);

c) The temperature at 100 metres depth ≥ 17°C (Zubkov et al. 2000b).

Considering the relationship between Z_{DCM} and sea-surface chlorophyll (*SSChlo*) found in our dataset of 12 AMT cruises (**Fig. 4.8**), we established a *SSChlo* threshold of 0.075 mg m^{-3} to delineate the area of the ocean gyres.

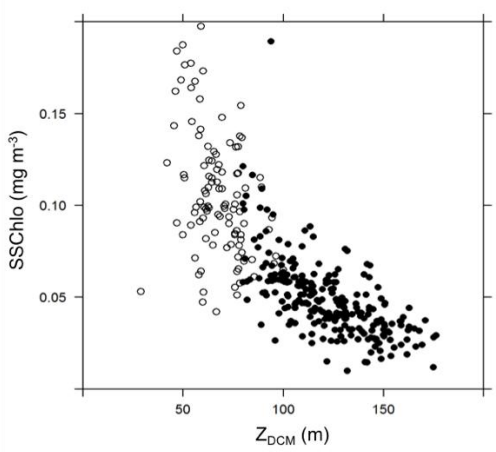


Figure 4.8. Relationship between the depth of the deep chlorophyll maximum (Z_{DCM}) and the sea-surface chlorophyll (*SSChlo*). Black dots show locations where Z_{DCM} ≥ 80 metres. Data from AMTs 12 to 24, provided by the British Oceanographic Data Centre (BODC).

4.2.5 *In-situ measurements of environmental variables*

The AMT dataset was provided by the British Oceanographic Data Centre – BODC, except flow cytometric picoplankton counts on AMTs 23 and 24, which were conducted by the author of this thesis. Data on remote sensing reflectance at 443 ($R_{rs}(443)$) and 488 nm ($R_{rs}(488)$) were extracted from match ups between the stations location and date and 8-day composite images (4-by-4 km resolution) acquired by the satellite Aqua-MODIS, provided by the NASA Ocean Color group (NASA 2014).

4.2.5.1 *Flow cytometric picoplankton cell counts*

Prochlorococcus cell counts were determined by fixing 0.8ml water samples using paraformaldehyde, and quantifying cells in these samples using a FACSCalibur (Becton Dickinson) flow cytometer. On the Atlantic Meridional Transect (AMT) cruises 12, 13, 16, 18, 19, 20, and 21, *Prochlorococcus* populations were determined based on their autofluorescence and right-angle light scatter (RALS) in unstained samples analysed following the method described in Heywood et al. (2006). On AMTs 14, 15, 17, 22, 23, and 24, samples were stained with 1% commercial stock solution of SYBR Green 1 (Molecular Probes, Inc.) in Milli-Q water mixed with 300mM tripotassium citrate (24.5mM final concentration), immediately following fixation (Marie et al. 1999; Zubkov et al. 2007). *Prochlorococcus* populations were determined using the cells' green fluorescence and right-angle light scatter, and yellow-green 0.5 and 1.0 μm reference beads were used as an internal standard for both fluorescence and flow rates (Zubkov and Burkill 2006).

4.2.5.2 *Calculation of in-situ variables*

In situ Z_{DCM} (Z_{DCM}') was defined as the depth at which the peak in chlorophyll (red) fluorescence was observed in each profile, using a SeaBird fluorometer mounted on a CTD rosette. The *in-situ* attenuation coefficient for PAR (K_dPAR') was calculated from profiles of downwelling PAR measured using a SeaBird CTD PAR sensor, according to equation [4.16] from Kirk (2011):

$$K_dPAR' = -d \ln E_d / dz \qquad [4.16]$$

where E_d is the downwelling irradiance (PAR), and z is the depth in metres.

K_dPAR' was used to calculate the *in situ* fractional PAR at depth ($fPAR_{(z)}'$), or the percent value of the surface irradiance at depth, in equation [4.17] from Kirk (2011):

$$fPAR_{(z)}' = \exp(-K_dPAR' \; z) \quad [4.17]$$

The compilation, processing, and analysis of the *in situ* dataset were performed using R packages *stats* (R Core Team 2017), *ggplot2* (Wickham 2009), *lattice* (Sarkar 2008) and *devtools* (Wickham and Chang 2016). Satellite data was assessed using the R packages *ncdf4* (Pierce 2015), *chron* (James and Hornik 2017), *fields* (Nychka et al. 2015), and *raster* (Hijmans 2016).

4.3 Results

4.3.1 *Model validation*

The derived parameters of the model (Z_{DCM}, K_dPAR, Pro_{surf}, Pro_{max}) that describe the shape of the abundance profile and the final products $Pro_{total(z),}$ and Pro_{int} were validated using 13 AMT cruises, which cover a broad swath of the Atlantic basin, and a global dataset of phytoplankton counts (http://doi.pangaea.de/10.1594/PANGAEA.777385), including data from the ocean time-series studies BATS (Bermuda Atlantic Time-Series Study) and HOTS (Hawaii Ocean Time-Series), as well as data collected from oceanographic cruises covering the global ocean (Buitenhuis et al. 2012).

Model estimates were compared with *in-situ* observations using the approach proposed by Brewin et al. (2015), which includes four statistical metrics: root mean square error (Ψ); average bias (δ); centre-pattern (or unbiased) root mean square error (Δ); and the adjusted coefficient of determination (r^2). For this, we assumed variables

present a normal frequency distribution in the natural environment. Results of the statistical tests are summarised in **Table 4.5**. The comparison between observed and predicted K_dPAR and Z_{DCM} are shown in **Figs. 4.5** and **4.6**, respectively.

When using *in-situ* observations of the derived parameters as inputs for the model, particularly Pro_{surf}' and Z_{DCM}' (in which case equations [4.3-4.5], and [4.12] are excluded), our model robustly predicts the vertical distribution of *Prochlorococcus* cells in the water column (i.e. $Pro_{total(z)}^{1}$, r^2 = 0.84, **Figs. 4.9b, 4.10a**) and, consequently, produces reasonable estimates of cell concentrations integrated in the top 200 metres of the water column (i.e. Pro_{int}^{1}, r^2 = 0.85, **Fig. 4.11**). However, when using remote-sensing environmental variables as inputs to estimate the derived parameters (full model from remote-sensing data), the predictive skill of the model to $Pro_{total(z)}$ and Pro_{int} decreases to r^2 = 0.58 and r^2 = 0.48, respectively (**Table 4.5**; **Fig. 4.9c**, **Fig. 4.12a,b**). This increase in the error is primarily caused by the difficulty in estimating Pro_{surf} from satellite (r^2 = 0.50; **Fig. 4.12c,d**; **Fig. 4.10b**). The reduction in performance may also be attributed to the nature of comparing observations at vastly different spatial and temporal scales: *in-situ* cell abundance was estimated using a few millilitres of seawater taken at a determined time point where environmental conditions can change in hours or days, whereas satellite data were extracted from 8 day composites and pixels cover an area of 16 km^2, and ARGO data were extracted from climatology (monthly average over 6 years). Overall, the satellite-derived model is negatively biased ($\delta = -0.572 \times 10^{12}$ cells cm^{-2}) and tends to underestimate cell concentrations at most depths (**Fig. 4.9b**). However, the spatial and temporal variability of integrated cell abundance is still well represented (**Fig. 4.12b**).

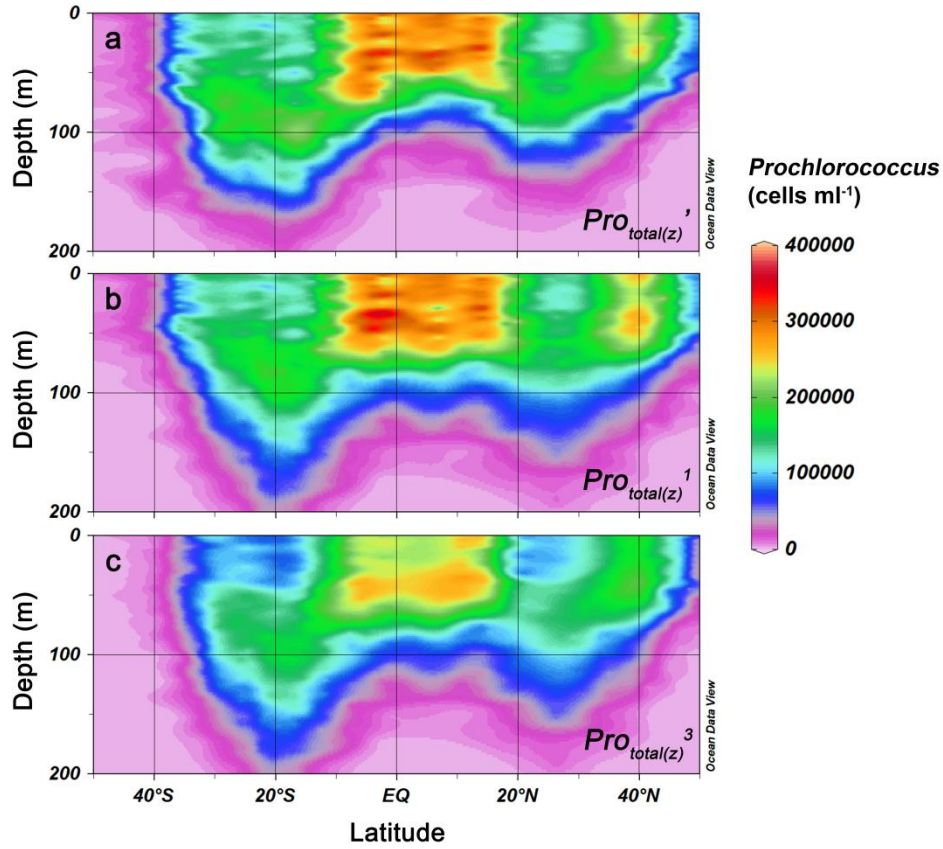


Figure 4.9. Vertical profiles of *Prochlorococcus* cell abundance over depth ($Pro_{total(z)}$) **a)** observed *in situ* on AMTs 12 to 24 ($Pro_{total(z)}$'); **b)** predicted using the partial model with observed inputs of Pro_{surf} and Z_{DCM} (equations [4.1] to [4.15] excluding equations [4.3-4.5] and [4.12]); and **c)** predicted using the full model with remote sensing inputs (equations [4.1-4.15]).

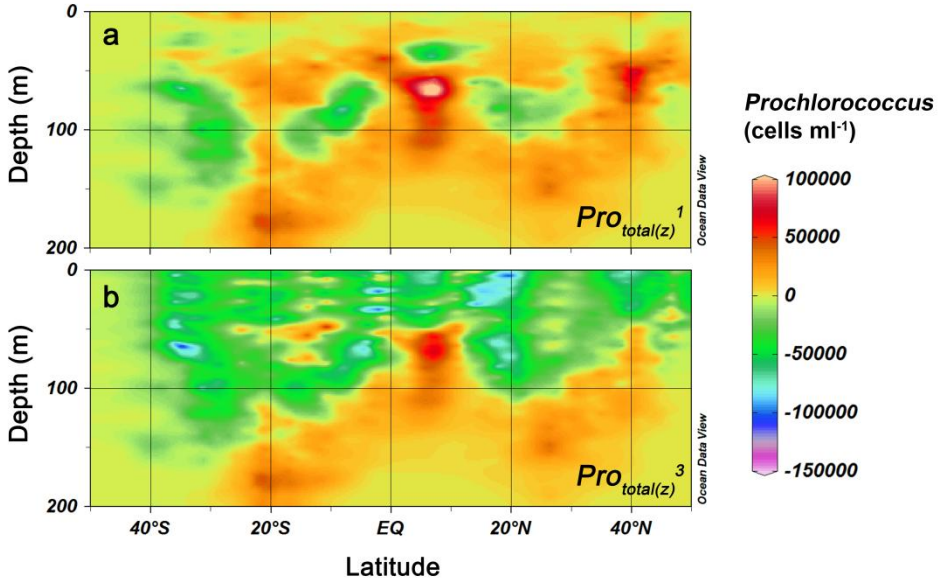


Figure 4.10. Difference (residual) between predicted and observed *Prochlorococcus* cell abundance over depth ($Pro_{total(z)}$) **a)** using the partial model partial model where *in-situ* observations of Z_{DCM}, K_dPAR, and Pro_{surf} are used as inputs to calculate $Pro_{total(z)}{}^{1}$ (excluding equations [4.3-4.5] and [4.12]); and **b)** using the full model with remote-sensing inputs (equations [4.1] to [4.15]).

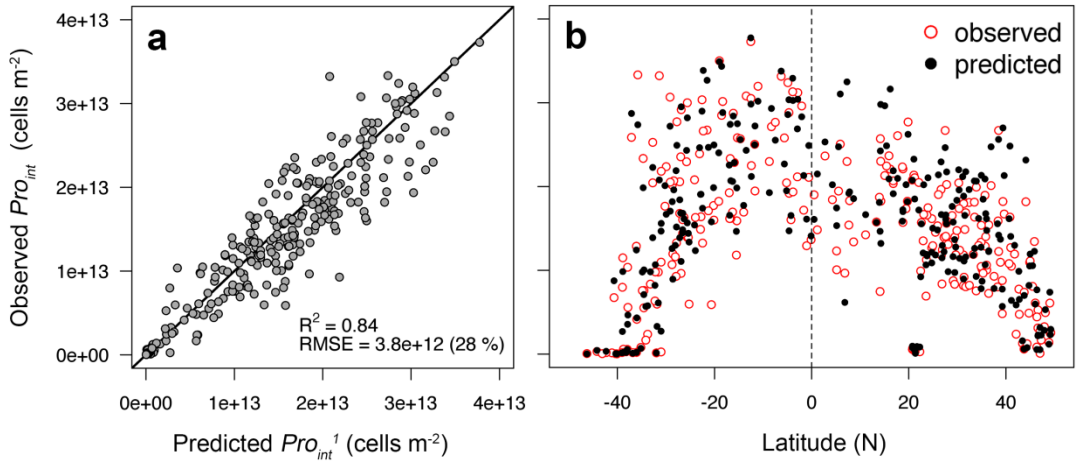


Figure 4.11. a) Comparison between observed and predicted *Prochlorococcus* cell abundance integrated in the water column (Pro_{int}^{1}) using the partial model where *in-situ* observations of Z_{DCM}, K_dPAR, and Pro_{surf} are used as inputs ($Pro_{total(z)}^{1}$ from equations [4.1] to [4.15] excluding equations [4.3-4.5] and [4.12]); **b)** Observed and predicted Pro_{int}^{1} across the Atlantic Ocean (AMTs 12 to 24).

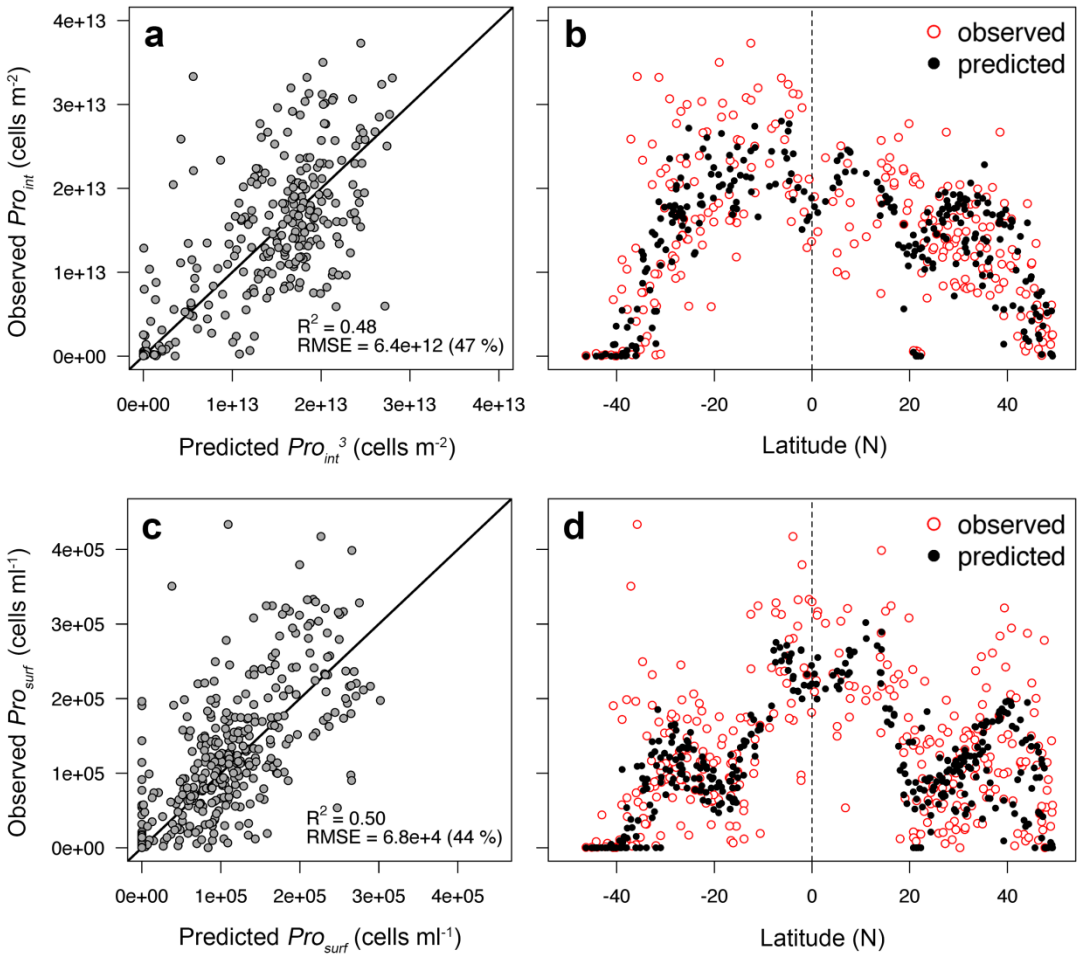


Figure 4.12. a) Comparison between observed and predicted *Prochlorococcus* cell abundance integrated in the water column (Pro_{int}^{3}) using the complete model (equations [4.1] to [4.15] of the present work); **b)** Observed and predicted Pro_{int}^{3} across the Atlantic Ocean (AMTs 12 to 24); **c)** Comparison between observed and predicted *Prochlorococcus* cell abundance at the sea surface (Pro_{surf}) using equations [4.3] to [4.5] of the present work; **d)** Observed and predicted Pro_{surf} across the Atlantic Ocean (AMTs 12 to 24).

Table 4.5. Response variables with their respective root mean square error (Ψ), bias (δ), centre-root (unbiased) mean square error (Δ), and correlation coefficient (r^2) when compared with *in situ* data from 13 AMT cruises (this work), and the PANGAEA dataset (Buitenhuis et al. 2012). Variable definitions are listed in **Table 4.4**.

Variable	Equation	Ψ AMT	δ AMT	Δ AMT	r^2 AMT	Δ PANGAEA	R^2 PANGAEA
K_dPAR	[4.11]	5.136×10^{-3}	-0.321×10^{-3}	0.512×10^{-3}	0.75		
Z_{DCM}	[4.12]	2.084×10^{1}	-0.101×10^{1}	2.081×10^{1}	0.73		
Pro_{max} [1]	[4.7]	5.872×10^{4}	-0.054×10^{4}	5.872×10^{4}	0.44		
$Pro_{total(z)}$ [1]	[4.9]	3.775×10^{4}	-0.361×10^{4}	3.758×10^{4}	0.84		
Pro_{int} [1]	[4.10]	3.682×10^{12}	-1.047×10^{12}	3.529×10^{12}	0.85		
Pro_{max} [2]	[4.7]	5.805×10^{4}	-0.349×10^{4}	5.794×10^{4}	0.40		
$Pro_{total(z)}$ [2]	[4.9]	4.038×10^{4}	-0.479×10^{4}	4.010×10^{4}	0.82	2.800×10^{4}	0.83
Pro_{int} [2]	[4.10]	4.146×10^{12}	-1.214×10^{12}	3.964×10^{12}	0.81	3.914×10^{12}	0.75
Pro_{surf} [3]	[4.3-4.5]	6.551×10^{4}	1.237×10^{4}	6.434×10^{4}	0.50	6.431×10^{4}	0.13
Pro_{max} [3]	[4.7]	6.210×10^{4}	0.297×10^{4}	6.203×10^{4}	0.32		
$Pro_{total(z)}$ [3]	[4.9]	6.176×10^{4}	0.466×10^{4}	6.159×10^{4}	0.58	6.471×10^{4}	0.38
Pro_{int} [3]	[4.10]	6.651×10^{12}	-0.572×10^{12}	6.651×10^{12}	0.48	7.601×10^{12}	0.14

Prochlorococcus cell abundances calculated using:
[1] *in situ* Pro_{surf} (Pro_{surf}') and *in situ* Z_{DCM} (Z_{DCM}');
[2] *in situ* Pro_{surf}' and modelled Z_{DCM} ;
[3] modelled Pro_{surf} and modelled Z_{DCM}.

4.3.2 *Choice of a two-component model*

The two-component model (*ProI* + *ProII*) described in the present work is able to determine a maximum in the abundance of *Prochlorococcus* cells when it occurs at depth (**Fig. 4.4d-h**). The depth of the deep *Prochlorococcus* maximum is henceforth called Z_{DPM}.

In vertical profiles of *Prochlorococcus* cell abundance, Z_{DPM} is often located a few metres above the depth of the deep chlorophyll maximum (Z_{DCM}), particularly in subtropical gyre waters. In the model, this deep *Prochlorococcus* maximum (*DPM*) is not generated from a peak in abundance of *ProI* or *ProII*, but from the sum of these two components. Therefore, Z_{DPM} is located at the depth where the *ProI* and *ProII* co-occur. When the *DCM* is shallower than 60 m, the maximum *Prochlorococcus* abundance in a

profile often occurs at the Z_{DCM} or at the sub-surface chlorophyll maximum because *ProII* is nearly absent (see **Fig. 4.4a-c**).

To test if the component *ProII* (*Prochlorococcus* at depth) is relevant to determine the vertical distribution of *Prochlorococcus* cells, curves of observed total *Prochlorococcus* cell abundance *versus fPAR* were fitted to equation [4.18] at each sampling station:

$$Pro_{total(z)} = Pro_{surf}{}' \left[1 - \exp\left(- \frac{\alpha}{Pro_{surf}{}'} fPAR_{(z)} \right) \right] \qquad [4.18]$$

where $Pro_{surf}{}'$ is the abundance of *Prochlorococcus* cells at the sea surface observed *in situ*, and is considered to be the maximum cell abundance *Prochlorococcus* can reach in a profile. In this equation, the deep maximum in the abundance of *Prochlorococcus* cells is neglected (*ProII* is absent).

To estimate the total *Prochlorococcus* abundance at each depth ($Pro_{total(z)}$) and the abundance of *Prochlorococcus* cells integrated in the surface 200 metres of the water column (Pro_{int}) using satellite observables, $fPAR_{(z)}$ was calculated using equation [4.1], and Pro_{surf} was calculated using equations [4.3-4.5]. The parameter alpha was taken from the fitted curves of *in situ* observations using equation [4.18], then averaged.

The comparison between values of Pro_{int} calculated using the two-component model ($Pro_{total(z)}$ = *ProI* + *ProII*) and the one-component model (where $Pro_{total(z)}$ is calculated using equation [4.18]) is shown in **Fig. 4.13**. The one-component model (r^2 = 0.36) underestimates Pro_{int} in the gyres, especially the South Atlantic gyre, as these are the areas where the deep *Prochlorococcus* maximum is most important and dictates the patterns in integrated cell abundances (**Fig. 4.13a-b**). In these areas, predictions made by the two-component model (r^2 = 0.48) are more accurate (**Fig. 4.13c-d**).

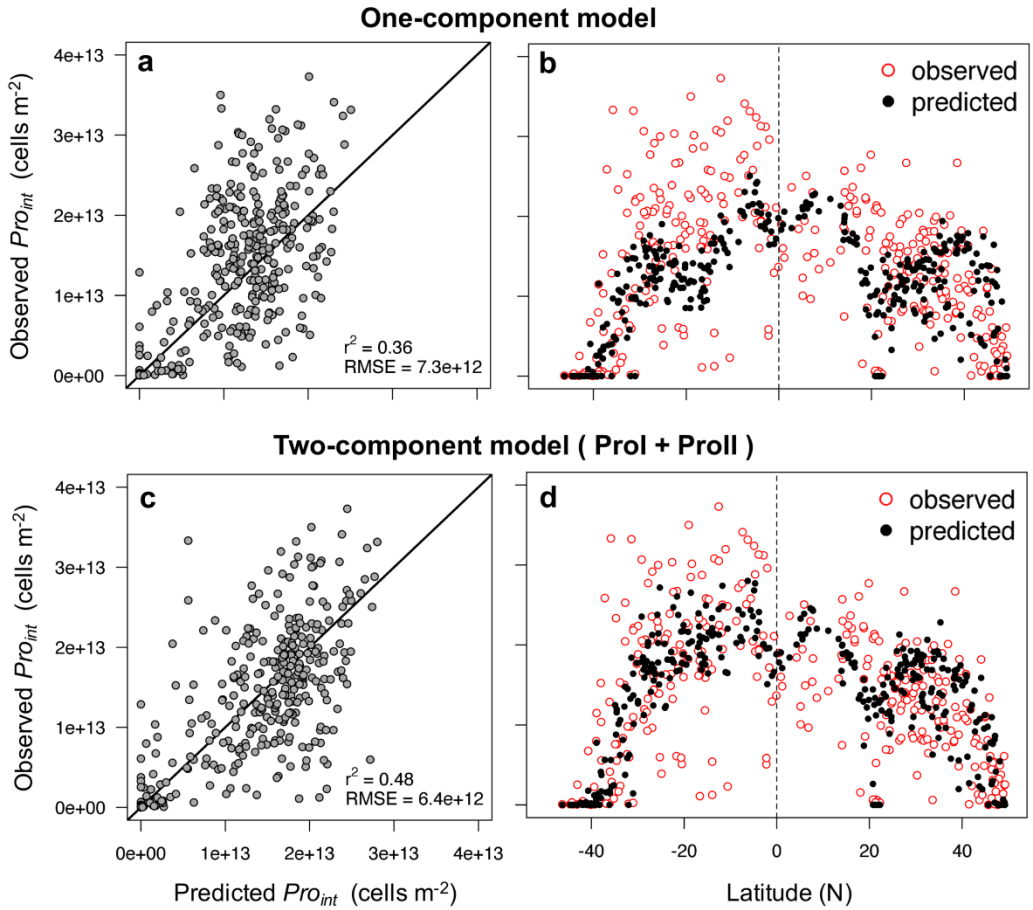


Figure 4.13. a) Comparison between observed and predicted *Prochlorococcus* cell abundance integrated in the water column (Pro_{int}) using the one-component model (equations [4.1-4.5] and [4.8-4.15], replacing equation [4.2] with equation [4.18]); **b)** Observed and predicted Pro_{int} across the Atlantic Ocean using the one-component model (AMT 12 to 24); **c)** Comparison between observed and predicted Pro_{int} using the two-component model (equations [4.1-4.15]); **d)** Observed and predicted Pro_{int} across the Atlantic Ocean (AMT 12 to 24) using the two-component model.

4.3.3 *Model output*

The two-component model estimates a global *Prochlorococcus* standing stock of approximately 3.4×10^{27} cells which equates to a biomass of 171 Mt of carbon (**Table 4.6**) (for 1 Mt = 10^{12} g). Most cells are accumulated within the subtropical gyres and at the Equatorial Convergence Zone (**Fig. 4.14a-c**), and reside within the top 200 metres of the surface ocean (**Fig. 4.4**), with 43% of the cells accumulated on the top 45 metres of the water column, and 57% between the depths of 45 and 200 metres. A marked seasonal

cycle in the global cell stock was observed from 2003 to 2014 (**Fig. 4.15a**), but no significant long-term temporal trend was evident (**Figs. 4.15b**). At the ocean's surface, where the global seasonal signal is strong (**Fig. 4.15c**), a slight decrease in cell abundance was observed from 2003 to 2011, followed by an increase from 2012 to 2014 (**Fig. 4.15d**).

Table 4.6. Predicted *Prochlorococcus* standing stock in the oceans, integrated spatially and vertically at each area. Values were computed using equations [4.1-4.15], with monthly climatology products used as input variables (Ocean Color, NASA 2014), then averaged over the year. Pro_{int}^{3}, Pro_{surf}^{3} and Pro_{max}^{3} were calculated at specific geographic locations within each Atlantic gyre (coordinates in the table).

	Standing stock (cells)	Total carbon* (megatonnes C)	Pro_{int}^{3} (cells m^{-2})	Pro_{surf}^{3} (cells ml^{-1})	Pro_{max}^{3} (cells ml^{-1})
Global	3.4×10^{27}	171			
Atlantic Ocean	7.4×10^{26}	37			
Equatorial Convergence Zone	2.2×10^{26}	11			
ECZ: 2° S , 22° W			1.7×10^{13}	2.2×10^{5}	0.7×10^{5}
North Atlantic Gyre	1.0×10^{26}	5.1			
NAG: 26° N , 50° W			1.6×10^{13}	0.7×10^{5}	1.3×10^{5}
South Atlantic Gyre	1.6×10^{26}	8.2			
SAG: 20° S , 20° W			2.2×10^{13}	1.0×10^{5}	1.7×10^{5}

* using 50 fg C $cell^{-1}$ to convert cell concentrations to carbon units (Bertilsson et al. 2003).

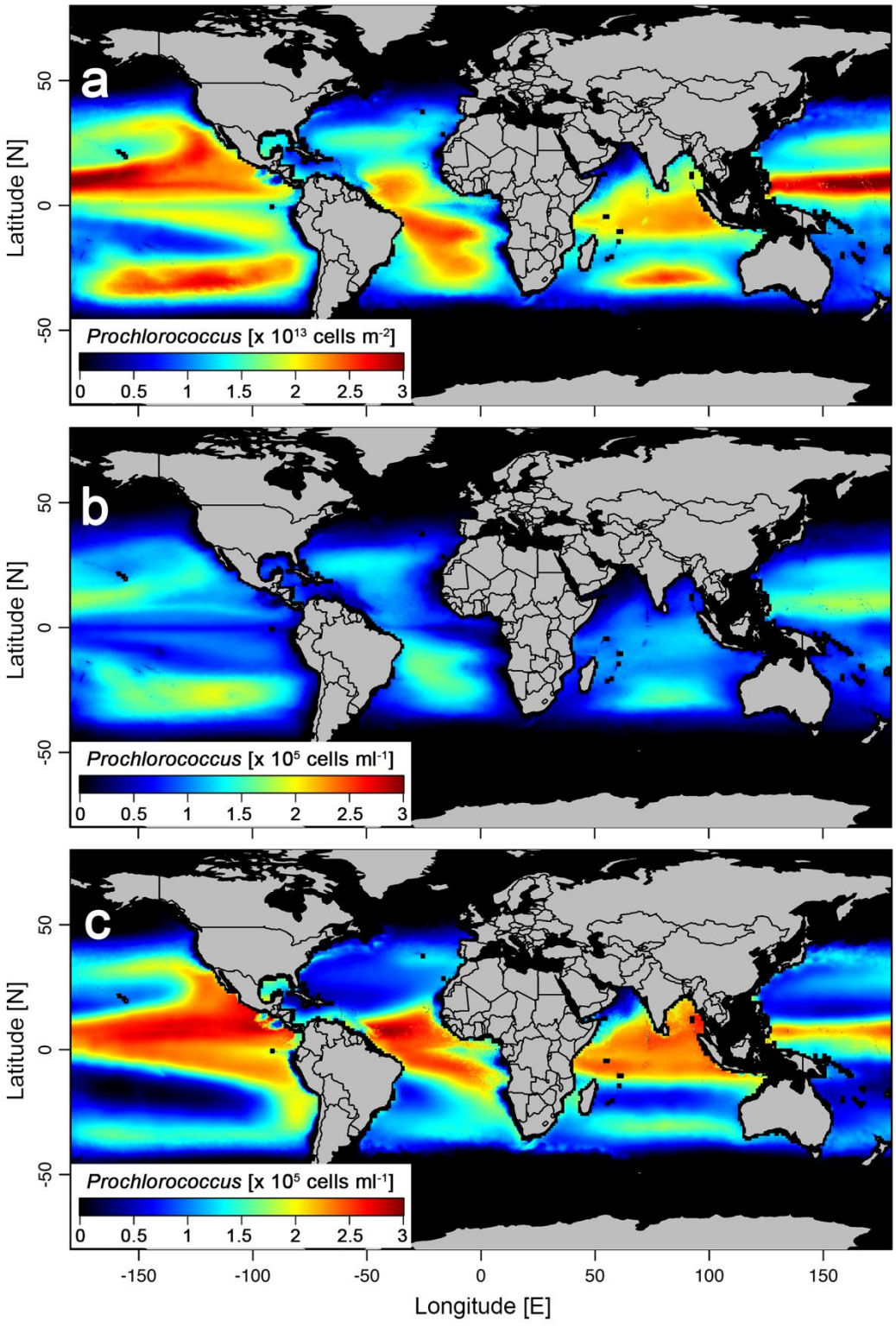


Figure 4.14. Annual mean of **a)** the predicted *Prochlorococcus* cell abundance integrated in the top 200 m of the water column (Pro_{int}^{3}) using the complete model (equations [4.1-4.15]); **b)** predicted maximum *Prochlorococcus* cell abundance at depth (Pro_{max}^{3}) using equation [4.7]; and **c)** predicted *Prochlorococcus* cell abundance at the sea surface (Pro_{surf}^{3}) from equations [4.1-4.5].

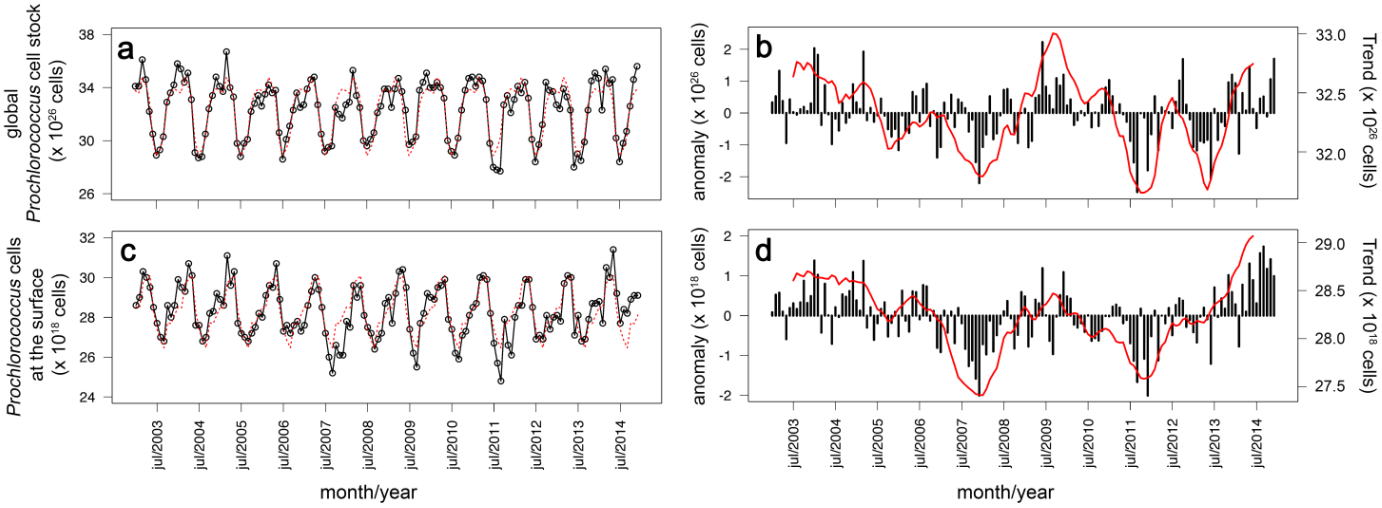


Figure 4.15. Time series of **a)** global horizontally- and vertically-integrated *Prochlorococcus* cell stocks and **c)** horizontally-integrated cell abundance near the ocean surface, with corresponding anomalies and trends **(b,d)**. Values were computed using monthly-composite input variables from the year 2002 to 2014 (NASA Ocean Color 2014). Anomalies were calculated by subtracting the monthly climatology (dashed red lines in figures **(a)** and **(c)**) from the calculated values for each month (black lines in figs. **(a)** and **(c)**). Red lines in figures **(b)** and **(d)** show the moving trend.

The Atlantic basin hosts 7.4×10^{26} *Prochlorococcus* cells (37 Mt of carbon), concentrated mainly in warm stratified waters. When combined, subtropical gyres hold the largest cell concentrations (35%), followed by areas near the Equatorial Convergence Zone (ECZ) which carry 30% of the Atlantic cell stock (**Table 4.6**). The total standing stock in the two Atlantic subtropical gyres varies according to both their areal extent, which expands and contracts seasonally (**Fig. 4.17a-b**), and to their euphotic depth (**Fig. 4.17c-d**), which governs the vertical distribution of cells and the depth range over which they occur. The monthly distribution of *Prochlorococcus* cells in the Atlantic Ocean is shown in **Fig. 4.16**.

To better visualize the seasonal dynamics of these two factors controlling the standing stock of *Prochlorococcus*, we assessed both of these ocean properties for the North and South Atlantic Gyres, hitherto referred to as the NAG and the SAG. In their respective summer months, both the northern and southern gyres expand (**Fig. 4.17e-f**) as

the sea surface temperature and the intensity of the incident irradiance (*PAR*) increase (Aiken et al. 2016). The increase in these two factors foster stratification of the water column that both reduces the supply of nutrients from depth and increases the average light intensity to which phytoplankton cells are exposed (Kirk 2011). The high incident irradiance leads to a reduction in the concentration of *Prochlorococcus* cells at surface (Pro_{surf}) (**Fig. 4.17g-h**), but since the light penetrates deeper in the water column, the growth of *Prochlorococcus* cells (Pro_{max}) is enhanced close to the DCM and higher concentrations are found at the DCM than at the sea surface (**Fig. 4.17i-j**). Thus, the vertical profiles of cell abundance vary over the annual cycle, with Pro_{max} reaching highest concentrations from spring to autumn (**Fig. 4.17i-j**; **Fig. 4.16**), whereas Pro_{surf} is highest during winter (**Fig. 4.17g-h**; **Fig. 4.16**). The integrated cell abundance in the water column (Pro_{int}) is influenced by both the depth of the euphotic layer and Pro_{max}, showing a seasonal variability that resembles that of Pro_{max}, and thus is inverse to Pro_{surf} (**Fig. 4.17k-l**). The resemblance between Pro_{int} and Pro_{max} was also observed in their inter-annual variability in both gyres (**Fig. 4.18c-d**; **Fig. 4.18i-j**).

In general, the standing stock of *Prochlorococcus* cells is 1.7 times higher in the SAG than in the NAG (**Table 4.4**), regardless of the season (**Fig. 4.17k-l**). No clear long-term temporal changes of Pro_{int} and Pro_{max} were observed in either of the gyres (**Fig. 4.18a-b**; **Fig. 4.18g-h**), although a mode shift (between positive and negative anomalies) of approximately 3 to 5 years was observed in the NAG (**Fig. 4.18a-b**). Pro_{surf} decreased in the SAG (**Fig. 4.18k-l**) whereas in the NAG there was an increase in cell abundance from 2002 to 2011, followed by a steep decrease from 2012 to 2014 (**Fig. 4.18e-f**), which could be associated with the degradation of MODIS R_{rs} signals that started in 2012.

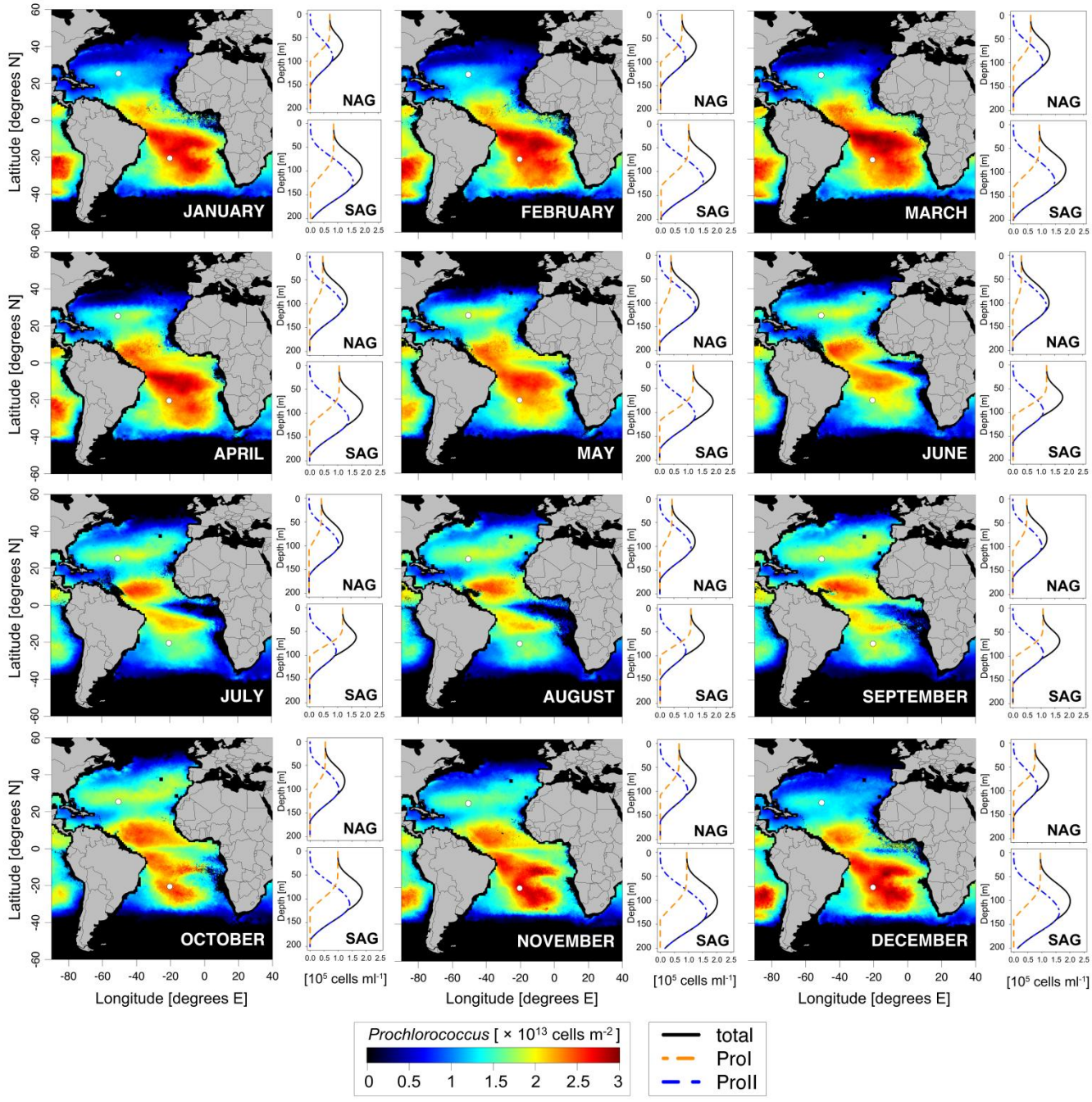


Figure 4.16. Estimated monthly distribution of the *Prochlorococcus* cells integrated in the top 200 m of the water column (Pro_{int}) (cells m^{-2}), with correspondent vertical profiles of estimated *Prochlorococcus* cell abundances (cells l^{-1}) at sites (white dots) in the North Atlantic Gyre (NAG) and South Atlantic Gyre (SAG): *ProI* is indicated by the orange dashed line, *ProII* by the blue dashed line, and the total *Prochlorococcus* abundance by the solid black line. Cell abundances were calculated based on the monthly climatology of environmental variables (NASA 2014).

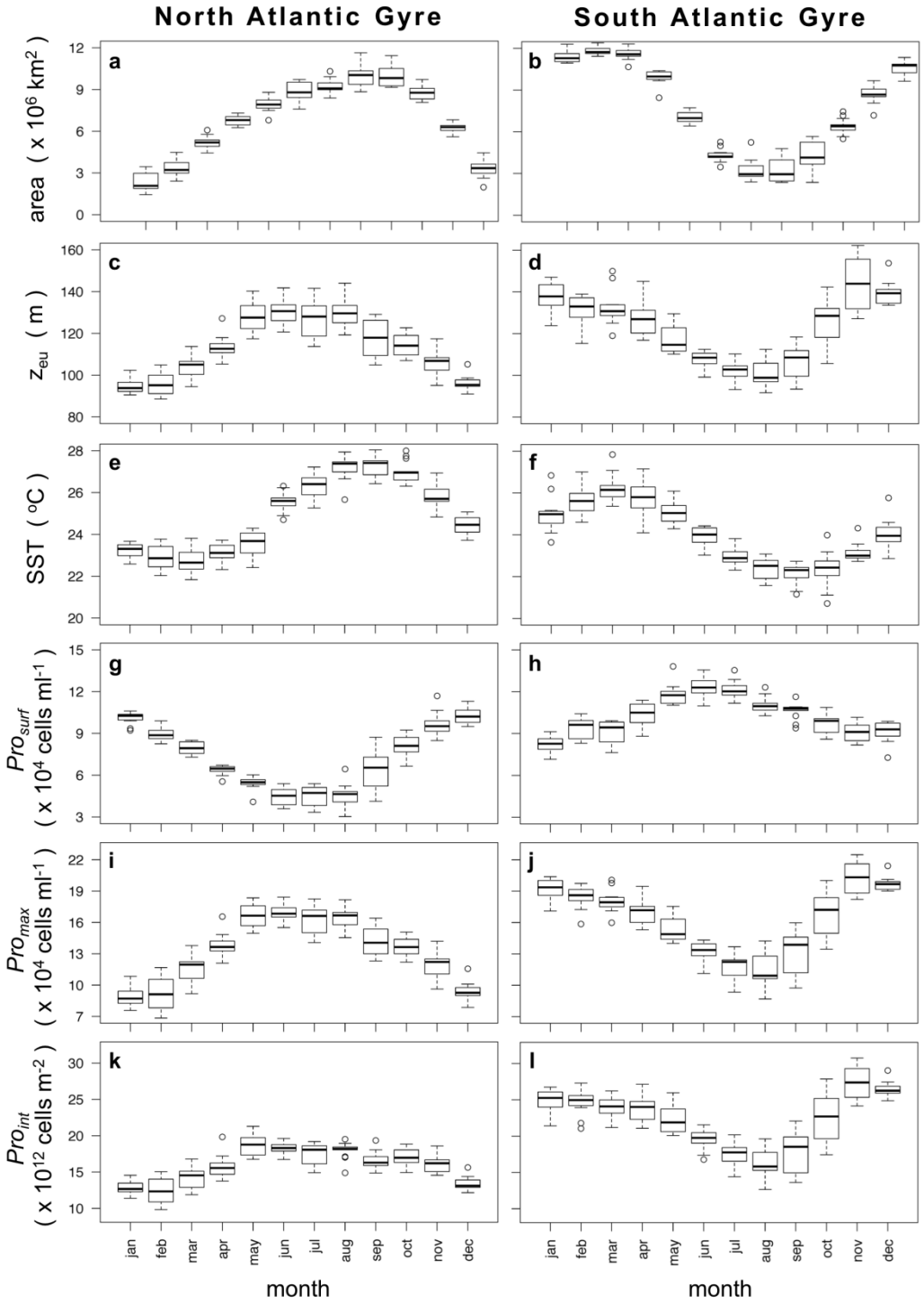


Figure 4.17. Monthly averages of **a)** the areal extent of the North Atlantic Gyre (NAG) and **b)** South Atlantic Gyre (SAG); **c)** the euphotic depth Z_{eu} at the NAG and **d)** the SAG; **e)** sea surface temperature *SST* at the NAG and **f)** the SAG; **g)** the estimated *Prochlorococcus* cell abundance at the sea surface (Pro_{surf}) at the NAG and **h)** the SAG; **i)** *Prochlorococcus* cell abundance at the deep maximum (Pro_{max}) at the NAG and **j)** the SAG; and **k)** *Prochlorococcus* cell abundance integrated in the water column (Pro_{int}) at the NAG and **l)** the SAG. *SST* measurements were taken from monthly satellite composites from Jan./2003 to Dec./2014 (NASA Ocean Color). *Prochlorococcus* cell abundances were computed using monthly-averaged input variables for the years 2003 to 2014, at specific locations inside the Atlantic gyres: NAG: 26°N, 50°W; SAG: 20°S, 20°W.

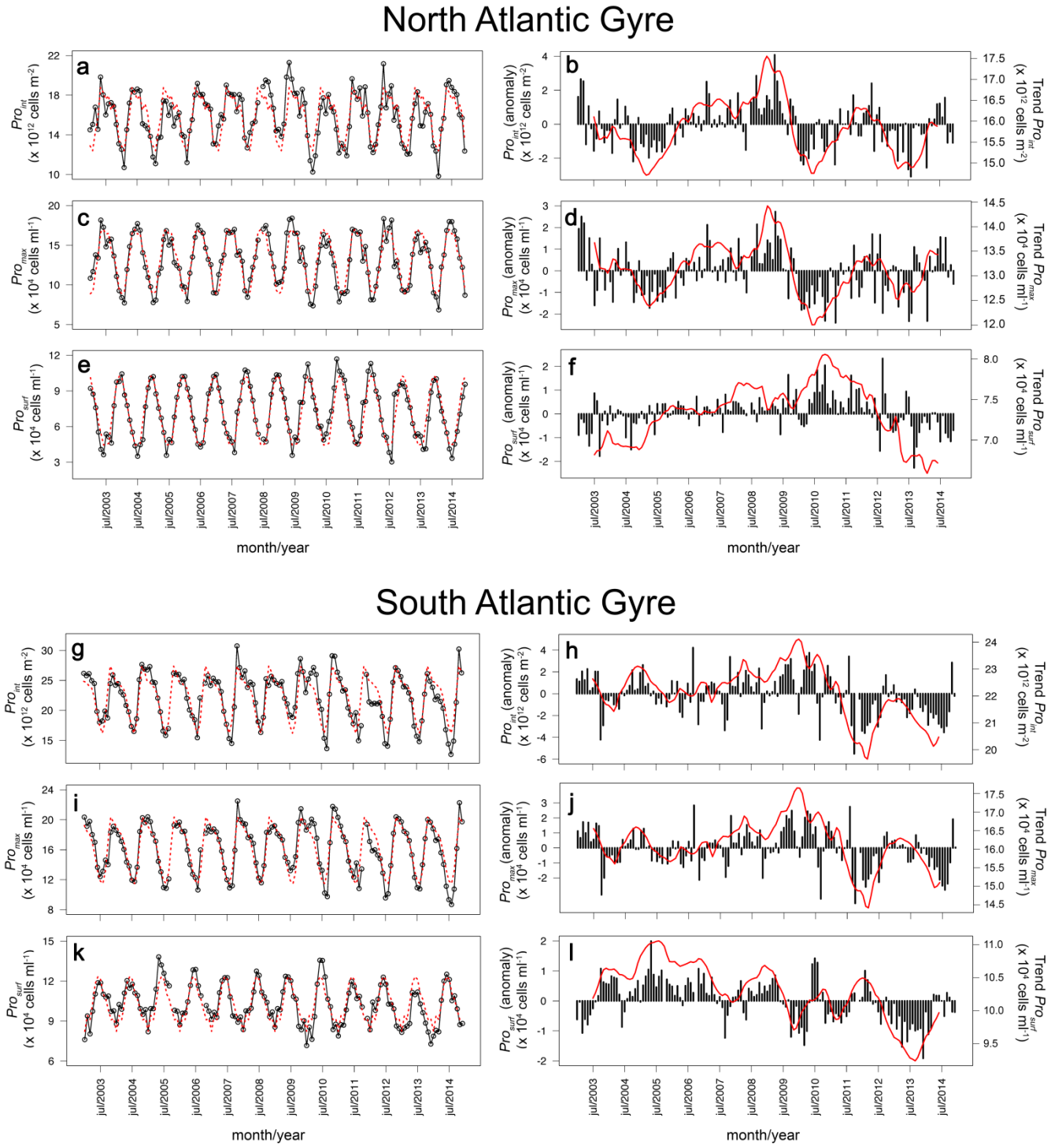


Figure 4.18. Time series of **a,g)** the estimated *Prochlorococcus* cell abundance integrated in the water column (Pro_{int}), **c,i)** estimated *Prochlorococcus* cell abundance at the deep maximum (Pro_{max}), and **e,k)** estimated *Prochlorococcus* cell abundance at surface (Pro_{surf}). All values calculated at **(a-f)** one location (26°N, 50°W) in the North Atlantic Gyre (NAG), and **(g-l)** one location (20°S, 20°W) in the South Atlantic Gyre (SAG). Figures on the right side show the time-series anomalies (black bars) and trends (red lines). Anomalies were calculated by subtracting the monthly climatology (dashed red lines in figures on the left side) from the calculated values for each month (black lines in figures on the left side).

4.4 Discussion

The model successfully reproduces the vertical distribution of the cell abundance of *Prochlorococcus*, especially across the Atlantic Basin, including the formation of a deep abundance maximum a few metres above the DCM (see **Fig. 4.4**). When provided with *in-situ* measurements of surface cell abundance (Pro_{surf}), the model accurately predicts the vertical distribution of cells (r^2 = 0.83, see **Table 4.5**), regardless of the geographic location, showing that physical and biological processes that take place in surface layers of the water column are tightly connected to what happens at depth. However, when satellite data are used to determine Pro_{surf}, model estimates of the integrated cell abundance in the water column (Pro_{int}) are more precise in the Atlantic Ocean than in other oceanic regions (see **Table 4.5**), and this is likely because the empirical relationships used in this algorithm were derived from data collected from the Atlantic.

The model estimates a global *Prochlorococcus* cell stock of 3.4×10^{27} cells, representing 171 Mt C, which is equivalent to 65% of the global phytoplankton carbon standing stock in the mixed layer (Behrenfeld et al. 2015; Kostadinov et al. 2016; Roy et al. 2017), and higher than the carbon contained in all picophytoplankton in the mixed layer (140 Mt C, Roy et al. 2017), highlighting the importance of picophytoplankton below the mixed layer in oligotrophic waters. Our estimates of global *Prochlorococcus* cell and carbon stocks are 3% lower than the estimate made by Williams and Follows (2011) (3.5×10^{27} cells, 180 Mt C), and 15% higher than the estimate of Flombaum et al. (2013) (2.9×10^{27} cells). Despite having roughly similar global estimates, the predicted global distribution patterns of *Prochlorococcus* cells are markedly different from previous studies, with our model showing higher surface cell concentrations in areas near the Equatorial Convergence Zone (ECZ) and on the periphery of subtropical gyres, and

lower surface cell abundance in the core of the gyres. This distribution pattern is supported by *in-situ* observations made in several transect cruises across the Atlantic Ocean (Zubkov et al. 2000b; Heywood et al. 2006). Conversely, surface distributions of *Prochlorococcus* presented by Flombaum et al. (2013) show higher cell concentrations not only in the ECZ, but also in the western sector of the ocean basins, which includes the central portion of subtropical gyres, due to the strong relationship between *Prochlorococcus* cell abundance and water temperature, especially if observations at depth are taken into account.

Similar to the present study, Flombaum et al. (2013) used a series of empirical equations that relate *Prochlorococcus* cell concentrations at the surface and at depth to the vertical structure in temperature and daily PAR. Thus, their model assumes that the same environmental factors that influence cell abundance at the surface govern also the variability in cell concentrations at depth.

In our model, the surface distribution of cells is primarily influenced by environmental conditions at the sea surface (except the variable T_{200} which is used as a proxy for stratification and hence nutrient input from depth). To estimate cell abundance at depth, we include an additional parameter: the maximum cell abundance at depth (Pro_{max}). The analysis of *in-situ* data shows that the profile of *Prochlorococcus* is directly influenced by Pro_{max}, which in turn is related to the remote sensing reflectance at 443nm ($R_{rs}(443)$). Thus, Pro_{max} is highest when $R_{rs}(443)$ is highest (i.e. in optically clear waters, there is less phytoplankton pigment at the surface, therefore less light absorption, leading to an increase in water leaving irradiance at blue wavelengths). Conversely, cell concentrations at the surface are inversely related to $R_{rs}(443)$ for high sea surface temperatures (see coefficient e_3 in **Table 4.3**), which occurs in the interior of subtropical gyres. Partitioning our *Prochlorococcus* population into two components (*ProI* near the

surface and *ProII* at depth) allowed us to include the deep peak in *Prochlorococcus* cell abundance that is routinely observed in subtropical waters (Zubkov et al. 2000b; Heywood et al. 2006; Rabouille et al. 2007; Brew et al. 2009) and which contributes significantly to the vertically integrated cell abundance, especially in periods when surface irradiance (PAR) is high or increasing over time (i.e. summer, spring). This deep abundance maximum is neglected in the previous models, which may explain why the global cell stock in Flombaum et al. (2013) is lower than that estimated in the present study.

Additionally, instead of using PAR, our model uses *fPAR* to determine the vertical distribution of cells, as *fPAR* shows a better relationship the abundance of *Prochlorococcus* cells than PAR at depth ($PAR_{(z)}$). This happens possibly because PAR varies over a time scale of hours, whereas *fPAR* reflects a longer-term (days or weeks) change the availability of light at depth and how the microbial community (including phytoplanktonic pigmented cells) responds to these variations over longer time periods. *Prochlorococcus* cells are not only dependent of the availability of light (PAR) but also respond to the microbial activity and community composition in the water body (Biller et al. 2014a).

As a consequence of the above-mentioned differences in approach between the present study and that of Flombaum et al. (2013), the seasonality and temporal variability of the global *Prochlococococcus* cell stock are markedly different between the two models. Our results show that global and regional cell stocks of *Prochlorococcus* are relatively constant over time, not showing any discernible long-term trend over the 12-year study period (2003-2014). This is in part due to the areal extent of the gyres being relatively uniform from 2003 to 2014 (if seasonal oscillations are discarded), when estimated on the basis of satellite observations of chlorophyll concentration at the sea surface (Aiken et al.

2016). Conversely, considering climate projections of environmental variables (mainly *SST*) from previously published climate models, Flombaum et al. (2013) predicted an increase of 29% in the global *Prochlorococcus* cell stock in the next 100 years, opposite to decreasing trends in phytoplankton global chlorophyll biomass projected by Boyce et al. (2010).

Despite the lack of a temporal trend, our model detected a positive-negative anomaly cycle of 3-5 years, similar to that observed between 1991 and 2004 in the North Pacific Gyre near Hawaii (HOTS time-series) (Rabouille et al. 2007). This cyclic oscillation may be associated with changes at depth such as variations in the volume and/or vertical oscillations of subtropical mode waters (STMW). The STMW are voluminous subsurface water masses (depths between ~150 and ~400 to 600 m in the Atlantic gyres) located in the subtropical gyres, and characterized by unique high temperature and salinity conditions that make this water mass vertically homogeneous (Tsubouchi et al. 2016). Therefore, in subtropical gyres, oscillations in the STMW directly influence nutrient supply from depth to surface and, consequently, phytoplankton growth, including the growth of *Prochlorococcus*.

Water column stability also varies seasonally, resulting in marked intra-annual changes in the concentrations of *Prochlorococcus* cells. As ~57% of the global ocean's area is located in the Southern Hemisphere (Boggs 1945), of which the occupation of subtropical gyres is vaster than in the Northern Hemisphere (i.e. **Fig. 4.17a-b**), the seasonal variability observed in the global *Prochlorococcus* cell stock (see **Fig. 4.16a**) is mostly influenced by a combination of environmental conditions in the Southern Hemisphere, such as the areal extent of the Southern Subtropical Gyres (see **Fig. 4.17b**), underwater light conditions, and vertical structure of the water column. As solar radiation levels increase during the summer, the gyres expand reaching their maximal extent, and

the water column becomes warmer and more stratified in the gyre's interior. This leads to extreme high-light and low-nutrient conditions that reduce the growth of phytoplankton at surface (Behrenfeld et al. 2015). High light levels at the sea surface also result in reduction in the intracellular concentration of photosynthetic pigments as a consequence of phytoplankton photoacclimation (Behrenfeld et al. 2015), which is another factor leading to lower concentrations of chlorophyll at the sea surface in the summer (Dave et al. 2015).

The increased surface irradiance and reduced phytoplankton pigment concentration at the surface allow solar irradiance to penetrate deeper within the water column, and the lower intracellular pigment concentrations induced by higher irradiance lead to a decrease in K_dPAR and consequently deepens the limits of the euphotic zone (see **Fig. 4.17c-d**). Therefore, the depth range over which *Prochlorococcus* has enough light to achieve net growth extends deeper, resulting in higher integrated cell abundances during the summer (see **Fig. 4.17k-l**). In contrast, during the winter, lower surface irradiances and increased mixing in the water column are accompanied by an increase in cellular chlorophyll concentrations at the sea surface, leading to the contraction of the gyre's extension (Polovina et al. 2008; Dave et al. 2015). Previous assessment of seasonal variations in *Prochlorococcus* populations based on *in-situ* observations show that, in the Atlantic subtropical gyres, standing stocks of *Prochlorococcus* and picoeukaryotes are larger during spring when compared with autumn (Zubkov et al. 2000b). Conversely, at the periphery of the North Atlantic gyre, *Prochlorococcus* is most abundant during summer and autumn (DuRand et al. 2001; Malmstrom et al. 2010). In the North Pacific Gyre (HOTS station), Rabouille et al. (2007) and Malmstrom et al. (2010) reported no significant seasonal changes in the integrated abundance of *Prochlorococcus* in the euphotic layer, but a noticeable seasonal shift in their vertical distribution was observed.

Differences between *Prochlorococcus* cell stocks in the NAG and the SAG may be a consequence of physical processes that govern nutrient delivery in the gyres: degree of water column stratification, and the proximity of the STMW to the bottom of the photic zone. In the SAG, the water column is strongly stratified at the bottom of the mixed layer, and a shallow pycnocline is formed during spring, when surface waters start to warm. The deep thermocline occurs at a depth of 80 to 120 metres and coincides with the nutricline, and above that the water column is homogeneous (see **Fig. 4.4i**), but the amount of total kinetic energy input at surface is low leading to low mixing (Barton et al. 2014). Additionally, the larger concentration of *Prochlorococcus* cells (Pro_{int} = 2.2 × 10^{13} cells m^{-2}) in the SAG when compared with the NAG may be a consequence of either a thinner underlying STMW in the SAG, or of the unique vertical structure of density of this STMW which compensates temperature and salinity stratification (Tsubouchi et al. 2016), and may influence nutrient input from depth to the euphotic layer. Conversely, the NAG has the thickest STMW in the world's oceans, and temperature at 200 m is considerably warmer (see **Fig. 4.4f**) than that found in the SAG, the ECZ, or even the NAG periphery (see **Fig. 4.4c**). The lower stratification combined with higher temperatures at depths between 100 and 200 m possibly indicates an even deeper thermocline and nutricline, leading to lower nutrient input from depth, and driving the lower *Prochlorococcus* cell stocks in the NAG (Pro_{int} = 1.6 × 10^{13} cells m^{-2}).

Prochlorococcus numerically dominates vast expanses of the warm and strongly-stratified open ocean (Heywood et al. 2006; Rabouille et al. 2007; Mella-Flores et al. 2012; Buitenhuis et al. 2012; Biller et al. 2014a). The sensitivity of the *Prochlorococcus* population as a whole to changes in physical forcing (Bouman et al. 2011) such as decreased kinetic energy input to the water column resulting in low turbulent mixing (Barton et al. 2014), and long-period internal oscillations in sub-surface water masses that

can lead to changes in nutrient supply from depth (Tsubouchi et al. 2016), makes this species an ideal indicator of water column dynamics. The preferred habitat of *Prochlorococcus*, the ocean's subtropical gyres, expands and contracts according to seasonal changes in stratification, leading to significant spatio-temporal changes in the global standing stocks of *Prochlorococcus* cells. Additionally, variations in *Prochlorococcus* cell stocks are a consequence of the collective physiological response of this genetically diverse assemblage of cells to both abiotic (temperature, nutrients), and biotic factors (grazing pressure, viral infection, sinking), the latter of which were not explored in the present study.

4.5 Conclusions

The model successfully predicts the vertical distribution of *Prochlorococcus* cells using remote-sensing data (R^2 = 0.58). However, the prediction of the abundance of *Prochlorococcus* cells at the sea surface (Pro_{surf}) can be improved, especially in the Pacific and Indian Oceans. Improving the prediction of Pro_{surf} will lead to significant improvement (R^2 increases up to 0.83) of the prediction of *Prochlorococcus* integrated cell abundances (Pro_{int}) in these ocean basins.

The deep maximum in the abundance of *Prochlorococcus* cells (Pro_{max}) contributes significantly to integrated cell abundances in the water column (Pro_{int}), such that oscillations in Pro_{int} follow that of Pro_{max} and are inversely correlated to cell abundances at the sea surface (Pro_{surf}).

Model predictions show that *Prochlorococcus* cells contribute approximately 171 Mt of carbon biomass (3.4×10^{27} cells) to the global ocean, with most of the biomass concentrated within the subtropical gyres and areas near the Equatorial Convergence

Zone (ECZ). In contrast to previous studies, the model shows no clear temporal change in cell standing stocks between the years 2003 and 2014, although marked seasonal variability in cell abundance is observed both globally and regionally.

The seasonal and spatial patters described by the present model, which predicts that *Prochlorococcus* cells are most abundant during spring and summer in the Atlantic subtropical gyres, are severely distinct from those predicted by the model of Flombaum et al. (2013). In addition, global estimates of *Prochlorococcus* cell abundance are 15% higher in the present model, which is similar to that calculated by Williams and Follows (2011).

The model developed in this study is able to recreate the basin-scale patterns in the vertical distribution of *Prochlorococcus* cells, which is a crucial first step to quantify the role of this globally important cyanobacterium in marine biogeochemical cycles. These results reveal that, despite their minute size, *Prochlorococcus* contributes significantly to total phytoplankton biomass in the Atlantic Ocean, and it is likely that previous models have underestimated these cell stocks by not capturing variations in cell abundance at depth. This empirical model improves our ability to predict the vertical distribution of *Prochlorococcus* by using either *in-situ* measurements of surface variables ($R^2 = 0.83$) or remote-sensing observables ($R^2 = 0.58$), which are crucial to assess the contribution of *Prochlorococcus* to the global carbon cycle.

Chapter 5.

Carbon fixation by *Prochlorococcus* in the global ocean

5.1 Introduction

By virtue of being the smallest and most abundant phytoplankton on Earth (Biller et al. 2014a), and being ubiquitous in warm oceanic waters between 40°N and 40°S (Partensky et al. 1999), *Prochlorococcus* has attracted the interest of global biogeochemists and marine ecologists since its discovery nearly three decades ago (Chisholm et al. 1988). The highest concentrations of *Prochlorococcus* biomass are found in oligotrophic regions such as subtropical gyres, where picoplankton (cells < 2μm) are dominant among primary producers, although *Prochlorococcus* also contributes a significant fraction of the phytoplankton biomass in the Equatorial Convergence Zone (ECZ), where it coexists with large diatoms and nanoplanktonic flagellates (Vaulot et al. 1995; Mann and Chisholm 2000; Zubkov et al. 2000b).

In spite of its small cell size and low intracellular carbon content (Bertilsson et al. 2003), *Prochlorococcus* is known to contribute significantly to the global marine phytoplankton carbon pool (**Chapter 4** of this thesis; Flombaum et al. 2013; Williams and Follows 2011) as a result of its numerical dominance over a vast area in the world's oceans. Although the abundance of *Prochlorococcus* cells can reach values of 10^5 cells ml^{-1} in subtropical waters, the actual concentration of carbon biomass is modest (~ 5 x 10^{-6} pg C ml^{-1}) when compared to blooms of nano- and micro- phytoplankton species with cell abundances of a similar order of magnitude (e.g. ~ 1 pg C ml^{-1} for the nanoplankter *Phaeocystis* sp., Rousseau et al. (1990)). However, when this biomass is integrated over ocean basins, the global contribution of *Prochlorococcus* (0.17 Gt C,

Chapter 4) to the organic carbon pool, allocated within and below the mixed layer in tropical and subtropical regions, is higher than the biomass of all picophytoplankton on the planet within the mixed layer (0.14 Gt C), which in turn is greater than the mixed-layer biomass of nano- and microphytoplankton cells combined (Roy et al. 2017).

In addition to their low intracellular carbon content, carbon-specific turnover rates of *Prochlorococcus* (~ 0.02 h^{-1}) are lower than rates observed in picoplanktonic eukaryotes (*Micromonas pusilla*: 0.07 h^{-1}), microplanktonic diatoms and dinoflagellates (i.e. *Coscinodiscus wailesii*: 0.05 h^{-1}; and *Alexandrium tamarense*: 0.04 h^{-1}), and nanoplanktonic organisms (i.e. 0.12 h^{-1} for the diatom *Thalassiosira weisflogii* and the coccolithophore *Emiliana huxleyi*) (López-Sandoval et al. 2014). When considering cell-specific carbon fixation rates, the difference between taxa increases to several orders of magnitude due to the difference in intra-cellular carbon content (López-Sandoval et al. 2014). However, *Prochlorococcus* is abundant and ubiquitous in oligotrophic areas throughout the whole year, forming a constant background of biomass, as opposed to other phytoplankton species that tend to oscillate seasonally or form episodic blooms in polar, temperate and shelf seas. As a consequence, *Prochlorococcus* should contribute a significant amount to the annual global carbon fixation budget. Rough estimates of carbon uptake by *Prochlorococcus* based on multiplying the cell abundance of *Prochlorococcus* by an average cell-specific daily carbon fixation rate (Li 1994) and then integrating over a year, provide a global carbon fixation rate of 4 Gt C $year^{-1}$ for *Prochlorococcus* (Flombaum et al. 2013), which is twice the annual primary productivity of the Southern Ocean (~ 2 Gt C $year^{-1}$) (Behrenfeld et al. 2005; Arrigo et al. 2008; Westberry et al. 2008). Note that such calculations make the general assumption of *Prochlorococcus* cells having the same rate of photosynthesis throughout the photic zone and across the global ocean, regardless of prevailing nutrients and light conditions.

Cell-specific carbon fixation for *Prochlorococcus* have been measured in natural populations (Li 1994; Jardillier et al. 2010; Hartmann et al. 2014) and cultures of different *Prochlorococcus* ecotypes (Partensky et al. 1993; Shimada et al. 1996; Moore and Chisholm 1999; Bruyant et al. 2005; Hopkinson et al. 2014). If combined with cell abundance distribution patterns and information on the underwater light field, rates of carbon fixation by *Prochlorococcus* in the global ocean can be estimated for the entire depth range which these cells are known to inhabit (down to the depth of ~ 200 metres), allowing the spatial and temporal variability in their metabolic activity to be systematically examined.

Remote-sensing observables have been broadly used to estimate carbon fixation rates of different phytoplankton size classes (Brewin et al. 2010a, 2014, 2017; Cabré et al. 2016; Kostadinov et al. 2016; Roy et al. 2017) and functional types (Nair et al. 2008; Uitz et al. 2008, 2010; Hirata et al. 2013), allowing the contribution of the total phytoplankton community to primary productivity on the biosphere to be assessed (Field et al. 1998). In this study, we combine remote-sensing estimates of the global vertical distribution of *Prochlorococcus* cells (**Chapter 4**) with cell-specific carbon fixation measurements made in the natural marine environment (Hartmann et al. 2014) to estimate the annual carbon uptake by *Prochlorococcus* in the global ocean and its contribution to the global marine primary production, in addition to accessing spatial and temporal distribution patterns in the carbon fixation by this important phytoplankton species. To do so, the vertically-resolved phytoplankton primary production model described in Sathyendranath and Platt (1989) was adapted to produce synoptic fields of *Prochlorococcus* productivity, which were then used to estimate carbon fixation by this globally important cyanobacterium at a high vertical resolution (1 m). This method produces depth-resolved estimates of *Prochlorococcus* primary production over basin scales, allowing the comparison between

the relative contribution of *Prochlorococcus* populations that inhabit the upper ocean (0-45 m) and deeper layers of the euphotic zone (45-200 m).

5.2 Methods

5.2.1 *Modelling approach*

Carbon fixation rates by *Prochlorococcus* were estimated in two steps. First, the vertical distribution of *Prochlorococcus* cells was estimated on a pixel-to-pixel basis from satellite observables using the model described in **Chapter 4**. Then, a pre-existing model used to calculate marine primary production from chlorophyll-specific carbon fixation parameters (Sathyendranath and Platt 1989) (**Fig. 5.1a**) was modified by substituting pigment biomass with cell abundance as the model's currency of phytoplankton biomass (**Fig. 5.1b**). The modified model required cell-specific rather than chlorophyll-specific photosynthetic parameters, obtained from the study by Hartmann et al. (2014). Finally, satellite observables were used as inputs to assign carbon fixation daily rates by *Prochlorococcus* cells.

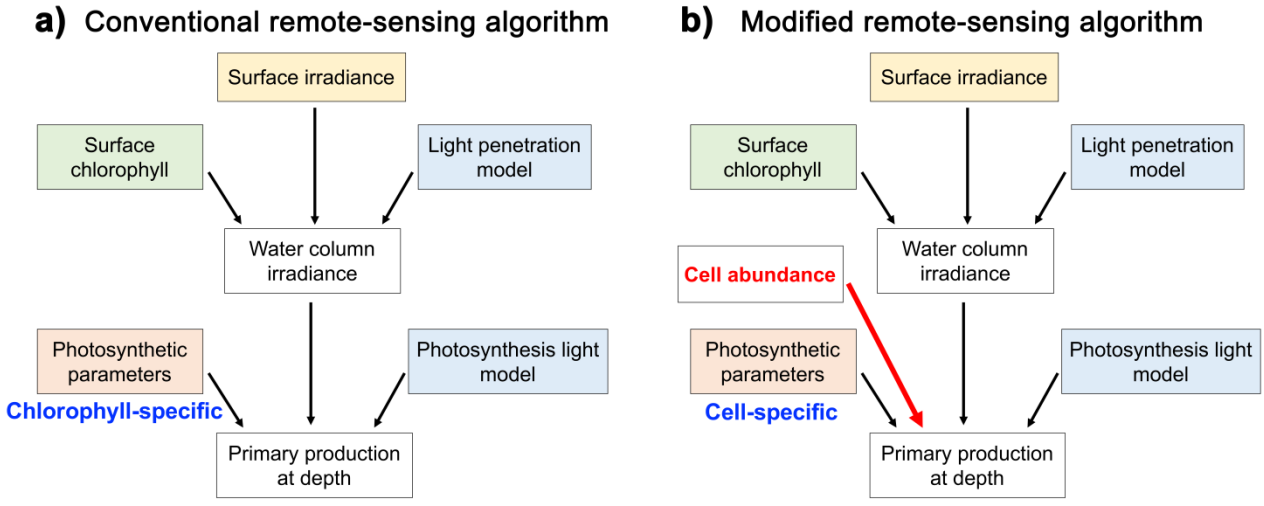


Figure 5.1. Flowchart of **a)** the primary production remote sensing algorithm that uses chlorophyll concentration as unit of biomass (Sathyendranath and Platt 1989), and **b)** the adapted primary production algorithm using cell abundance as the biomass unit.

The primary productivity model of Sathyendranath and Platt (1989) (**Fig. 5.1a**) calculates the surface irradiance $E(\lambda)$ at hourly time steps throughout the day using information on geographic location and day of the year. The penetration of the visible irradiance in the water column is modelled hyperspectrally using the vertical attenuation coefficient $K_d(\lambda)$, which is a function of the concentration of chlorophyll in the water column. Due to its large dynamic range of concentrations in the surface ocean, chlorophyll is the main component that governs variations in the absorptive properties of seawater in open ocean regions such as the subtropical gyres (Kirk 2011). In addition, the other optically relevant constituents (non-algal particulates and coloured dissolved organic matter) tend to co-vary with the concentration of chlorophyll *a* (Gordon and Morel 1983) in such areas. Once the vertical distribution of $E(\lambda)$ is known, primary production (carbon uptake) by a given phytoplankton group is calculated based on the relationship between available light and the rate of carbon fixation, which is described by a photosynthesis-irradiance (*PE*) response curve and can be expressed in the absence of photoinhibition by the following equation [5.1] (Platt et al. 1980):

$$P^b = P_m^b \left[1 - \exp\left(- \frac{\alpha^b}{P_m^b} PAR \right) \right] \quad [5.1]$$

where P^b is the primary production (carbon fixation) per unit of biomass, $P_m{}^b$ is the maximum carbon fixation rate per unit of biomass, and α^b is the initial slope of the *PE* curve. An example of a *PE* curve is shown in **Fig. 5.2**.

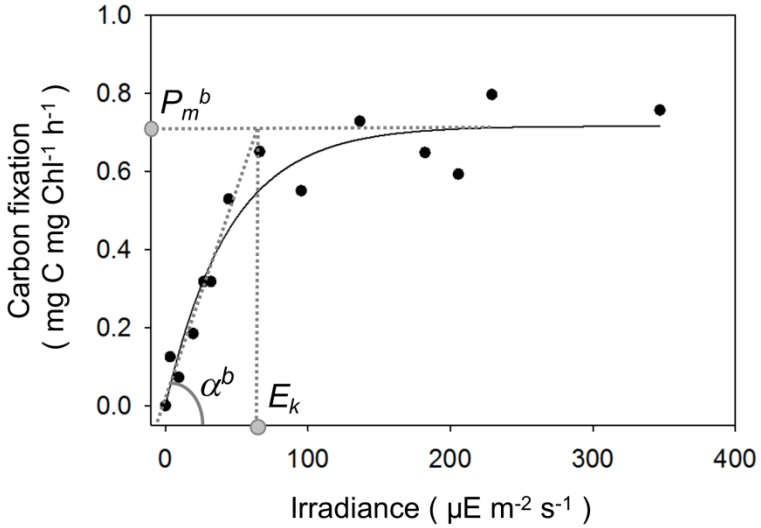


Figure 5.2. Example of a photosynthesis-irradiance (*PE*) curve for picophytoplankton in the North Atlantic gyre (13.9° N, 33.6° W), with photosynthetic parameters P_m^b (maximum carbon fixation rate per unit of biomass), α^b (initial slope), and E_k (saturating irradiance). Data provided by Gavin Tilstone (Plymouth Marine Laboratory), collected on AMT22.

The rationale for normalising the parameters to biomass is so that the major source of variability in carbon uptake, the concentration of phytoplankton biomass, is removed, allowing for changes in secondary factors, such as nutrient stress and light history, to be examined. Although the unit of biomass (*b*) is conventionally chlorophyll concentration or cell carbon, in this modified version of the Sathyendranath and Platt (1989) model, cell abundance per unit volume is used as the unit of biomass, thus the photosynthetic parameters become the maximum carbon uptake rate per cell P_m^{cell} and the initial slope α^{cell} (**Fig. 5.1a**). The photoadaptation parameter E_k, which is used as a proxy for photoacclimation, can also be retrieved by simply dividing P_m^b by α^b. As this parameter has units of irradiance (µmol quanta m^{-2} s^{-1}), its magnitude is independent of the currency of biomass used to normalise the rates of production. Thus, regardless of the biomass used to derive photosynthetic parameters, E_k values retrieved from the literature can be used to estimate α^{cell} once P_m^{cell} is known. Last, it is important to point out that, in this modified

model, the sea surface chlorophyll concentration is still used to estimate $K_d(\lambda)$ and hence calculate the vertical attenuation of light in the water column at each time step of the day.

5.2.2 *Photosynthetic parameters for Prochlorococcus*

In order to calculate the carbon uptake by *Prochlorococcus* cells, species-specific photosynthetic parameters must be assigned. In remotely-sensed models of marine primary production, parameters describing the rate of carbon fixation by marine phytoplankton are typically derived from photosynthesis-irradiance (*PE*) experiments. To obtain information on the photosynthetic response of phytoplankton to light, seawater samples or cultured isolates are spiked with a known quantity of labelled bicarbonate (conventionally with ^{14}C) and incubated over a range of light intensities for a given time interval. Phytoplankton is then harvested onto filters and the amount of carbon incorporated into the cells over the course of the experiment is measured (Tilstone et al. 2009).

Although several studies have obtained light-response curves for various *Prochlorococcus* ecotypes in culture (Partensky et al. 1993; Shimada et al. 1996; Moore and Chisholm 1999; Bruyant et al. 2005; Kulk et al. 2011; Hopkinson et al. 2014), only a few studies have measured cell-specific rates of carbon fixation by *Prochlorococcus* in the natural environment (Li 1994; Jardillier et al. 2010; Hartmann et al. 2014; Rii et al. 2016). Field-based experiments are preferable for modelling *in-situ* marine primary production since they integrate the physiological response of the cells to a variety of biotic and abiotic factors, including light history and nutrient availability, which is difficult to simulate in the laboratory. However, obtaining cell-specific rates of carbon uptake for *Prochlorococcus* is extremely labour intensive, as it requires that the *Prochlorococcus* cells are physically separated from the rest of the phytoplankton

community using a flow cytometer, and cells need to be sorted for a long period of time before enough cells are collected to obtain a detectable rate of uptake. Consequently, such rates have been obtained at a single light level. Nevertheless, cell-specific maximum photosynthetic rates can be recovered from such field experiments if we can establish that the light intensities used in the experiments were sufficiently high that the surface population of cells were achieving their maximum photosynthetic rates P_m^{cell} (i.e. the plateau of the photosynthesis-irradiance curve).

In this study, maximum rates of carbon fixation were obtained from the study of Hartmann et al. (2014). Seawater samples were spiked with ^{14}C-labelled bicarbonate and incubated for a total of 10 hours. Every 2 hours, aliquots were sampled for cell sorting using a flow cytometer. The sorted cells were then filtered and the amount of radioactive carbon incorporated in the particulate fraction retained on the filter was measured. To ascertain whether the rates measured by Hartmann et al. (2014) were equivalent to P_m^{cell}, *Prochlorococcus*-specific E_k values measured in cultures and natural samples were compared with measurements of E_k taken from the total picophytoplankton population in areas dominated by *Prochlorococcus* cells (i.e. subtropical gyres), provided by the MAPPS database (European Space Agency – ESA) (**Table 5.1**). The photoadapation parameter E_k is considered to be a useful indicator of the irradiance necessary for a phytoplanktonic cell to achieve the maximum carbon fixation rate P_m^{cell}. Given that the irradiance used in the incubations of natural populations of *Prochlorococcus* by Hartmann et al (2014) was higher (E_{inc} = 500 μmol quanta m^{-2} s^{-1}) than the average E_k measured both in subtropical gyre waters and in *Prochlorococcus* cultures (44 μmol quanta m^{-2} s^{-1}), the cell-specific carbon uptake rates measured by Hartmann et al. (2014) were considered to be representative of the maximum carbon fixation rates of *Prochlorococcus* cells (P_m^{cell}). (**Table 5.1**; **Fig. 5.3a**).

Thenceforth, the cell-specific rates of carbon fixation by *Prochlorococcus* from the Hartmann et al. (2014) study were adopted and assigned to the biogeochemical provinces of the Atlantic Ocean, where *Prochlorococcus* is an important phytoplankton component (Longhurst 1998). Province-specific P_m^{cell} values are used because the photosynthetic parameters vary in a systematic manner with geographical area: P_m^{cell} values are higher in the equatorial region when compared with the oceanic gyres (**Fig. 5.3b**).

The value for α^{cell} was taken from a literature compilation of *Prochlorococcus* cell-specific *PE* parameters measured on culture strains adapted to different light levels (Partensky et al. 1993; Shimada et al. 1996; Moore and Chisholm 1999; Hopkinson et al. 2014) (**Table 5.1**). Although this compilation from culture studies shows the difference between the α^{cell} of high- and low-light acclimated cells and various ecotypes, we assigned a constant value of α^{cell} because the model used to estimate the abundance of *Prochlorococcus* cells does not distinguish between high- and low-light ecotypes.

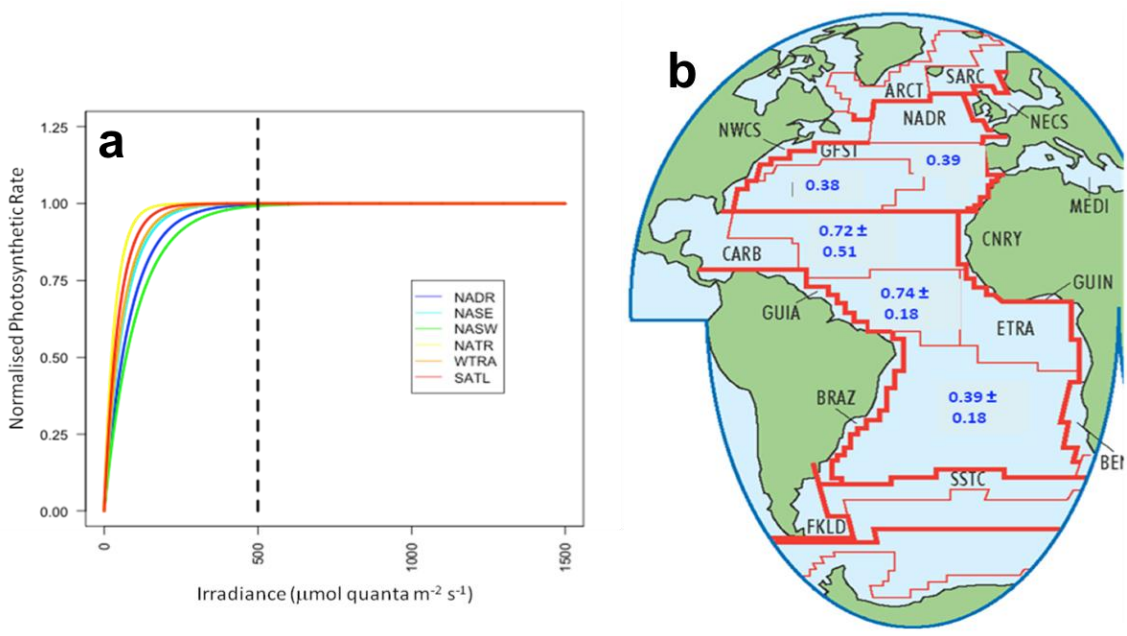


Figure 5.3. a) Shape of average phytoplankton community PE curves for various Atlantic provinces (MAPPS database). Growth irradiance used in the AMT20 incubations (Hartmann et al. 2014) indicated by dashed line; **b)** Cell-specific carbon uptake rates (fg C $cell^{-1}$ h^{-1}) by *Prochlorococcus* (Hartmann et al. 2014) in the different oceanic biogeochemical provinces (Longhurst 1998).

Table 5.1. Compilation of photosynthesis-irradiance curve parameters for *Prochlorococcus*, taken from Bruyant et al. (2005), Hartmann et al. (2014) , Hopkinson et al. (2014) , Li (1994) , Moore and Chisholm (1999) , Partensky et al. (1993) , Shimada et al. (1996). Total phytoplankton E_k data provided by the MAPPS dataset (Bouman et al. 2017).

	ecotype	P_m^{cell} fg C cell^{-1} h^{-1}	α fg C cell^{-1} h^{-1} (µmol quanta m^{-2} s^{-1})$^{-1}$	E_k µmol quanta m^{-2} s^{-1}
n		28	20	24
mean		4.17	0.171	44
σ	*Pro* HL+LL	3.26	0.149	22
min		0.03	0.020	17
max		12.00	0.600	100
n		20	12	15
mean		3.12	0.113	47
σ	*Pro* HL	2.31	0.043	19
min		0.03	0.050	24
max		6.20	0.190	90
n		8	8	9
mean		6.81	0.258	40
σ	*Pro* LL	3.91	0.208	28
min		2.00	0.020	17
max		12.00	0.600	100
n				44
mean				44.2
σ	Total phytoplankton			
min				17
max				100

HL - ecotypes adapted to high light; LL - ecotypes adapted to low light; n - number of observations; σ - standard deviation;

Differences between *PE* parameters obtained from culture experiments of high light (HL) and low light (LL) *Prochlorococcus* ecotypes (**Table 5.1**) suggest there is a depth-dependency of P_m^{cell} and α^{cell}, as these parameters vary according to the light level to which cells are acclimated: HL ecotypes show lower P_m^{cell} and α^{cell} than LL-adapted cells, although values are not significantly different since parameters obtained from experiments using LL ecotypes are highly variable. Nevertheless, it is important to note that LL ecotypes dominate the *Prochlorococcus* population at depths > 80 m in the

natural environment (Johnson et al. 2006), thus these cells are rarely exposed to high irradiances (i.e. rarely reaching P_m^{cell}) in natural conditions. Additionally, HL ecotypes numerically dominate *Prochlorococcus* populations in areas where *Prochlorococcus* is most abundant (Johnson et al. 2006), especially in the upper ocean (0-45 metres depth).

Although the higher E_k values exhibited by HL ecotypes reflect the suitability of these cells to thrive under high sea-surface irradiances, differences between HL and LL populations are not significant when values from all studies are combined. However, measurements taken from 6 HL ecotypes and 4 LL ecotypes by Moore and Chisholm (1999) show that E_k increases when cells are pre-acclimated to high light before *PE* parameters are measured, regardless of the ecotype: in HL ecotypes, E_k increased from 34 μmol quanta m^{-2} s^{-1} in cells pre-acclimated to low light to 62 μmol quanta m^{-2} s^{-1} under high light, whereas LL ecotypes showed an increase in E_k from 19 to 63 μmol quanta m^{-2} s^{-1} when cells were acclimated to high light (Moore and Chisholm 1999). These observations agree with E_k values of natural phytoplankton populations measured in areas where picophytoplankton is dominant (i.e. subtropical gyres – data from the MAPPS database, ESA) (**Fig. 5.3**; **Table 5.1**), and *Prochlorococcus* is the most abundant primary producer (Zubkov et al. 2000a).

5.3 Results

When carbon fixation rates are integrated globally, the depth-resolved primary production model estimates that *Prochlorococcus* is responsible for assimilating 4.7 Gt C $year^{-1}$ (**Fig. 5.4**). The Pacific Ocean basin is responsible for 59% of the global carbon fixation by *Prochlorococcus* (**Table 5.2**) due to its vast areal extent (**Fig. 5.4a**). The Atlantic Ocean is responsible for 22% of the global carbon fixation by *Prochlorococcus*,

with 44% occurring in the Equatorial convergence area and 35% in the subtropical gyres (**Table 5.2**; **Fig. 5.4a**).

On a global perspective, most of the carbon fixation by *Prochlorococcus* (61%) occurs on the upper water column (from surface to 45 metres depth), with a significant fraction of this surface productivity occurring in oceanic areas located near the equator (**Fig. 5.4b**). However, when rates of carbon fixation are integrated vertically for all the subtropical gyres (**Fig. 5.5**), the annual carbon fixation by *Prochlorococcus* is highest (62%) at depths below 45 metres (46-200 m) (**Fig. 5.4c**), reaching values up to 68% during summer.

Table 5.2. Annual carbon fixation by *Prochlorococcus* integrated spatially and vertically in each area. Values were computed with monthly climatology products used as input variables (Ocean Color, NASA 2014), then integrated monthly and over the year. The annual mean of the daily carbon fixation was calculated at specific geographic locations within the Atlantic gyres (coordinates in the table).

Prochlorococcus	Annual carbon fixation (Gt C $year^{-1}$)	Fraction of global annual C fixation (%)	Fraction of global biomass (%)	Daily carbon fixation (mg C m^{-2} d^{-1})
Global	4.74			
depth: 0 to 45 m		61	43	
depth: 45 m to 200 m		39	57	
Indian Ocean	2.8	19	20	
Pacific Ocean	8.9	59	58	
Atlantic Ocean	1.0	22	22	
Atlantic Equatorial Convergence ECZ: 2° S , 22° W	0.44	9.4	5	90
North Atlantic Gyre NAG: 26° N , 50° W	0.14	2.9	3.5	61
South Atlantic Gyre SAG: 20° S , 20° W	0.21	4.4	5.6	80

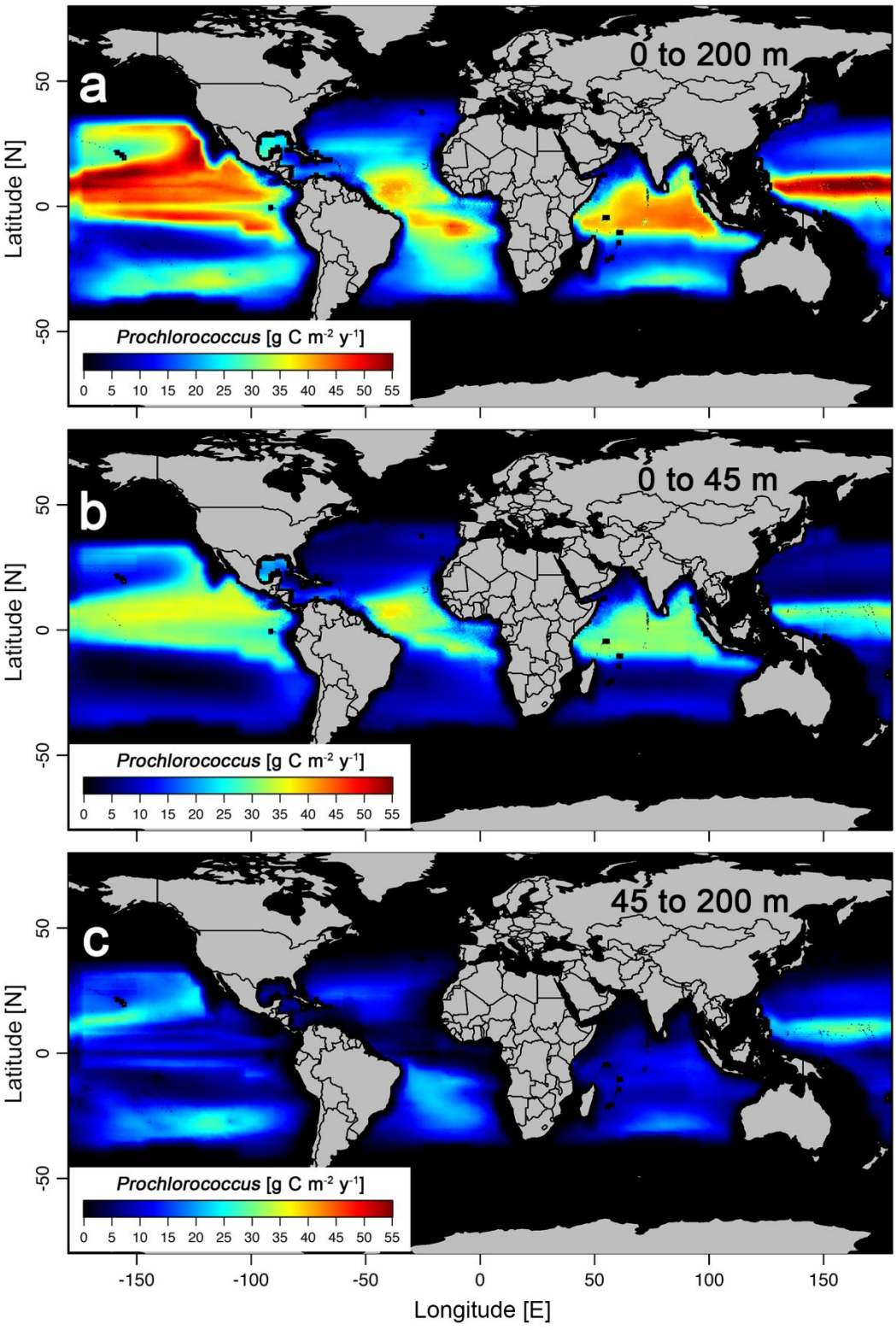


Figure 5.4. a) Global distribution of the annual carbon fixation by *Prochlorococcus* in the euphotic layer; **b)** in the upper water column (surface to 45 metres depth), and; **c)** from 45 to 200 metres.

To examine the seasonality, one location was selected in each subtropical gyre (i.e. North Atlantic Gyre - NAG, South Atlantic Gyre - SAG, North Pacific Gyre - NPG, South Pacific Gyre - SPG, and Indian Gyre - IG), in addition to one location in the Northern Indian Ocean to highlight the difference between the gyres and areas near the Equatorial Convergence (**Fig. 5.5**). *Prochlorococcus* carbon fixation rates show strong seasonality in the interior of subtropical gyres, with the lowest daily rates of carbon fixation by *Prochlorococcus* occurring in the winter, and the highest rates during the summer in the North Atlantic Gyre (NAG) and Indian Gyre (IG) (**Fig. 5.5a,f**, respectively), late spring in the South Atlantic Gyre (SAG) and North Pacific Gyre (NPG) (**Fig. 5.5b,c**), and early spring in the South Pacific Gyre (SPG) (**Fig. 5.5d**). The seasonality observed in the gyres is primarily governed by seasonal oscillations in carbon fixation rates in the lower euphotic layer (45 to 200 metres) (**Fig. 5.5a-f**). In contrast, the contribution of the upper water column (surface to 45 metres) to the daily carbon fixation in the water column is low in subtropical gyres (33%, varying between 9 to 61%) and only reaches values higher than 50% in the North Atlantic and Pacific Gyres during autumn and early winter (**Fig. 5.5a-f**).

The seasonal variation in the spatial distribution of daily carbon fixation rates by *Prochlorococcus* in the Atlantic Ocean is shown in **Fig. 5.6**, where the significance of the Equatorial Convergence Zone and strong seasonality in subtropical gyres is clearly observed.

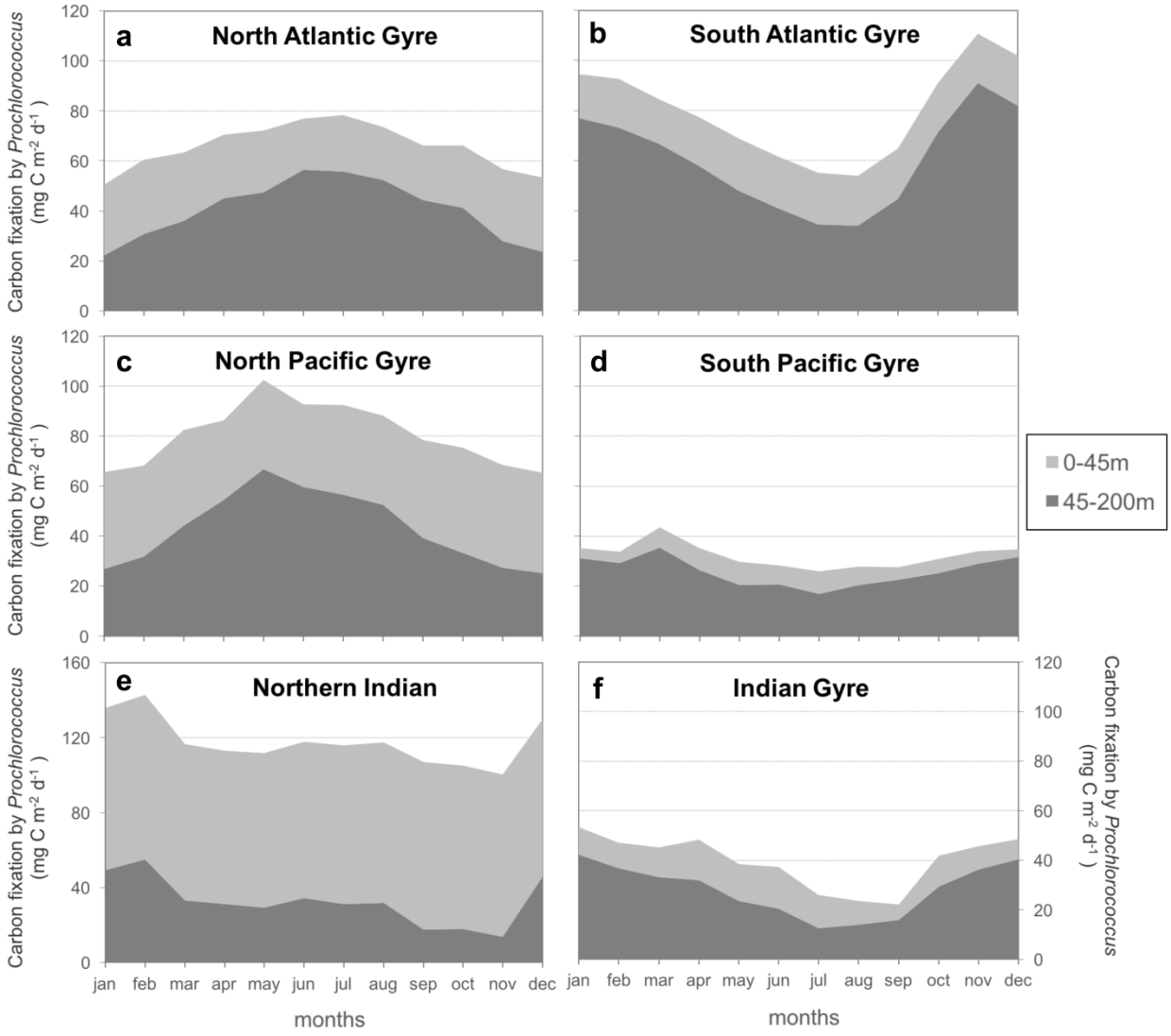


Figure 5.5. Seasonal variability in the carbon fixation rates by *Prochlorococcus* integrated in the water column (mg C m^{-2} d^{-1}) down to the depth of 200 metres, in the **a)** North Atlantic Gyre (22°N, 50°W), **b)** South Atlantic Gyre (20°S, 20°W), **c)** North Pacific Gyre (22°N, 166°W), **d)** South Pacific Gyre (20°S, 150°W), **e)** Northern Indian Ocean (2°S, 80°E), and **f)** Indian Gyre (20°S, 80°E). Light grey indicates values integrated in the upper ocean (0 to 45 metres depth), and dark grey represents carbon fixation integrated in the lower euphotic zone (45 to 200 metres deep).

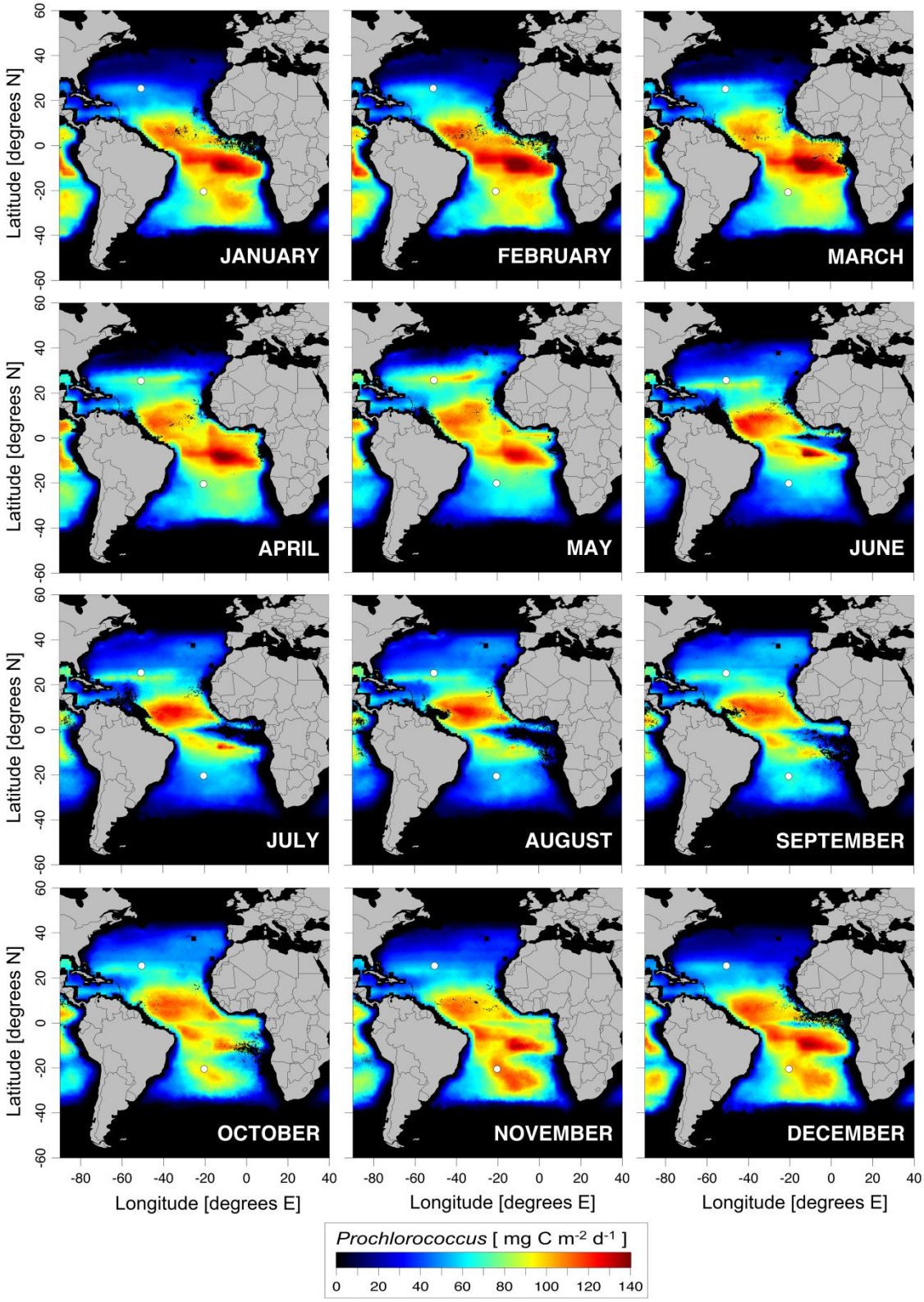


Figure 5.6. Estimated monthly distribution of the *Prochlorococcus* carbon uptake integrated in the top 200 m of the water column (mg C m^{-2} d^{-1}). White dots indicate the location of the sites in the North Atlantic Gyre (NAG) and South Atlantic Gyre where data from **Fig. 5.5** was taken from. Carbon fixation was calculated based on the monthly climatology of environmental variables (NASA 2014).

5.4 Discussion

The cell abundance-based model used to estimate *Prochlorococcus* primary production predicts that these cells assimilate 4.7 Gt C $year^{-1}$ in the global ocean, which corresponds to approximately 43% of the global picophytoplankton primary production estimated using pigment markers (Uitz et al. 2010), 10% of the carbon assimilated by all phytoplankton within the mixed layer in the global ocean using remotely-sensed chlorophyll (Field et al. 1998; Behrenfeld et al. 2005; Westberry et al. 2008; Brewin et al. 2010a), and 4.5% of the total net primary production on planet Earth derived from satellite estimates of the marine and terrestrial biospheres (Field et al. 1998). Due to the sustained growth of this cyanobacterium in warm stratified waters through all seasons, *Prochlorococcus* annually fixes twice the amount of carbon as all phytoplankton in the Southern Ocean, one of the most productive areas in the globe (Behrenfeld et al. 2005; Arrigo et al. 2008; Westberry et al. 2008), and an amount equivalent to about one quarter of the carbon assimilated by tropical rainforests or savannahs (Field et al. 1998).

Estimates of the vertical distribution of carbon fixation by *Prochlorococcus* in the water column show that, globally, 61% of the carbon is fixed in the upper water column (depth < 45 metres), where only 43% of the *Prochlorococcus* biomass is accumulated (**Chapter 4**). Although a significant fraction of the carbon fixation by *Prochlorococcus* occurs in the upper water column, a substantial amount of the carbon is fixed by this cyanobacterium at layers deeper than 45 metres in subtropical gyres, where *Prochlorococcus* cells are dominant among primary producers (Zubkov et al. 2000b; Heywood et al. 2006; Rabouille et al. 2007). Similar seasonal patterns of carbon fixation were predicted in this study for all five subtropical gyres (North and South Atlantic gyres, North and South Pacific gyres, and Indian gyre), with highest carbon fixation rates in

spring and summer and lowest during winter. The cyclic trends respond to oscillations in cell abundance (**Chapter 4**) combined with changes in photosynthetic rates due to seasonal fluctuations in light and nutrient conditions.

Measurements of vertical profiles of carbon fixation by *Prochlorococcus* in the natural environment are scarce, thus validating the model results is challenging. A recent study by Rii et al. (2016) measured carbon fixation of dominant picophytoplankton groups, including *Prochlorococcus*, at six discrete depths at the ALOHA station (22^{o}45'N, 158^{o} W) in the North Pacific gyre, at monthly intervals for over a year. In the present study, the lower variability in the range of *Prochlorococcus* productivity rates in the top 45 m of the water column (32 to 42 mg C m^{-2} d^{-1}) at a site in the NPG (22^{o} N, 166^{o} W) was within the range of measurements (17 to 81 mg C m^{-2} d^{-1}) made at the ALOHA station (22^{o}45'N, 158^{o} W) (Rii et al. 2016). Additionally, the present model predicts that the carbon fixation by *Prochlorococcus* is higher in deeper layers of the euphotic zone (45 to 200 m), except for the autumn and early winter periods when the contribution of the upper water column is higher than 50% (see **Fig. 5.5c**). Unfortunately, the deeper carbon fixation rates reported by Rii et al. (2016) are not directly comparable with the present study, since they consider the deep euphotic layer between depths of 75 and 125 metres. Thus, the study by Rii et al. (2016) disregards the depth interval between 45 and 75 metres, where *Prochlorococcus* cells can be most abundant (Rabouille et al. 2007) and consequently carbon fixation rates in this depth horizon may contribute a significant fraction of the water column productivity.

The spatial patterns of *Prochlorococcus* carbon fixation produced in the present study resemble those estimated by Rousseaux and Gregg (2013) for picocyanobacteria (*Prochlorococcus* and *Synechococcus*) using the NASA Ocean Biogeochemical Model (NOBM), although the estimated annual rate of global carbon fixation by cyanobacteria

in the biogeochemical model (4 Gt C year^{-1}) is lower than that predicted only for *Prochlorococcus* in the present study (4.7 Gt C year^{-1}). The spatial distribution patterns found in the studies above are in contrast to those found by Uitz et al. (2010), who estimated an annual carbon fixation of 11 Gt C year^{-1} for picophytoplankton (consisting of marine cyanobacteria *Prochlorococcus* and *Synechococcus*, and green flagellates) using marker pigments. The use of pigments is efficient to discriminate cyanobacteria, as they are the dominant phytoplankton members that contain zeaxanthin in the oligotrophic ocean (Roy et al. 2013). However, using diagnostic pigments as indicators of phytoplankton biomass disregards the effects of photoacclimation on the intracellular pigment concentration and pigment ratios (Partensky et al. 1993; Raven 2011), and thus may lead to a different estimate of phytoplankton biomass and carbon fixation in the surface ocean than estimates based on cell counts. In the case of *Prochlorococcus,* surface populations often present a reduced intracellular pigment content when subjected to high light intensities (Partensky et al. 1993). The present approach of using cell abundance data has the advantage of not being vulnerable to changes in the cellular pigmentation that may lead to errors in the estimation of the biomass and carbon fixation rates of *Prochlorococcus*.

The global estimate of carbon fixation by *Prochlorococcus* reported in this study is slightly higher than that calculated by Flombaum et al. (2013) (4 Gt C year^{-1}) based on a global abundance of 2.9 x 10^{27} *Prochlorococcus* cells and cell-specific carbon fixation rates measured by Li (1994), which are similar to the rates used in this study, measured by Hartmann et al. (2014) in the Atlantic subtropical gyres. This extrapolation of productivity rates by Flombaum et al. (2013) is calculated under the assumption that the annual carbon fixation depends exclusively on cell abundance, and that carbon fixation rates do not vary in response to environmental conditions (e.g. light and nutrients). The

present model demonstrates, for the first time, how the vertical distribution of carbon fixation of *Prochlorococcus* varies both globally and seasonally, accounting for light-dependent variations not only in cell abundance but also in carbon fixation rates. Moreover, this model has the potential of providing a three-dimensional view of the water-column *Prochlorococcus* productivity across different ocean basins in an operational manner.

The highest fraction of carbon fixation by *Prochlorococcus* takes place in the Pacific Ocean (58%), followed by the Atlantic (22%) and Indian (20%) Oceans, with most of the carbon fixation taking place in the North Pacific near the Equatorial Convergence Zone and in the Northern Indian Ocean, and a substantial amount of carbon fixed in the subtropical gyres (see **Fig.5.4**). In the Atlantic, where the cell-specific carbon fixation rates were measured, the high rates of carbon fixation by *Prochlorococcus* estimated in the Equatorial Convergence region and areas around subtropical gyres are a consequence of higher cell-specific carbon fixation rates measured in these areas when compared to the subtropical gyres (Hartmann et al. 2014) (**Fig. 5.3b**). This difference in carbon fixation rates can be attributed to the dominance of different *Prochlorococcus* ecotypes (Johnson et al. 2006), which respond distinctly to environmental forcing in these regions (Partensky et al. 1993; Shimada et al. 1996; Moore and Chisholm 1999; Hopkinson et al. 2014). Although nutrient input has been shown to increase carbon fixation rates in oligotrophic areas without changing the taxonomic composition or size structure of the phytoplankton communities (Marañón et al. 2003), this is likely a consequence of the physiological response of picoeukaryotes to nutrient availability (Marañón et al. 2003; Zubkov 2014). As *Prochlorococcus* utilizes nutrients in a variety of reduced and organic forms such as ammonia and amino-acids (Zubkov et al. 2004a; Zubkov and Tarran 2005a; Mary et al. 2008a; Casey et al. 2016), it is possible that the production of these

organic compounds may increase in response to the higher abundance and metabolism of herbivores in nutrient-enriched areas (where primary production is highest) such as the Equatorial Convergence Zone, fuelling the growth of *Prochlorococcus*.

5.5 Conclusions

Using the wealth of information on the depth distribution of *Prochlorococcus* and cell-specific carbon fixation rates from field and culture studies, a depth-resolved production model that includes the light-driven photosynthetic response of *Prochlorococcus* cells was developed and used to assess how surface and deep populations of these cells contribute to ocean productivity over basin scales and seasonal cycles.

The modified primary production model predicts that, over the global ocean, this minute cyanobacterium fixes 4.7 Gt C $year^{-1}$. Thus, *Prochlorococcus* contributes 10% of the global marine phytoplankton primary production, and 4.5% of the primary production on Earth including both marine and terrestrial biospheres. Although this contribution may appear modest, the global carbon fixation by *Prochlorococcus* shows little seasonal variability when compared to other algae, representing a stable supply of organic carbon that sustains the largest pelagic ecosystems in the world ocean.

When the subtropical gyres are examined separately, seasonal variations become more pronounced. The gyres cover vast areas of the global ocean (~50%, Longhurst 1998) where *Prochlorococcus* is the dominant primary producer (Zubkov et al. 1998b; Karl 1999). Rates of carbon fixation by *Prochlorococcus* in all gyres are highest during spring and summer and decrease in winter, following seasonal variations in light (which

influence both carbon fixation rates and cell abundance), and the thermal structure of the water column (an important determinant of cell abundance).

Most of the global carbon fixation by *Prochlorococcus* occurs at the top 45 metres of the water column (61%), where 43% of the *Prochlorococcus* cells reside. This vertical distribution occurs globally because light intensity is highest in the upper water column and decreases exponentially with depth, and higher *Prochlorococcus* cell-specific carbon fixation rates occur in areas where cells are most abundant in the upper water column, such as the Equatorial Convergence region (see **Fig. 5.3**) (Hartmann et al. 2014). In the central gyres, most of the carbon fixation occurs in the deeper euphotic layer between 45 and 200 metres, except during autumn and early winter in the North Atlantic and Pacific gyres, when cells are most abundant in the upper water column leading to an increase in carbon fixation.

The results generated by this model provide a synoptic view of the depth dependence of carbon fixation by *Prochlorococcus*, the most numerically abundant phytoplankton on Earth. The model builds on previous estimates by including parameters that describe the light-dependence of phytoplankton photosynthesis, providing a realistic representation of the depth dependence of *Prochlorococcu*s primary production. The relevance of light as a key driver governing the ecology and physiology of *Prochlorococcus* cells is well established, allowing the model developed in this study to be used to examine how surface and deep populations of this species contribute to ocean productivity. This approach also provides a useful framework for obtaining depth-resolved estimates of primary production for other picophytoplankton groups.

Chapter 6.

Final remarks and future perspectives

6.1 General conclusions

The main objective of this thesis was to develop a new tool to estimate the vertical distribution of the different functional groups of picophytoplankton on a global scale using remote-sensing observations. To accomplished this goal, one taxonomic group was chosen as a model organism: the cyanobacterium *Prochlorococcus*, which is not only ubiquitous in tropical and subtropical waters, but also the most numerically abundant phytoplankton on the planet. The remote-sensing models were developed using a compilation of empirical equations based on relationships between the abundance of *Prochlorococcus* and environmental variables that can be measured from satellites or ARGO sensors.

Although sometimes grouped together for conveniences in global biogeochemical models, it is widely known that the functional groups of picophytoplankton (*Prochlorococcus*, *Synechococcus*, and picoeukaryotes) respond to environmental variables in a different manner and, consequently, they play different roles in the marine biogeochemical cycles. **Chapter 1** presents a general background on the ecology and physiology of these picoplankton functional groups, as well as the methods used to quantify and identify these cells. The chapter also explores how this information can be used in remote-sensing models, providing an unprecedented view of the global distribution of these cells, including their vertical distribution in the water column, and their contribution to carbon fixation in the global ocean.

To better understand the response of two major groups of picophytoplankton, the cyanobacteria *Prochlorococcus* and *Synechococcus*, to the two main drivers governing their biogeography, the availability of light and nutrients, results of experiments set in the South Atlantic Gyre, where these groups are dominant, are described in **Chapter 2**. By testing the combined effects of different light levels and the addition of nutrients (nitrogen and iron) on the growth of picocyanobacteria, it was observed that light is the primary agent influencing the growth and optical properties (red fluorescence and right-angle light scatter - RALS) of these cells. However, in the gyre centre, *Prochlorococcus* cells showed an increase in their RALS signal when subjected to saturating light levels (> 700 μE m^{-2} s^{-1}) and nutrients (nitrogen and iron) were added, leading to a decrease in cell abundance. We speculate that these variations are a consequence of the increase in the iron availability, which would make *Prochlorococcus* cells more vulnerable to photodamage when exposed to high light. Iron addition is known to increase the photosynthetic electron transfer (Lea-Smith et al. 2016), which could damage other molecular components of the photosynthetic apparatus further down the photosynthesis reaction chain such as RuBisCO (Berepiki et al. 2016). This would lead to a decrease in red fluorescence, which was also observed in these cells subjected to high light and nutrient addition. These changes in optical characteristics were not observed in the gyre periphery, where the ambient concentration of nutrients is higher (Moore et al. 2013) and surface light intensities tend to be lower due to the presence of other phytoplankton groups absorbing and scattering light, resulting in increased light attenuation in the water column.

Taking into consideration the relevance of light in controlling the abundance of *Prochlorococcus* cells across different nutrient regimes, a large dataset was assembled for the development of empirical algorithms to predict the surface and depth-resolved

distribution of *Prochlorococcus* cells. The dataset included flow cytometric measurements of cell abundance, as well as environmental variables such as light, temperature, and water column attributes that are sensitive to the concentration of phytoplankton biomass (reflectance – R_{rs} at the wavebands of 443 and 488 nm), or indicators of water column stratification and hence nutrient input (temperature at 200 metres depth). For developing this algorithm, *Prochlorococcus* is an ideal model organism due to the wealth of available *in-situ* data, and for being ubiquitous in a vast region of the world's oceans, occurring from the latitude of 40°N to 40°S (Partensky et al. 1999). To ensure that the information contained in the different datasets compiled for this study was comparable, the different flow-cytometric methods used to quantify the abundance of *Prochlorococcus* cells were compared in **Chapter 3**. Results show that the difference between cell abundances quantified using the 'stained' (Zubkov et al. 2007) and 'unstained' (Olson et al. 1993) flow-cytometric methods is less than 20% (with an average of 17%), thus datasets that use the two approaches were assembled together. In addition, the efficiency of GF/F filters (used in the analysis of pigments and phytoplankton absorption) to retain the smallest *Prochlorococcus* cells that inhabit the sea surface of subtropical gyres was examined. More than 95% of these cells were retained on the filters, providing confidence that the filtration method is reliable to quantify pigments and absorption by picophytoplankton, even in regions where cells are extremely small.

Following this check for potential methodological bias, a dataset of flow cytometric picophytoplankton counts and environmental variables (temperature, light, chlorophyll fluorescence) measured in 13 Atlantic Meridional Transect (AMT) cruises was compiled for the development of empirical algorithms to predict the abundance of *Prochlorococcus* cells throughout the water column. **Chapter 4** describes how these empirical algorithms

were developed, including details on the selection of input variables, and the parameterization and validation of equations used to estimate the abundance of *Prochlorococcus* at the sea surface and near the deep chlorophyll maximum (*DCM*). The vertical distribution of the total abundance of *Prochlorococcus* cells was estimated by summing up the predicted abundances of two subpopulations, *ProI* and *ProII*, which in turn have their vertical distribution calculated as a function of the fraction of the sea surface light present at each depth (fractional PAR – *fPAR*). The subpopulation *ProI* occurs where *fPAR* levels are higher, ranging from 100% of the surface light intensity to the 1% light level, whereas *ProII* is abundant under low-light conditions near the *DCM*. The final model uses information from satellite observations (sea-surface temperature and R_{rs} at the wavebands of 443 and 488 nm, and ARGO data of the water temperature at 200 metres) to estimate the vertical distribution of *Prochlorococcus* cells anywhere in the global ocean. Results from the cell abundance model show that, despite their minute size and cellular biomass (Partensky et al. 1999), *Prochlorococcus* represents a significant amount of global carbon biomass: 171 Mt C contained in ~ 3.4×10^{27} cells. Most of this biomass is concentrated in areas near the Equatorial Convergence Zone and in the subtropical gyres. Globally, no significant temporal change was observed over the period of 2003 to 2014, but marked seasonal variations in cell abundance occur inside the subtropical gyres: in the Atlantic gyres, cell abundances are highest in the spring and summer, and lowest during the winter. Although the global estimate is similar to that calculated in a previous model (Flombaum et al. 2013), the spatial and temporal patterns in the abundance of *Prochlorococcus* cells predicted in this previous model differ from that estimated in the present study. However, results from the present study are in agreement with observations made in the natural environment (Zubkov et al. 2000b; Heywood et al. 2006; Rabouille et al. 2007; Brew et al. 2009), and provide a detailed

three-dimensional view of the distribution of *Prochlorococcus* biomass in the global ocean using remote-sensing observations.

Using the modelled fields of *Prochlorococcus* cell abundance, **Chapter 5** uses an adapted primary production model to estimate the vertical distribution of carbon fixation rates by *Prochlorococcus* in the global ocean. The primary production model, modified from the model described by Sathyendranath and Platt (1989), replaces chlorophyll biomass and chlorophyll-normalized carbon fixation rates with *Prochlorococcus* cell abundance and cell-specific carbon fixation rates (Hartmann et al. 2014) measured in the different provinces of the Atlantic Ocean (Longhurst 1998). The model estimates that, on a global scale, *Prochlorococcus* cells fix 4.7 Gt C $year^{-1}$. In general, spatial patterns of water-column primary production by *Prochlorococcus* coincide with the global distribution of cell abundance. However, an interesting feature was observed in the vertical distribution of primary production: globally, 61% of the carbon fixation occurs in the upper water column (0-45 metres), whereas over half of the cell stock (57%) is located below the surface layer (45-200m). This difference is in part a consequence of higher cell-specific carbon fixation rates measured in the Equatorial Convergence Zone (Hartmann et al. 2014), where productivity is more confined to the surface layers whereas, in the subtropical gyres, cell-specific rates are lower and the biomass resides in the low-light region of the water column. When only the subtropical gyres are considered, highest carbon fixation (62%) occurs at deeper layers (45-200m), and carbon fixation shows a marked seasonal pattern: highest values are found in spring (North Atlantic and Pacific gyres) and summer (South Atlantic, Pacific and Indian gyres), and lowest during winter. This seasonal cycle of carbon fixation in the central gyres is governed by seasonal variations in light and the thermal structure of the water column, which are primary factors governing rates of cell growth. Because of the difficulty of making species-

specific carbon fixation measurements in the natural environment, *in-situ* measurements of the vertical distribution of carbon fixation by *Prochlorococcus* in the water column are scarce (Rii et al. 2016), making these modelled estimates difficult to validate. However, the model is robust and considers most of the possible factors that can influence *Prochlorococcus* primary production. The *Prochlorococcus*-specific carbon fixation model provides, for the first time, a vertically-resolved estimate of primary production of this important cyanobacterium in the global ocean, considering the influence of light on not only cell abundance, but also on the photosynthetic rates by these cells.

Prochlorococcus contributes 171 Mt C to the global phytoplankton biomass, which is higher than the picophytoplankton biomass estimated in the mixed layer (140 Mt C, Roy et al. 2017), and fixes 4.7 Gt C $year^{-1}$, which is equivalent to 10% of the global carbon fixation in the oceans, and 4.5% of total net primary production on Earth. Although 61% of the carbon fixation occurs at the upper ocean (depth < 45 m), a significant fraction takes place in layers below 45 metres, and likely below the limits of the mixed layer. These results reinforce the fact that an important fraction of the carbon fixation by *Prochlorococcus* occurs below the mixed layer, especially in the subtropical gyres. This sub-surface carbon fixation must be taken into account in global biogeocheminal models, since subtropical gyres represent ~50% of the area of the global oceans (Longhurst 1998).

Although previous models have estimated the global abundance of *Prochlorococcus* cells, these models did not capture variations in cell abundance at depth, which may explain why estimates calculated by Flombaum et al. (2013) are 15% lower when compared to the estimate of the global *Prochlorococcus* standing stock computed in the present study. The model results generated in this thesis provide an unprecedented global view of the vertical distribution of biomass and carbon fixation by *Prochlorococcus*, a marine cyanobacterium of global importance.

6.2 Future perspectives

The results produced by this thesis advance our ability to examine temporal changes in the production of *Prochlorococcus* over basin scales. Although the model captures the light-dependence of *Prochlorococcus* photosynthesis, which drives its global distribution, there is scope for further refinements. The parameterisation of the cell abundance model is based on a dataset that is geographically biased to the Atlantic basin, whereas data from the Pacific and Indian Oceans (PANGAEA dataset after 2002) were used only for validation. A broader coverage of spatial *in-situ* data can improve the equation used to estimate the abundance of *Prochlorococcus* cells at the sea surface (Pro_{surf}) by regionally tuning it for each ocean basin. Improvement of estimates of Pro_{surf} will increase the model's ability to accurately predict of the vertical distribution of *Prochlorococcus* cells in other ocean basins.

Estimates of carbon fixation by *Prochlorococcus* can also be improved through two modifications: 1) by using province-specific measurements of P_m^{cell} from the Pacific and Indian Oceans to estimate carbon fixation in these ocean basins, as P_m^{cell} values used in this study were measured in the Atlantic; 2) by using a depth- (or light-) dependent α^{cell} instead of an average α^{cell} taken from the literature, although this will likely not lead to a significant change in model outputs, since integrated models of light limited photosynthesis are less sensitive to changes in α than in P_m (Bouman et al. 2000).

The models developed in this thesis are useful tools to estimate the contribution of a single species to the global phytoplankton biomass and primary production using Earth observations. The cell-based carbon fixation model developed for *Prochlorococcus* has the potential to be applied to other picophytoplankton groups contained in large *in-situ* datasets, such as *Synechococcus* and possibly to some species of picoeukaryotes. Once

relationships between remotely-sensed variables and the abundance of the target organism or group are established, the vertical distribution of cells can be predicted if, as in the case of *Prochlorococcus*, its vertical structure is primarily governed by depth-dependent changes in light. Another requirement to apply this model to other phytoplankton groups is that cell-specific carbon fixation rates are well known. Refined models of species-specific productivity that capture the light-dependence of carbon fixation will provide a more robust assessment of the contribution of different phytoplankton species to the global carbon cycle, and aid our understanding of their ecological and biogeochemical significance.

***

References

Aiken, J., Brewin, R.J.W., Dufois, F., Polimene, L., Hardman-Mountford, N.J., Jackson, T., Loveday, B., Hoya, S.M., Dall'Olmo, G., Stephens, J., Hirata, T., 2016. A synthesis of the environmental response of the North and South Atlantic Sub-Tropical Gyres during two decades of AMT. *Prog. Oceanogr.* doi:10.1016/j.pocean.2016.08.004

Arrigo, K.R., Van Dijken, G.L., Bushinsky, S., 2008. Primary production in the Southern Ocean, 1997-2006. *J. Geophys. Res. Ocean.* 113. doi:10.1029/2007JC004551

Barker, S., Higgins, J., Elderfield, H., 2003. The future of the carbon cycle: review, calcification response, ballast and feedback on atmospheric CO_2. *Philos. Trans. A. Math. Phys. Eng. Sci.* 361, 1977-98–9. doi:10.1098/rsta.2003.1238

Barton, A.D., Ward, B.A., Williams, R.G., Follows, M.J., 2014. The impact of fine-scale turbulence on phytoplankton community structure. *Limnol. Oceanogr. Fluids Environ.* 4, 34–49. doi:10.1215/21573689-2651533

Behrenfeld, M.J., Falkowski, P.G., 1997. Photosynthetic rates derived from satellite-based chlorophyll concentration. *Limnol. Oceanogr.* 42, 1–20. doi:10.4319/lo.1997.42.1.0001

Behrenfeld, M.J., Boss, E., Siegel, D.A., Shea, D.M., 2005. Carbon-based ocean productivity and phytoplankton physiology from space. *Global Biogeochem. Cycles* 19. doi:10.1029/2004GB002299

Behrenfeld, M.J., O'Malley, R.T., Boss, E.S., Westberry, T.K., Graff, J.R., Halsey, K.H., Milligan, A.J., Siegel, D.A., Brown, M.B., 2015. Revaluating ocean warming impacts on global phytoplankton. *Nat. Clim. Chang.* 6, 323–330. doi:10.1038/nclimate2838

Berepiki, A., Hitchcock, A., Moore, C.M., Bibby, T.S., 2016. Tapping the unused potential of photosynthesis with a heterologous electron sink. *ACS Synth. Biol.* 5, 1369–1375. doi:10.1021/acssynbio.6b00100

Berg, H.C., Purcell, E.M., 1977. Physics of chemoreception. *Biophys. J.* 20, 193–219. doi:10.1016/S0006-3495(77)85544-6

Berglund, J., Müren, U., Båmstedt, U., Andersson, A., 2007. Efficiency of a phytoplankton-based and a bacterial-based food web in a pelagic marine system. *Limnol. Oceanogr.* 52, 121–131. doi:10.4319/lo.2007.52.1.0121

Bertilsson, S., Berglund, O., Karl, D.M., Chisholm, S.W., 2003. Elemental composition of marine *Prochlorococcus* and *Synechococcus*: Implications for the ecological stoichiometry of the sea. *Limnol. Oceanogr.* 48, 1721–1731. doi:10.4319/lo.2003.48.5.1721

Berube, P.M., Biller, S.J., Kent, A.G., Berta-Thompson, J.W., Roggensack, S.E., Roache-Johnson, K.H., Ackerman, M., Moore, L.R., Meisel, J.D., Sher, D., Thompson, L.R., Campbell, L., Martiny, A.C., Chisholm, S.W., 2015. Physiology and evolution of nitrate acquisition in *Prochlorococcus*. *ISME J.* 9, 1195–1207. doi:10.1038/ismej.2014.211

Biller, S.J., Berube, P.M., Lindell, D., Chisholm, S.W., 2014a. *Prochlorococcus*: the structure and function of collective diversity. *Nat. Rev. Microbiol.* 13, 13–27. doi:10.1038/nrmicro3378

Biller, S.J., Schubotz, F., Roggensack, S.E., Thompson, A.W., Summons, R.E., Chisholm, S.W., 2014b. Bacterial vesicles in marine ecosystems. *Science* 343, 183–6. doi:10.1126/science.1243457

Boggs, S.W., 1945. This Hemisphere. *J. Geog.* 44, 345–355.

Boney, A.D., 1976. *Phytoplankton*. Institute of Biology/Studies in Biology 52, Edward Arnold, London, UK.

Bouman, H.A., Platt, T., Kraay, G.W., Sathyendranath, S., Irwin, B.D., 2000. Bio-optical properties of the subtropical North Atlantic. I. Vertical variability. *Mar. Ecol. Prog. Ser.* 200, 3–18. doi:10.3354/meps200003

Bouman, H.A., Ulloa, O., Scanlan, D.J., Zwirglmaier, K., Li, W.K.W., Platt, T., Stuart, V., Barlow, R., Leth, O., Clementson, L., Lutz, V., Fukasawa, M., Watanabe, S., Sathyendranath, S., 2006. Oceanographic basis of the global surface distribution of *Prochlorococcus* ecotypes. *Science* 312, 918–21. doi:10.1126/science.1122692

Bouman, H.A., Ulloa, O., Barlow, R., Li, W.K.W., Platt, T., Zwirglmaier, K., Scanlan, D.J., Sathyendranath, S., 2011. Water-column stratification governs the community structure of subtropical marine picophytoplankton. *Environ. Microbiol. Rep.* 3, 473–482. doi:10.1111/j.1758-2229.2011.00241.x

Bouman, H.A., Platt, T., Doblin, M.A., Figueiras, F.G, Gudmundsson, K.,;Gudfinnsson, H.G, Huang, B., Hickman, A., Hiscock, M.R., Jackson, T., Lutz, V.A., Melin, F., Rey, F., Pepin, P., Segura, V., Tilstone, G., van Dongen-Vogels, V., Sathyendranath, S., 2017. A global dataset of photosynthesis-irradiance parameters for marine phytoplankton. *PANGAEA*, https://doi.org/10.1594/PANGAEA.874087

Boyce, D.G., Lewis, M.R., Worm, B., 2010. Global phytoplankton decline over the past century. *Nature* 466, 591–6. doi:10.1038/nature09268

Brew, H.S., Moran, S.B., Lomas, M.W., Burd, A.B., 2009. Plankton community composition, organic carbon and thorium-234 particle size distributions, and particle export in the Sargasso Sea. *J. Mar. Res.* 67, 845–868. doi:10.1357/002224009792006124

Brewin, R.J.W., Lavender, S.J., Hardman-Mountford, N.J., 2010a. Mapping size-specific phytoplankton primary production on a global scale. *J. Maps* 6, 448–462. doi:10.4113/jom.2010.1122

Brewin, R.J.W., Sathyendranath, S., Hirata, T., Lavender, S.J., Barciela, R.M., Hardman-Mountford, N.J., 2010b. A three-component model of phytoplankton size class for the Atlantic Ocean. *Ecol. Modell.* 221, 1472–1483. doi:10.1016/j.ecolmodel.2010.02.014

Brewin, R.J.W., Hardman-Mountford, N.J., Lavender, S.J., Raitsos, D.E., Hirata, T., Uitz, J., Devred, E., Bricaud, A., Ciotti, A., Gentili, B., 2011. An intercomparison of bio-optical techniques for detecting dominant phytoplankton size class from satellite remote sensing. *Remote Sens. Environ.* 115, 325–339. doi:10.1016/j.rse.2010.09.004

Brewin, R.J.W., Sathyendranath, S., Lange, P.K., Tilstone, G., 2013. Comparison of two methods to derive the size-structure of natural populations of phytoplankton. *Deep-Sea Res. Part I* 85, 72–79. doi:10.1016/j.dsr.2013.11.007

Brewin, R.J.W., Sathyendranath, S., Tilstone, G., Lange, P.K., Platt, T., 2014. A multicomponent model of phytoplankton size structure. *J. Geophys. Res. Ocean.* 119, 3478–3496. doi:10.1002/2014JC009859

Brewin, R.J.W., Sathyendranath, S., Müller, D., Brockmann, C., Deschamps, P.Y., Devred, E., Doerffer, R., Fomferra, N., Franz, B., Grant, M., Groom, S., Horseman, A., Hu, C., Krasemann, H., Lee, Z.P., Maritorena, S., Mélin, F., Peters, M., Platt, T., Regner, P., Smyth, T., Steinmetz, F., Swinton, J., Werdell, J., White, G.N., 2015. The Ocean Colour Climate Change Initiative: III. A round-robin comparison on in-water bio-optical algorithms. *Remote Sens. Environ.* 162, 271–294. doi:10.1016/j.rse.2013.09.016

Brewin, R.J.W., Tilstone, G.H., Jackson, T., Cain, T., Miller, P.I., Lange, P.K., Misra, A., Airs, R.L., 2017. Modelling size-fractionated primary production in the Atlantic Ocean from remote sensing. *Prog. Oceanogr.* doi:10.1016/j.pocean.2017.02.002

Briat, J.F., Dubos, C., Gaymard, F., 2015. Iron nutrition, biomass production, and plant product quality. *Trends Plant Sci.* doi:10.1016/j.tplants.2014.07.005

Bruyant, F., Babin, M., Genty, B., Prasil, O., Behrenfeld, M.J., Claustre, H., Bricaud, A., Garczarek, L., Holtzendorff, J., Koblizek, M., 2005. Diel variations in the photosynthetic parameters of *Prochlorococcus* strain PCC 9511: Combined effects of light and cell cycle. *Limnol. Oceanogr.* 50, 850–863. doi:10.4319/lo.2005.50.3.0850

Bryant, D.A., 2003. The beauty in small things revealed. *Proc. Natl. Acad. Sci.* 100, 9647–9649. doi:10.1073/pnas.1834558100

Buitenhuis, E.T., Li, W.K.W., Vaulot, D., Lomas, M.W., Landry, M.R., Partensky, F., Karl, D.M., Ulloa, O., Campbell, L., Jacquet, S., Lantoine, F., Chavez, F., Macias, D., Gosselin, M., McManus, G.B., 2012. Picophytoplankton biomass distribution in the global ocean. *Earth Syst. Sci. Data* 4, 37–46. doi:10.5194/essd-4-37-2012

Butcher, R.W., 1952. Contributions to our knowledge of the smaller marine algae. *J. Mar. Biol. Assoc. UK* 31, 175–191. doi:10.1017/S0025315400003751

Cabré, A., Shields, D., Marinov, I., Kostadinov, T.S., 2016. Phenology of size-partitioned phytoplankton carbon-biomass from ocean color remote sensing and CMIP5 models. *Front. Mar. Sci.* 3, 1–20. doi:10.3389/fmars.2016.00039

Casey, J.R., Mardinoglu, A., Nielsen, J., Karl, D.M., 2016. Adaptive evolution of phosphorus metabolism in *Prochlorococcus*. *mSystems* 1, 1–15. doi:10.1128/mSystems.00065-16.Editor

Chen, B.Z., Liu, H.B., 2010. Relationships between phytoplankton growth and cell size in surface oceans: Interactive effects of temperature, nutrients, and grazing. *Limnol. Ocean.* 55, 965–972. doi:10.4319/lo.2010.55.3.0965

Chisholm, S.W., Olson, R.J., Zettler, E.R., Goericke, R., Waterbury, J.B., 1988. A novel free-living prochlorophyte abundant in the oceanic euphotic zone. *Nature* 334, 340–343.

Chisholm, S.W., Frankel, S.L., Goericke, R., Olson, R.J., Palenik, B., Waterbury, J.B., West-Johnsrud, L., Zettler, E.R., 1992. *Prochlorococcus marinus* nov. gen. nov. sp.: an oxyphototrophic marine prokaryote containing divinyl chlorophyll *a* and *b*. *Arch. Microbiol.* 157, 297–300. doi:10.1007/BF00245165

Church, M.J., Ducklow, H.W., Karl, D.M., 2004. Light dependence of [^{3}H]leucine incorporation in the oligotrophic North Pacific ocean. *Appl. Environ. Microbiol.* 70, 4079–4087. doi:10.1128/AEM.70.7.4079-4087.2004

Claustre, H., Bricaud, A., Babin, M., Bruyant, F., Guillou, L., Le Gall, F., Marie, D., Partensky, F., 2002. Diel variations in *Prochlorococcus* optical properties. *Limnol. Oceanogr.* 47, 1637–1647. doi:10.4319/lo.2002.47.6.1637

Cooper, P.I., 1969. The absorption of radiation in solar stills. *Sol. Energy* 12, 333–346. doi:10.1016/0038-092X(69)90047-4

Cubillos-ruiz, A., Berta-thompson, J.W., Becker, J.W., Donk, W.A., 2017. Evolutionary radiation of lanthipeptides in marine cyanobacteria. *Proc. Natl. Acad. Sci. USA*. 201700990. doi:10.1073/pnas.1700990114

Cullen, J.J., 1982. The deep chlorophyll maximum: comparing vertical profiles of chlorophyll *a*. *Can. J. Fish. Aquat. Sci.* 39, 791–803.

Dave, A.C., Barton, A.D., Lozier, M.S., McKinley, G.A., 2015. What drives seasonal change in oligotrophic area in the subtropical North Atlantic? *J. Geophys. Res. C Ocean.* 120, 3958–3969. doi:10.1002/2015JC010787

de Boyer Montégut, C., Madec, G., Fischer, A.S., Lazar, A., Iudicone, D., 2004. Mixed layer depth over the global ocean: An examination of profile data and a profile-based climatology. *J. Geophys. Res. Ocean.* 109, 1–20. doi:10.1029/2004JC002378

Ducklow, H.W., Steinberg, D.K., Buesseler, K.O., 2001. Upper ocean carbon export and the biological pump. *Oceanography* 14, 50–58. doi:10.5670/oceanog.2001.06

DuRand, M.D., Olson, R.J., 1998. Diel patterns in optical properties of the chlorophyte *Nannochloris* sp.: Relating individual-cell to bulk measurements. *Limnol. Oceanogr.* 43, 1107–1118. doi:10.4319/lo.1998.43.6.1107

DuRand, M.D., Olson, R.J., Chisholm, S.W., 2001. Phytoplankton population dynamics at the Bermuda Atlantic Time-series station in the Sargasso Sea. *Deep-Res. Part II* 48, 1983–2003. doi:10.1016/S0967-0645(00)00166-1

DuRand, M.D., Green, R.E., Sosik, H.M., Olson, R.J., 2002. Diel variations in optical properties of *Micromonas pusilla* (Prasinophyceae). *J. Phycol.* 38, 1132–1142. doi:10.1046/j.1529-8817.2002.02008.x

Feely, R., Sabine, C., Takahashi, T., Wanninkhof, R., 2001. Uptake and storage of carbon dioxide in the ocean: the global CO_2 survey. *Oceanography* 14, 18–32. doi:10.5670/oceanog.2001.03

Field, C.B., Behrenfeld, M.J., Randerson, J.T., Falkowski, P., 1998. Primary production of the biosphere: integrating terrestrial and oceanic components. *Science* 281, 237–240. doi:10.1126/science.281.5374.237

Flombaum, P., Gallegos, J.L., Gordillo, R.A., Rincon, J., Zabala, L.L., Jiao, N., Karl, D.M., Li, W.K.W., Lomas, M.W., Veneziano, D., Vera, C.S., Vrugt, J.A., Martiny, A.C., 2013. Present and future global distributions of the marine cyanobacteria *Prochlorococcus* and *Synechococcus*. *Proc. Natl. Acad. Sci.* 110, 9824–9829. doi:10.1073/pnas.1307701110

Goericke, R., Repeta, D., 1993. Chlorophylls *a* and *b* and divinyl chlorophylls *a* and *b* in the open subtropical North Atlantic Ocean. *Mar. Ecol. Prog. Ser.* 101, 307–313. doi:10.3354/meps101307

Gómez-Pereira, P.R., Hartmann, M., Grob, C., Tarran, G. a, Martin, A.P., Fuchs, B.M., Scanlan, D.J., Zubkov, M.V., 2013. Comparable light stimulation of organic nutrient uptake by *SAR11* and *Prochlorococcus* in the North Atlantic subtropical gyre. *ISME J.* 7, 603–14. doi:10.1038/ismej.2012.126

Gordon, H.R., Morel, A.Y., 1983. *Remote assessment of ocean color for interpretation of satellite visible imagery.* Springer-Verlag New York, New York, USA.

Grace, J., San Jose, J., Meir, P., Miranda, H.S., Montes, R.A., 2006. Productivity and carbon fluxes of tropical savannas. *J. Biogeogr.*, 387–400. doi:10.1111/j.1365-2699.2005.01448.x

Grob, C., Hartmann, M., Zubkov, M. V., Scanlan, D.J., 2011. Invariable biomass-specific primary production of taxonomically discrete picoeukaryote groups across the Atlantic Ocean. *Environ. Microbiol.* 13, 3266–3274. doi:10.1111/j.1462-2920.2011.02586.x

Hartmann, M., Zubkov, M. V., Scanlan, D.J., Lepère, C., 2013. *In situ* interactions between photosynthetic picoeukaryotes and bacterioplankton in the Atlantic Ocean: Evidence for mixotrophy. *Environ. Microbiol. Rep.* 5, 835–840. doi:10.1111/1758-2229.12084

Hartmann, M., Gomez-Pereira, P., Grob, C., Ostrowski, M., Scanlan, D.J., Zubkov, M. V, 2014. Efficient CO_2 fixation by surface *Prochlorococcus* in the Atlantic Ocean. *ISME J.* 8, 2280–2289. doi:10.1038/ismej.2014.56

Heywood, J.L., Zubkov, M.V., Tarran, G.A., Fuchs, B.M., Holligan, P.M., 2006. Prokaryoplankton standing stocks in oligotrophic gyre and equatorial provinces of the Atlantic Ocean: Evaluation of inter-annual variability. *Deep-Sea Res. Part II* 53, 1530–1547. doi:10.1016/j.dsr2.2006.05.005

Hickman, A.E., Holligan, P.M., Moore, C.M., Sharples, J., Krivtsov, V., Palmer, M.R., 2009. Distribution and chromatic adaptation of phytoplankton within a shelf sea thermocline. *Limnol. Oceanogr.* 54, 525–536. doi:10.4319/lo.2009.54.2.0525

Hijmans, R.J., 2016. *raster: Geographic data analysis and modelling.* R package version 2.5-8.

Hirata, T., Aiken, J., Hardman-mountford, N., Smyth, T.J., Barlow, R.G., 2008. An absorption model to determine phytoplankton size classes from satellite ocean colour, *Rem. Sens. Envir.* 112, 3153–3159. doi:10.1016/j.rse.2008.03.011

Hirata, T., Saux-Picart, S., Hashioka, T., Aita-Noguchi, M., Sumata, H., Shigemitsu, M., Allen, J.I., Yamanaka, Y., 2013. A comparison between phytoplankton community structures derived from a global 3D ecosystem model and satellite observation. *J. Mar. Syst.* 109–110, 129–137. doi:10.1016/j.jmarsys.2012.01.009

Hopkinson, B.M., Young, J.N., Tansik, A.L., Binder, B.J., 2014. The minimal CO_2-concentrating mechanism of *Prochlorococcus* spp. MED4 is effective and efficient. *Plant Physiol.* 166, 2205–2217. doi:10.1104/pp.114.247049

Hosoda, S., Ohira, T., Nakamura, T., 2008. A monthly mean dataset of global oceanic temperature and salinity derived from Argo float observations. *JAMSTEC Rep. Res. Dev.* 8, 47–59. doi:10.5918/jamstecr.8.47

Huot, Y., Babin, M., 2010. Overview of fluorescence protocols: theory, basic concepts, and practice. *In: Chlorophyll a fluorescence in aquatic science: Methods and applications,* 31–74. doi:10.1007/978-90-481-9268-7

Hynes, A.M., Blythe, B.J., Binder, B.J., 2015. An individual-based model for the analysis of *Prochlorococcus* diel cycle behavior. *Ecol. Modell.* 301, 1–15. doi:10.1016/j.ecolmodel.2015.01.011

Jacquet, S., Partensky, F., Marie, D., Casotti, R., Vaulot, D., 2001. Cell cycle regulation by light in *Prochlorococcus* strains. *Appl. Environ. Microbiol.* 67, 782–790. doi:10.1128/AEM.67.2.782-790.2001

James, D., Hornik, K., 2017. *chron: Chronological objects which can handle dates and times*. R package version 2.3-50.

Jardillier, L., Zubkov, M.V., Pearman, J., Scanlan, D.J., 2010. Significant CO_2 fixation by small prymnesiophytes in the subtropical and tropical northeast Atlantic Ocean. *ISME J.* 4, 1180–1192. doi:10.1038/ismej.2010.36

Johnson, Z.I., Zinser, E.R., Coe, A., McNulty, N.P., Woodward, E.M., Chisholm, S.W., 2006. Niche partitioning among *Prochlorococcus* ecotypes along ocean-scale environmental gradients. *Science* 311, 1737–1740. doi:10.1126/science.1118052

Johnson, Z.I., Lin, Y., 2009. *Prochlorococcus*: approved for export. *Proc. Natl. Acad. Sci.* 106, 10400–10401. doi:10.1073/pnas.0905187106

Karl, D.M., 1999. Minireviews: A sea of change: biogeochemical variability in the North Pacific Subtropical Gyre. *Ecosystems* 2, 181–214. doi:10.1007/s100219900068

Karl, D.M., Bidigare, R.R., Letelier, R.M., 2001. Long-term changes in plankton community structure and productivity in the North Pacifc Subtropical Gyre: The domain shift hypothesis. *Deep-Sea Res. Part II* 48 (8-9), 1449-1470. doi: 10.1016/S0967-0645(00)00149-1

Kettler, G.C., Martiny, A.C., Huang, K., Zucker, J., Coleman, M.L., Rodrigue, S., Chen, F., Lapidus, A., Ferriera, S., Johnson, J., Steglich, C., Church, G.M., Richardson, P., Chisholm, S.W., 2007. Patterns and implications of gene gain and loss in the evolution of *Prochlorococcus*. *PLoS Genet.* 3, 2515–2528. doi:10.1371/journal.pgen.0030231

Kiørboe, T., 1993. Turbulence, phytoplankton cell size, and the structure of pelagic food webs. *Advances in Marine Biology* 29, 1-72. doi:10.1016/S0065-2881(08)60129-7

Kirk, J.T.O., 2011. *Light and photosynthesis in aquatic ecosystems*, 3rd ed. Cambridge University Press, Cambridge.

Kirkham, A.R., Jardillier, L.E., Holland, R., Zubkov, M. V., Scanlan, D.J., 2011. Analysis of photosynthetic picoeukaryote community structure along an extended Ellett Line transect in the northern North Atlantic reveals a dominance of novel prymnesiophyte and prasinophyte phylotypes. *Deep-Sea Res. Part I* 58, 733–744. doi:10.1016/j.dsr.2011.05.004

Kirkham, A.R., Lepère, C., Jardillier, L.E., Not, F., Bouman, H., Mead, A., Scanlan, D.J., 2013. A global perspective on marine photosynthetic picoeukaryote community structure. *ISME J.* 7, 922–36. doi:10.1038/ismej.2012.166

Kletou, D., Hall-Spencer, J.M., 2010. Threats to ultraoligotrophic marine ecosystems. *Mar. Ecosyst.* 1–35. doi:10.5772/34842

Kostadinov, T.S., Milutinovi, S., Marinov, I., Cabre, A., 2016. Carbon-based phytoplankton size classes retrieved via ocean color estimates of the particle size distribution. *Ocean Sci.* 12, 561–575. doi:10.5194/os-12-561-2016

Kulk, G., de Poll, W.H. Van, Visser, R.J.W., Buma, A.G.J., 2011. Distinct differences in photoacclimation potential between prokaryotic and eukaryotic oceanic phytoplankton. *J. Exp. Mar. Bio. Ecol.* 398, 63–72. doi:10.1016/j.jembe.2010.12.011

Landolfi, A., Dietze, H., Volpe, G., 2016. Longitudinal variability of organic nutrients in the North Atlantic subtropical gyre. *Deep-Sea Res. Part I* 111, 50–60. doi:10.1016/j.dsr.2015.11.009

Le Quéré, C., Harrison, S.P., Prentice, I.C., Buitenhuis, E.T., Aumont, O.,Bopp, L.,Claustre, H., Da Cunha, L.C., Geider, R., Giraud, X., Klaas, C., Kohfeld, K.E., Legendre, L., Manizza, M., Platt, T., Rivkin, R.B., Sathyendranath, S., Uitz, J., Watson, A.J., Wolf-Gladrow, D., 2005. Ecosystem dynamics based on plankton functional types for global ocean biogeochemistry models. *Global Change Biol.* 11(11), 2016-2040.

Lea-Smith, D.J., Bombelli, P., Vasudevan, R., Howe, C.J., 2016. Photosynthetic, respiratory and extracellular electron transport pathways in cyanobacteria. *Biochim. Biophys. Acta - Bioenerg.* 1857, 247–255. doi:10.1016/j.bbabio.2015.10.007

Lefort, T., Gasol, J.M., 2014. Short-time scale coupling of picoplankton community structure and single-cell heterotrophic activity in winter in coastal NW Mediterranean Sea waters. *J. Plankton Res.* 36, 243–258. doi:10.1093/plankt/fbt073

Legendre, L., Le Févre, J., 1989. Hydrodynamical singularities as control of recycled versus export production in oceans. *In: Berger W.H. et al. (eds.) Productivity of the ocean: Present Past*, 49–63.

Li, W.K.W., 1994. Primary production of prochlorophytes, cyanobacteria, and eucaryotic ultraphytoplankton: Measurements from flow cytometric sorting. *Limnol. Oceanogr.* 39, 169–175. doi:10.4319/lo.1994.39.1.0169

Li, W.K.W., 2002. Macroecological patterns of phytoplankton in the northwestern North Atlantic Ocean. *Nature* 419, 154–7. doi:10.1038/nature00994

Li, W.K.W., 2007. Macroscopic patterns in marine plankton, *In: Levin, S.A. (Ed.), Encyclopedia of Biodiversity*. Elsevier.

Lin, Y., Gazsi, K., Lance, V.P., Larkin, A.A., Chandler, J.W., Zinser, E.R., Johnson, Z.I., 2013. *In situ* activity of a dominant *Prochlorococcus* ecotype (eHL-II) from rRNA content and cell size. *Environ. Microbiol.* 15, 2736–2747. doi:10.1111/1462-2920.12135

Lomas, M.W., Moran, S.B., 2011. Evidence for aggregation and export of cyanobacteria and nano-eukaryotes from the Sargasso Sea euphotic zone. *Biogeosciences* 8, 203–216. doi:10.5194/bg-8-203-2011

Longhurst, A., 1998. *Ecological geography of the sea.* San Diego: Academic Press, San Diego.

López-Sandoval, D.C., Rodríguez-Ramos, T., Cermeño, P., Sobrino, C., Marañón, E., 2014. Photosynthesis and respiration in marine phytoplankton: Relationship with cell size, taxonomic affiliation, and growth phase. *J. Exp. Mar. Bio. Ecol.* 457, 151–159. doi:10.1016/j.jembe.2014.04.013

Malmstrom, R.R., Coe, A., Kettler, G.C., Martiny, A.C., Frias-Lopez, J., Zinser, E.R., Chisholm, S.W., 2010. Temporal dynamics of *Prochlorococcus* ecotypes in the Atlantic and Pacific oceans. *ISME J.* 4, 1252–1264. doi:10.1038/ismej.2010.60

Mann, E.L., Chisholm, S.W., 2000. Iron limits the cell division rate of *Prochlorococcus* in the eastern equatorial Pacific. *Limnol. Oceanogr.* 45, 1067–1076. doi:10.4319/lo.2000.45.5.1067

Marañón, E., Behrenfeld, M.J., Gonzalez, N., Mourino, B., Zubkov, M.V., 2003. High variability of primary production in oligotrophic waters of the Atlantic Ocean: uncoupling from phytoplankton biomass and size structure. *Mar. Ecol. Prog. Ser.* 257, 1–11.

Marañón, E., Cermeno, P., Rodriguez, J., Zubkov, M.V., Harris, R.P., 2007. Scaling of phytoplankton photosynthesis and cell size in the ocean. *Limnol. Oceanogr.* 52, 2190–2198. doi:10.4319/lo.2007.52.5.2190

Marañón, E., 2014. Cell size as a key determinant of phytoplankton metabolism and community structure. *Ann. Rev. Mar. Sci.* 7, 241–64. doi:10.1146/annurev-marine-010814-015955

Marchetti, A., Parker, M.S., Moccia, L.P., Lin, E.O., Arrieta, A.L., Ribalet, F., Murphy, M.E.P., Maldonado, M.T., Armbrust, E.V., 2009. Ferritin is used for iron storage in bloom-forming marine pennate diatoms. *Nature* 457, 467–70. doi:10.1038/nature07539

Margalef, R., 1968. *Perspectives in ecological theory.* Univ. Chicago Press, Chicago doi:10.1515/9781400860180

Marie, D., Partensky, F., Vaulot, D., Brussard, C., 1999. Enumeration of phytoplankton, bacteria, and viruses in marine samples. *Curr. Protoc. Cytom.* doi:10.1002/0471142956.cy0706s02

Marquis, E., Niquil, N., Delmas, D., Hartmann, H.J., Bonnet, D., Carlotti, F., Herbland, A., Labry, C., Sautour, B., Laborde, P., Vézina, A., Dupuy, C., 2007. Inverse analysis of the planktonic food web dynamics related to phytoplankton bloom development on the continental shelf of the Bay of Biscay, French coast. *Estuar. Coast. Shelf Sci.* 73, 223–235. doi:10.1016/j.ecss.2007.01.003

Mary, I., Garczarek, L., Tarran, G.A., Kolowrat, C., Terry, M.J., Scanlan, D.J., Burkill, P.H., Zubkov, M.V., 2008a. Diel rhythmicity in amino acid uptake by *Prochlorococcus*. *Environ. Microbiol.* 10, 2124–31. doi:10.1111/j.1462-2920.2008.01633.x

Mary, I., Tarran, G.A., Warwick, P.E., Terry, M.J., Scanlan, D.J., Burkill, P.H., Zubkov, M.V., 2008b. Light enhanced amino acid uptake by dominant bacterioplankton groups in surface waters of the Atlantic Ocean. *FEMS Microbiol. Ecol.* 63, 36–45. doi:10.1111/j.1574-6941.2007.00414.x

McClain, C.R., Signorini, S.R., Christian, J.R., 2004. Subtropical gyre variability observed by ocean-color satellites. *Deep-Res. Part II* 51, 281–301. doi:10.1016/j.dsr2.2003.08.002

Mella-Flores, D., Six, C., Ratin, M., Partensky, F., Boutte, C., Le Corguillé, G., Marie, D., Blot, N., Gourvil, P., Kolowrat, C., Garczarek, L., 2012. *Prochlorococcus* and *Synechococcus* have evolved different adaptive mechanisms to cope with light and uv stress. *Front. Microbiol.* 3. doi:10.3389/fmicb.2012.00285

Moore, C.M., Mills, M.M., Arrigo, K.R., Berman-Frank, I., Bopp, L., Boyd, P.W., Galbraith, E.D., Geider, R.J., Guieu, C., Jaccard, S.L., Jickells, T.D., La Roche, J., Lenton, T.M., Mahowald, N.M., Marañón, E., Marinov, I., Moore, J.K., Nakatsuka, T., Oschlies, A., Saito, M.A., Thingstad, T.F., Tsuda, A., Ulloa, O., 2013. Processes and patterns of oceanic nutrient limitation. *Nat. Geosci.* 6, 701–710. doi:10.1038/ngeo1765

Moore, L.R., Chisholm, S.W., 1999. Photophysiology of the marine cyanobacterium *Prochlorococcus*: ecotypic differences among cultured isolates. *Limnol. Oceanogr.* 44, 628–638. doi:10.4319/lo.1999.44.3.0628

Moore, L.R., Post, A.F., Rocap, G., Chisholm, S.W., 2002. Utilization of different nitrogen sources by the marine cyanobacteria *Prochlorococcus* and *Synechococcus*. *Limnol. Oceanogr.* 47, 989–996. doi:10.4319/lo.2002.47.4.0989

Moran, S.B., Lomas, M.W., Kelly, R.P., Gradinger, R., Iken, K., Mathis, J.T., 2012. Seasonal succession of net primary productivity, particulate organic carbon export, and autotrophic community composition in the eastern Bering Sea. *Deep-Sea Res. Part II* 65–70, 84–97. doi:10.1016/j.dsr2.2012.02.011

Morel, A., Berthon, J.-F., 1989. Surface pigments, algal biomass profiles, and potential production of the euphotic layer: Relationships reinvestigated in view of remote-sensing applications. *Limnol. Oceanogr.* 34, 1545–1562. doi:10.4319/lo.1989.34.8.1545

Morel, A., Huot, Y., Gentili, B., Werdell, P.J., Hooker, S.B., Franz, B.A., 2007. Examining the consistency of products derived from various ocean color sensors in open ocean (Case 1) waters in the perspective of a multi-sensor approach. *Remote Sens. Environ.* 111, 69–88. doi:10.1016/j.rse.2007.03.012

Morris, R.M., Rappé, M.S., Connon, S., Vergin, K.L., Siebold, W., Carlson, C., Giovannoni, S.J., 2002. *SAR11* clade dominates ocean surface bacterioplankton communities. *Nature* 420, 806–810. doi:10.1038/nature01240

Morris, J.J., Kirkegaard, R., Szul, M.J., Johnson, Z.I., Zinser, E.R., 2008. Facilitation of robust growth of *Prochlorococcus* colonies and dilute liquid cultures by "helper" heterotrophic bacteria. *Appl. Environ. Microbiol.* 74, 4530–4534. doi:10.1128/AEM.02479-07

Morris, J.J., Johnson, Z.I., Szul, M.J., Keller, M., Zinser, E.R., 2011. Dependence of the cyanobacterium *Prochlorococcus* on hydrogen peroxide scavenging microbes for growth at the ocean's surface. *PLoS One* 6. doi:10.1371/journal.pone.0016805

Morrissey, J., Bowler, C., 2012. Iron utilization in marine cyanobacteria and eukaryotic algae. *Front. Microbiol.* 3. doi:10.3389/fmicb.2012.00043

Mouriño-Carballido, B., Hojas, E., Cermeño, P., Chouciño, P., Fernández-Castro, B., Latasa, M., Marañón, E., Morán, X.A.G., Vidal, M., 2016. Nutrient supply controls picoplankton community structure during three contrasting seasons in the northwestern Mediterranean Sea. *Mar. Ecol. Prog. Ser.* 543, 1–19. doi:10.3354/meps11558

Nair, A., Sathyendranath, S., Platt, T., Morales, J., Stuart, V., Forget, M.H., Devred, E., Bouman, H., 2008. Remote sensing of phytoplankton functional types. *Remote Sens. Environ.* 112, 3366–3375. doi:10.1016/j.rse.2008.01.021

NASA, 2014. Moderate Resolution Imaging Spectroradiometer (MODIS-Aqua) Ocean Color Data. NASA Goddard Space Flight Center, Ocean Ecology Laboratory, Ocean Biology Processing Group, NASA OB.DAAC, Greenbelt, MD, USA.

Nychka, D., Furrer, R., Paige, J., Sain, D., 2015. *fields: Tools for spatial data.* R package version 8.10. doi:10.5065/D6W957CT

Olson, D.M., Dinerstein, E., Wikramanayake, E.D., Burgess, N.D., Powell, G.V.N., Underwood, E.C., D'amico, J.A., Itoua, I., Strand, H.E., Morrison, J.C., Loucks, C.J., Allnutt, T.F., Ricketts, T.H., Kura, Y., Lamoreux, J.F., Wettengel, W.W., Hedao, P., Kassem, K.R., 2001. Terrestrial ecoregions of the world: a new map of life on Earth. *Bioscience* 51, 933. doi:10.1641/0006-3568(2001)051[0933:TEOTWA]2.0.CO;2

Olson, R.J., Chisholm, S.W., Zettler, E.R., 1990. Pigments, size, and distribution of *Synechococcus* in the North Atlantic and Pacific Oceans. *Limnol. Oceanogr.* 35 (1), 45-58.

Olson, R.J., Zettler, E.R., DuRand, M.D., 1993. Phytoplankton analysis using flow cytometry. *In: Kemp, P.F., Sherr, E.B., Cole, J.J. (eds.), Handbook of Methods in Aquatic Microbial Ecology.* Lewis Publishers, Boca Raton, USA, pp. 175–186.

Partensky, F., Hoepffner, N., Li, W., 1993. Photoacclimation of *Prochlorococcus* sp. (Prochlorophyta) strains isolated from the North Atlantic and the Mediterranean Sea. *Plant Physiol.* 101, 285–296. doi:101/1/285 [pii]

Partensky, F., Hess, W.R., Vaulot, D., 1999. *Prochlorococcus*, a marine photosynthetic prokaryote of global significance. *Microbiol. Mol. Biol. Rev.* 63, 106–127. doi:doi:1092-2172/99/$04.00

Partensky, F., Garczarek, L., 2010. *Prochlorococcus* : advantages and limits of minimalism. *Ann. Rev. Mar. Sci.* 2, 305–331. doi:10.1146/annurev-marine-120308-081034

Pérez, V., Fernández, E., Marañón, E., Morán, X.A.G., Zubkov, M.V., 2006. Vertical distribution of phytoplankton biomass, production and growth in the Atlantic subtropical gyres. *Deep-Sea Res. Part I* 53, 1616–1634. doi:10.1016/j.dsr.2006.07.008

Pierce, D., 2015. *ncdf4: Interface to unidata netCDF (Version 4 or Earlier) format data files.* R package version 1.15.

Platt, T., Gallegos, C.L., Harrison, W.G., 1980. Photoinhibition of photosynthesis in natural assemblages of marine phytoplankton. *J. Mar. Res.* 38, 687–701.

Polovina, J.J., Howell, E.A., Abecassis, M., 2008. Ocean's least productive waters are expanding. *Geophys. Res. Lett.* 35, L03618. doi:10.1029/2007GL031745

Rabouille, S., Edwards, C.A., Zehr, J.P., 2007. Modelling the vertical distribution of *Prochlorococcus* and *Synechococcus* in the North Pacific Subtropical Ocean. *Environ. Microbiol.* 9, 2588–2602. doi:10.1111/j.1462-2920.2007.01376.x

R Core Team, 2017. *R: A language and environment for statistical computing.* Viena.

Raimbault, P., Garcia, N., Cerutti, F., 2008. Distribution of inorganic and organic nutrients in the South Pacific Ocean - evidence for long-term accumulation of organic matter in nitrogen-depleted waters. *Biogeosciences* 5, 281–298. doi:10.5194/bgd-4-3041-2007

Raven, J.A., 1994. Why are there no picoplanktonic O_2 evolvers with volumes less than 10^{-19} m^3? *J. Plankton Res.* 16, 565–580. doi:10.1093/plankt/16.5.565

Raven, J.A., 2011. The cost of photoinhibition. *Physiol. Plant.* 142, 87–104. doi:10.1111/j.1399-3054.2011.01465.x

Renz, M., 2013. Fluorescence microscopy-A historical and technical perspective. *Cytom. Part A.* doi:10.1002/cyto.a.22295

Ribalet, F., Swalwell, J., Clayton, S., Jiménez, V., Sudek, S., Lin, Y., Johnson, Z.I., Worden, A.Z., Armbrust, E.V., 2015. Light-driven synchrony of *Prochlorococcus* growth and mortality in the subtropical Pacific gyre. *Proc. Natl. Acad. Sci.* 112, 8008–8012. doi:10.1073/pnas.1424279112

Richardson, T.L., Jackson, G. a, 2007. Small phytoplankton and carbon export from the surface ocean. *Science* 315, 838–40. doi:10.1126/science.1133471

Rii, Y.M., Karl, D.M., Church, M.J., 2016. Temporal and vertical variability in picophytoplankton primary productivity in the North Pacific Subtropical Gyre. *Mar. Ecol. Prog. Ser.* 562, 1–18. doi:10.3354/meps11954

Rippka, R., Coursin, T., Hess, W., Lichtle, C., Scanlan, D.J., Palinska, K.A., Iteman, I., Partensky, F., Houmard, J., Herdman, M., 2000. *Prochlorococcus marinus* Chisholm et al. 1992 subsp. *pastoris* subsp. nov. strain PCC 9511, the first axenic chlorophyll a2/b2-containing cyanobacterium (Oxyphotobacteria). *Int. J. Syst. Evol. Microbiol.* 50, 1833–1847. doi:10.1099/00207713-50-5-1833

Robertson, B.R., Button, D.K., Koch, A.L., 1998. Determination of the biomasses of small bacteria at low concentrations in a mixture of species with forward light scatter measurements by flow cytometry. *Appl. Environ. Microbiol.* 64, 3900–3909.

Roesler, C.S., Barnard, A.H., 2013. Optical proxy for phytoplankton biomass in the absence of photophysiology: Rethinking the absorption line height. *Methods Oceanogr.* 7, 79–94. doi:10.1016/j.mio.2013.12.003

Rousseau, V., Mathot, S., Lancelot, C., 1990. Calculating carbon biomass of *Phaeocystis* sp. from microscopic observations. *Mar. Biol.* 107, 305–314. doi:10.1007/BF01319830

Rousseaux, C.S., Gregg, W.W., 2013. Interannual variation in phytoplankton primary production at a global scale. *Remote Sens.* 6, 1–19. doi:10.3390/rs6010001

Roy, S., Llewellyn, C., Egeland, E.S., Johnsen, G., 2013. Phytoplankton pigments: characterization, chemotaxonomy and applications in oceanography. *J. Phycol.* 1–2. doi:10.1111/jpy.12035

Roy, S., Sathyendranath, S., Platt, T., 2017. Size-partitioned phytoplankton carbon and carbon-to-chlorophyll ratio from ocean colour by an absorption-based bio-optical algorithm. *Remote Sens. Environ.* 194, 177–189. doi:10.1016/j.rse.2017.02.015

Rusch, D.B., Martiny, A.C., Dupont, C.L., Halpern, A.L., Venter, J.C., 2010. Characterization of *Prochlorococcus* clades from iron-depleted oceanic regions. *Proc. Natl. Acad. Sci.* 107, 16184–16189. doi:10.1073/pnas.1009513107

Šantić, D., Krstulović, N., Šolić, M., Kušpilić, G., 2011. Distribution of *Synechococcus* and *Prochlorococcus* in the central Adriatic Sea. *Acta Adriat.* 52, 101–114.

Sarkar, D., 2008. *lattice: Multivariate data visualization with R.* Springer, New York.

Sathyendranath, S., Platt, T., 1989. Computation of aquatic primary production: Extended formalism to include effect of angular and spectral distribution of light. *Limnol. Oceanogr.* 34, 188–198. doi:10.4319/lo.1989.34.1.0188

Sathyendranath, S., Watts, L., Devred, E., Platt, T., Caverhill, C., Maass, H., 2004. Discrimination of diatoms from other phytoplankton using ocean-colour data. *Mar. Ecol. Prog. Ser.* 272, 59–68. doi:10.3354/meps272059

Sathyendranath, S., Platt, T., 2007. Spectral effects in bio-optical control on the ocean system. *Oceanologia* 49, 5–39.

Scanlan, D.J., West, N.J., 2002. Molecular ecology of the marine cyanobacterial genera *Prochlorococcus* and *Synechococcus*. *FEMS Microbiol. Ecol.* 40, 1–12. doi:10.1111/j.1574-6941.2002.tb00930.x

Schauer, M., Balagué, V., Pedrós-Alió, C., Massana, R., 2003. Seasonal changes in the taxonomic composition of bacterioplankton in a oligotrophic coastal system. *Aquat. Microb. Ecol.* 31, 163–174. doi:10.3354/ame031163

Shapiro, H.M., 2003. *Practical flow cytometry.* John Wiley and Sons, Inc., Hoboken, NJ, USA. doi:10.1002/0471722731

Shimada, A., Maruyama, T., Miyachi, S., 1996. Vertical distributions and photosynthetic action spectra of two oceanic picophytoplankters, *Prochlorococcus* and *Synechococcus* sp. *Mar. Biol.* 127, 15–23.

Shire, D.M., Kustka, A.B., 2015. Luxury uptake, iron storage and ferritin abundance in *Prochlorococcus marinus* (Synechococcales) strain MED4. *Phycologia* 54, 398–406.

Shukla, A., Biswas, A., Blot, N., Partensky, F., Karty, J.A., Hammad, L.A., Garczarek, L., Gutu, A., Schluchter, W.M., Kehoe, D.M., 2012. Phycoerythrin-specific bilin lyase-isomerase controls blue-green chromatic acclimation in marine *Synechococcus*. *Proc. Natl. Acad. Sci. USA* 109, 20136–41. doi:10.1073/pnas.1211777109

Sieburth, J.M., Smetacek, V., Lenz, J., 1978. Pelagic ecosystem structure: Heterotrophic compartments of the plankton and their relationship to plankton size fractions. *Limnol. Oceanogr.* 23, 1256–1263. doi:10.4319/lo.1978.23.6.1256

Siegel, D.A., Buesseler, K.O., Doney, S.C., Sailley, S.F., Behrenfeld, M.J., Boyd, P.W., 2014. Global assessment of ocean carbon export by combining satellite observations and food-web models. *Global Biogeochem. Cycles* 28, 181–196. doi:10.1002/2013GB004743

Smayda, T., 1958. Biogeographical studies of marine phytoplankton. *Oikos* 9, 158–191.

Smayda, T.J., 1997. Bloom dynamics: Physiology, behavior, and trophic effects. *Limnol. Oceanogr.* 42, 1132–1136.

Steglich, C., Mullineaux, C.W., Teuchner, K., Hess, W.R., Lokstein, H., 2003. Photophysical properties of *Prochlorococcus marinus* SS120 divinyl chlorophylls and phycoerythrin *in vitro* and *in vivo*. *FEBS Lett.* 553, 79–84. doi:10.1016/S0014-5793(03)00971-2

Stomp, M., Huisman, J., Stal, L.J., Matthijs, H.C.P., 2007. Colorful niches of phototrophic microorganisms shaped by vibrations of the water molecule. *ISME J.* doi:10.1038/ismej.2007.59

Stramski, D., Morel, A., 1990. Optical properties of photosynthetic picoplankton in different physiological states as affected by growth irradiance. *Deep-Sea Res. Part A* 37, 245–266.

Stramski, D., Reynolds, R.A., 1993. Diel variations in the optical properties of a marine diatom. *Limnol. Oceanogr.* 38, 1347–1364.

Stramski, D., Shalapyonok, A., Reynolds, R.A., 1995. Optical characterization of the oceanic unicellular cyanobacterium *Synechococcus* grown under a day-night cycle in natural irradiance. *J. Geophys. Res.* 100, 13,295-13,307.

Striebel, M., Schabhttl, S., Hodapp, D., Hingsamer, P., Hillebrand, H., 2016. Phytoplankton responses to temperature increases are constrained by abiotic conditions and community composition. *Oecologia* 182, 815–827. doi:10.1007/s00442-016-3693-3

Tarran, G., Heywood, J.L., Zubkov, M.V., 2006. Latitudinal changes in the standing stocks of nano- and picoeukaryotic phytoplankton in the Atlantic Ocean. *Deep-Sea Res. Part II* 53, 1516–1529. doi:10.1016/j.dsr2.2006.05.004

Tilstone, G.H., Smyth, T., Poulton, A., Hutson, R., 2009. Measured and remotely sensed estimates of primary production in the Atlantic Ocean from 1998 to 2005. *Deep-Sea Res. Part II* 56, 918–930. doi:10.1016/j.dsr2.2008.10.034

Tilstone, G.H., Lange, P.K., Misra, A., Brewin, R.J.W., Cain, T., 2017. Micro-phytoplankton photosynthesis, primary production and potential export production in the Atlantic Ocean. *Prog. Oceanogr.* doi:10.1016/j.pocean.2017.01.006

Tissot, N., Przybyla-Toscano, J., Reyt, G., Castel, B., Duc, C., Boucherez, J., Gaymard, F., Briat, J.F., Dubos, C., 2014. Iron around the clock. *Plant Sci.* doi:10.1016/j.plantsci.2014.03.015

Torres-Valdés, S., Roussenov, V.M., Sanders, R., Reynolds, S., Pan, X., Mather, R., Landolfi, A., Wolff, G.A., Achterberg, E.P., Williams, R.G., 2009. Distribution of dissolved organic nutrients and their effect on export production over the Atlantic Ocean. *Global Biogeochem. Cycles* 23. doi:10.1029/2008GB003389

Tsubouchi, T., Suga, T., Hanawa, K., 2016. Comparison study of subtropical mode waters in the world ocean. *Front. Mar. Sci.* 3, 270.

Uitz, J., Huot, Y., Bruyant, F., Babin, M., Claustre, H., 2008. Relating phytoplankton photophysiological properties to community structure on large scales. *Limnol. Oceanogr.* 53, 614–630. doi:10.4319/lo.2008.53.2.0614

Uitz, J., Claustre, H., Gentili, B., Stramski, D., 2010. Phytoplankton class-specific primary production in the world's oceans: Seasonal and interannual variability from satellite observations. *Global Biogeochem. Cycles* 24, n/a-n/a. doi:10.1029/2009GB003680

Urbach, E., Robertson, D.L., Chisholm, S.W., 1992. Multiple evolutionary origins of prochlorophytes within the cyanobacterial radiation. *Nature* 355, 267–270. doi:10.1038/355267a0 [doi]

Vaulot, D., Marie, D., Olson, R.J., Chisholm, S.W., 1995. Growth of *Prochlorococcus*, a photosynthetic prokaryote, in the Equatorial Pacific Ocean. *Science* 268, 1480–1482.

Vaulot, D., Eikrem, W., Viprey, M., Moreau, H., 2008. The diversity of small eukaryotic phytoplankton (≤ 3 μm) in marine ecosystems. *FEMS Microbiol. Rev.* doi:10.1111/j.1574-6976.2008.00121.x

Veldhuis, M.J.W., Kraay, G.W., 2004. Phytoplankton in the subtropical Atlantic Ocean: Towards a better assessment of biomass and composition. *Deep-Res. Part I* 51, 507–530. doi:10.1016/j.dsr.2003.12.002

Veldhuis, M.J.W., Timmermans, K.R., Croot, P., van der Wagt, B., 2005. Picophytoplankton; a comparative study of their biochemical composition and photosynthetic properties. *J. Sea Res.* 53, 7–24. doi:10.1016/j.seares.2004.01.006

Venables, W.N., Ripley, B.D., 2002. *Modern Applied Statistics with S*, Fourth ed., World. Springer, New York, New York, USA. doi:10.2307/2685660

Waterbury, J.B., Watson, S.W., Guillard, R.R.L., Brand, L.E., 1979. Widespread occurrence of a unicellular, marine, planktonic, cyanobacterium. *Nature* 277, 293–294. doi:10.1038/277293a0

Waterbury, J.B., Watson, S.W., Valois, F.W., Franks, D.G., 1986. Biological and ecological characterization of the marine unicellular cyanobacterium *Synechococcus*. *Can. Bull. Fish. Aquat. Sci.* 214, 71–120.

West, N.J., Scanlan, D.J., 1999. Niche-partitioning of *Prochlorococcus* populations in a stratified water column in the eastern North Atlantic Ocean. *Appl. Environ. Microbiol.* 65, 2585–2591.

Westberry, T., Behrenfeld, M.J., Siegel, D.A., Boss, E., 2008. Carbon-based primary productivity modeling with vertically resolved photoacclimation. *Global Biogeochem. Cycles* 22. doi:10.1029/2007GB003078

Wickham, H., 2009. *ggplot2: Elegant graphics for data analysis.* Springer-Verlag, New York.

Wickham, H., Chang, W., 2016. *devtools: Tools to make developing R packages easier*. R package version 1.12.0.

Wiethaus, J., Busch, A.W.U., Dammeyer, T., Frankenberg-Dinkel, N., 2010. Phycobiliproteins in *Prochlorococcus marinus*: biosynthesis of pigments and their assembly into proteins. *Eur. J. Cell Biol.* 89, 1005–10. doi:10.1016/j.ejcb.2010.06.017

Williams, R.G., Follows, M.J., 2011. Biological Fundamentals. *In: Williams, R.G., Follows, M.J. (Eds.), Ocean Dynamics and the Carbon Cycle: Principles and Mechanisms*. Cambridge University Press, New York, USA.

Winder, M., Sommer, U., 2012. Phytoplankton response to a changing climate. *Hydrobiologia*. doi:10.1007/s10750-012-1149-2

Wyman, M., Gregory, R.P., Carr, N.G., 1985. Novel role for phycoerythrin in a marine cyanobacterium, *Synechococcus* strain DC2. *Science* 230, 818–20. doi:10.1126/science.230.4727.818

Zhang, Y., Jiao, N., Hong, N., 2008. Comparative study of picoplankton biomass and community structure in different provinces from subarctic to subtropical oceans. *Deep. Res. Part II* 55, 1605–1614. doi:10.1016/j.dsr2.2008.04.014

Zinser, E.R., Johnson, Z.I., Coe, A., Karaca, E., Veneziano, D., Chisholm, S.W., 2007. Influence of light and temperature on *Prochlorococcus* ecotype distributions in the Atlantic Ocean. *Limnol. Oceanogr.* 52, 2205–2220. doi:10.4319/lo.2007.52.5.2205

Zinser, E.R., Lindell, D., Johnson, Z.I., Futschik, M.E., Steglich, C., Coleman, M.L., Wright, M.A., Rector, T., Steen, R., McNulty, N., Thompson, L.R., Chisholm, S.W., 2009. Choreography of the transcriptome, photophysiology, and cell cycle of a minimal photoautotroph, *Prochlorococcus*. *PLoS One* 4. doi:10.1371/journal.pone.0005135

Zubkov, M.V., Sleigh, M.A., Tarran, G.A., Burkill, P.H., Leakey, R.J.G., 1998a. Picoplanktonic community structure on an Atlantic transect from 50 degrees N to 50 degrees S. *Deep Sea Res. Part I* 45, 1339–1355. doi:10.1016/s0967-0637(98)00015-6

Zubkov, M.V., Sleigh, M., Burkill, P.H., 1998b. Measurement of bacterivory by protists in open ocean waters. *FEMS Microbiol. Ecol.* 27, 85–102. doi:10.1111/j.1574-6941.1998.tb00527.x

Zubkov, M.V., Fuchs, B.M., Eilers, H., Burkill, P.H., Amann, R., 1999. Determination of total protein content of bacterial cells by SYPRO staining and flow cytometry. *Appl. Environ. Microbiol.* 65, 3251–7.

Zubkov, M.V., Sleigh, M.A., Burkill, P.H., 2000a. Assaying picoplankton distribution by flow cytometry of underway samples collected along a meridional transect across the Atlantic Ocean. *Aquat. Microb. Ecol.* 21, 13–20. doi:10.3354/ame021013

Zubkov, M.V., Sleigh, M.A., Burkill, P.H., Leakey, R.J.G., 2000b. Picoplankton community structure on the Atlantic Meridional Transect: a comparison between seasons. *Prog. Oceanogr.* 45, 369–386. doi:10.1016/S0079-6611(00)00008-2

Zubkov, M.V., Fuchs, B.M., Tarran, G.A., Burkill, P.H., Amann, R., 2003. High rate of uptake of organic nitrogen compounds by *Prochlorococcus* cyanobacteria as a key to their dominance in oligotrophic oceanic waters. *Appl. Envir. Microb.* 69, 1299–1304. doi:10.1128/AEM.69.2.1299

Zubkov, M.V., Tarran, G.A., Fuchs, B.M., 2004. Depth related amino acid uptake by *Prochlorococcus* cyanobacteria in the Southern Atlantic tropical gyre. *FEMS Microbiol. Ecol.* 50, 153–61. doi:10.1016/j.femsec.2004.06.009

Zubkov, M.V., Tarran, G.A., 2005. Amino-acid uptake of *Prochlorococcus* spp. in surface waters across the South Atlantic Subtropical Front. *Aquat. Microb. Ecol.* 40, 241–249. doi:10.3354/ame040241

Zubkov, M.V., Burkill, P.H., 2006. Syringe pumped high speed flow cytometry of oceanic phytoplankton. *Cytometry A*. 69(9), 1010–1019. doi: 10.1002/cyto.a.20332

Zubkov, M.V., Burkill, P.H., Topping, J.N., 2007. Flow cytometric enumeration of DNA-stained oceanic planktonic protists. *J. Plankton Res.* 29, 79–86. doi:10.1093/plankt/fbl059

Zubkov, M.V., 2009. Photoheterotrophy in marine prokaryotes. *J. Plankton Res.* 31, 933–938. doi:10.1093/plankt/fbp043

Zubkov, M.V., 2014. Faster growth of the major prokaryotic versus eukaryotic CO_2 fixers in the oligotrophic ocean. *Nat. Commun.* 5. doi:10.1038/ncomms4776